Finite Element Modelling of Large Area Maintenance Shelters and Comparison to Experimental Results

by

Culver Norred

A thesis submitted to the Graduate Faculty of
Auburn University
in partial fulfillment of the
requirements for the Degree of
Master of Science

Auburn, Alabama
December 11, 2021

Keywords: structural engineering, finite element modelling, large area maintenance shelter

Approved by

Justin D. Marshall, Ph.D., P.E., Chair, Associate Professor of Civil and Environmental Engineering.
David Roueche, Ph.D., Co-Chair, Assistant Professor of Civil and Environmental Engineering.
James S. Davidson, Ph.D., Gottlieb Professor of Civil and Environmental Engineering.
J. Brian Anderson, Ph.D., Associate Professor of Civil and Environmental Engineering.

Abstract

Large area maintenance shelters (LAMS) are used as temporary structures by the United States Air Force to provide shelter for helicopters, tanks, wheeled vehicles, and aircraft. There are several different brands of LAMS used throughout the military, however the one focused on in this study is specifically used by the Air Force. These structures are lightweight and easy to construct, take down, and ship and are used throughout the world on military bases by the United States Air Force. However, several of these shelters have experienced failure due to wind loads below those the structure was designed to withstand.

The objective of this study is to investigate the structural response of a typical LAMS to design wind load cases and identify any systemic factors that may be contributing to premature failure. In this study, the structure is modeled using SAP 2000. Simple load cases were applied to understand the vertical and lateral load paths through the structure. Design wind loads were then developed and applied to the structure. Modeled demands under design wind loads were compared against preliminary strains, forces, and displacements measured in-situ in an existing, instrumented LAMS. The comparison demonstrated mixed agreements between the model output and responses of the in-service LAMS under transverse and longitudinal wind loads. Finally, the design wind loads were used to analyze the maximum demands on the structure.

Some stresses within the model were found to be larger than the allowable stress. This was the case at the eave of the windward door frames under longitudinal wind loads. The failures that have occurred in several LAMS show similar mechanisms and locations. The high uncertainty of the wind loads on the door frames, along with the uncertainty of the tightness of the cables, purlins, and fabric could all be contributing factors to these failures.

Acknowledgments

I want to thank my advisors, Dr. Marshall, and Dr. Roueche, for their support and encouragement through my study at Auburn University. Their knowledge and skills are valuable to me.

A special thanks to my parents and my sister who supported me through my life to be where I am now. Also, I would like to thank my good friend Hunter Chitty for his continued support and encouragement through my undergraduate and graduate experience. I am glad to have him as my friend and peer. Finally, I would like to thank the United States Air Force for the funding provided to make this research possible.

I want to thank all my professors, friends, and classmates at Auburn University for their supports during my life in Auburn.

Table of Contents

List of Tables

List of Figures

Chapter 1 Introduction

Large Area Maintenance Shelters (LAMS) are temporary structures used by the United States military all around the world to provide shelter and protection for helicopters, tanks, wheeled vehicles, and aircraft on military bases or other forward operating positions (JOCOTAS, 2012). These shelters are typically either constructed as aluminum-framed structures or inflatable structures. The specific LAMS studied in this research is constructed by Clamshell Buildings with the NSN of 5410-01-533-7395 (JOCOTAS, 2012). Throughout this study, this structure is simply referred to as the large area maintenance shelter, or simply LAMS. This LAMS is a frame-supported fabric membrane structure composed of short aluminum frame members that are built in sections and spliced together to form the framing system. Steel cables, aluminum purlins, and fabric are used to hold the structure together. These shelters are lightweight, easy to pack and ship, and easy to construct, which makes them ideal for expeditionary use around the world.

Unfortunately, these lightweight structures have experienced premature collapses, potentially causing costly damage to airplanes and injuries to occupants. Stiles (2021) documented several cases of premature collapses of LAMS due to high winds, from which several potential causal factors were suggested. More rigorous study is needed however to identify any systemic flaws in design, assembly, or operational use that are contributing to the premature failures.

This study is one component of a larger project focused on improving guidance and specifications for the design and erection of LAMS. The entire project includes load path evaluations of typical LAMS through field monitoring the response of an in-service LAMS and construction of 2D and 3D numerical models. Other components involve experimental testing of structural members used in LAMS and review of design criteria and specifications.

The objective of this thesis is to investigate the structural response of a typical LAMS to design wind load cases and identify any systemic structural factors that may be contributing to premature failure. The development, validation, and analysis of a 3D numerical model of the instrumented LAMS being used for field monitoring was the approach used to meet the objective.

A load path analysis was conducted on the finite element model to understand how the forces and stresses are distributed throughout the model. This was also performed as a check to validate that the model transfers loads in a manner that is expected.

At an existing LAMS, the research team implemented a detailed instrumentation plan on the structure that recorded forces, displacements, and strains at numerous selected locations. A weather monitoring station was also installed nearby the LAMS to record wind speeds and directions that were occurring at the structure. The demands in the LAMS recorded by the instrumentation system was compared to the stresses and forces in the finite element model at the same locations for the measured wind loads to verify that the model correctly represented the in-service LAMS. The model was then used to determine the location of maximum stresses and forces under the design wind loads to gain a better understanding of possible failure locations.

Chapter 1 introduces this research by defining the problem, introducing the proposed solution, and discussing the work scope and the approach used during this research. Chapter 2 provides a literature review designed to give background on LAMS and to deliver the necessary background on the behavior and design of these types of structures. Chapter 3 presents a description of the finite element model developed and how the structure was modeled. The calculation of the wind loads, along with the application of these loads are also discussed in this chapter. Chapter 4 focuses on the validation of the model using the results of the load path analysis conducted on the finite element model. This chapter also presents the results from the comparison of the finite element model to the instrumentation recordings. The stresses and forces at the location of the instrumentation are presented for the model as well as the recordings for multiple wind scenarios. Chapter 5 presents the maximum demands on the model based on the design wind loads. Potential failure locations are also presented. Chapter 6 presents alternative model analysis scenarios. Variables in the structure and wind loads are explored to determine their effect on the model. Chapter 7 summarizes the research, presents conclusions, and provides recommendations for future studies.

Chapter 2 Literature Review

The purpose of this chapter is to provide background information on tension fabric structures along. Case studies are conducted on the failure of two tensile fabric structures along with failure in LAMS. Further background is then provided to explore common mistakes in tensile fabric structure design and construction.

2.1 Tension Fabric Structure Background

Tension fabric structures are used to provide a covered area with protection from the environment. These usually consist of a light and simple structural system that is covered by a fabric to provide the protection. Most fabric structures have an arched type of structural system that allows the area under the protection to be free of any supports. Aluminum pipes and frames are typically used for the structural system (Huntington, 2013). These are chosen for their lightweight properties which allow these structures to be easily erected.

The design and selection of the tensile fabric membrane is a critical part of the overall design process in tension fabric structures. Woven or laid yards inside the membrane give it its tensile strength. The majority of membranes have fibers made of polyester, glass fibers, Teflon, and aramids (Huntington, 2013). The fibers are parallel to each other and are either woven or laid on top of each other in the perpendicular direction to give the fabric a biaxial strength. Polyester fibers are used in the LAMS fabric. Polyesters have been in use since the early 1960s and are the most common type of fiber used on tensile fabric membranes. They are cost-effective and have lifespans normally around 15 years (Huntington, 2013). Once the fibers are laid in the appropriate position, a coating is applied to protect the fibers and keep them in the proper position. The most common type of coating, that is mostly used with polyester fibers, is polyvinylchloride (PVC). These coatings are flexible and easy to work with. UV rays deteriorate the coating, giving it a life of about 15 years. PVC polyester fabrics are selected for structures like the LAMS because of their blackout capabilities (Huntington, 2013).

2.2 Large Area Maintenance Shelter Background

The United States Department of Defense (DoD) uses a wide range of tactical shelters for a multitude of purposes. These shelters are preferred for their light weight, limited footprint, and ease of erection. The Air Force began using lightweight fabric structures in the late 1980s. While these structures are much simpler to deploy and erect, there has been an increase in failures of these structures (JOCOTAS, 2012).

In 2012, the Joint Committee on Tactical Shelters (JOCOTAS) was created by the DoD and tasked with the duty of developing a standard family of tactical shelters. Before this, hundreds of different types of tactical shelters were used by the military. This caused many logistical issues and clutter. The JOCOTAS reduced the types of tactical shelters to 21. By DoD definition, a tactical shelter is described as “A mobile, transportable structure designed for a functional requirement. It provides an environmentally controllable space for human habitation and use, and/or permanent equipment storage or operation.” (JOCOTAS, 2012). Tactical Shelters are then categorized into three groups, rigid wall shelters, soft wall shelters, and hybrid shelters. Hybrid shelters are defined as “a combination of rigid and soft wall shelters that are transported and erected or assembled on-site” (JOCOTAS, 2012). Large area maintenance shelters, LAMS, fall under this category. The JOCOTAS has selected one specific LAMS to be used by the United States Air Force, which is the subject of this study.

A large area maintenance shelter is defined as a frame-supported shelter with the purpose of being a “larger area maintenance/repair shelter for helicopters, tanks, wheeled vehicles and aircraft” (JOCOTAS, 2012). This specific LAMS is “used as a mobile facility in the US Air Force

BEAR inventory supporting combat maintenance for the US Air Force F-15, F-16, and F-22 aircraft" (Clamshell Buildings, 2019).

2.3 Tensioned Fabric Structure Failure Cases

While the specific LAMS considered in this study is manufactured specifically for the US Air Force, the broad class of tensioned fabric or frame-supported fabric membrane structures has seen widespread use in many industries and has also experienced several notable failures. This section provides fabric structure failure examples in common fabric-designed structures along with failures that occurred in LAMS. A likely reason for failure is specified for each failure example to demonstrate how each of the problems can lead to failure.

2.3.1 Collapse of the Dallas Cowboys Indoor Practice Facility, 2009

On May 2nd, 2009, during a practice session at the Dallas Cowboys practice facility, a severe thunderstorm caused the practice facility to collapse (NIST, 2010). At the time of the collapse, there were approximately 70 people inside the facility. Twelve people were injured, including one severely injured. The practice facility was a gable-roof, steel frame structure with tensioned fabric covering (NIST, 2010). The building was 204 feet wide by 406 feet long. At the ridge, the height of the structure was 86 feet. The structure was designed and constructed for the Cowboys in 2003 and it was upgraded with a new roof and reinforcement added to some members in 2008 (NIST, 2010).

The design wind loads for the structure were calculated using a design wind speed of 90 mph. Based on data received from the National Oceanic and Atmospheric Administration, the wind speeds were estimated to be around 55 mph to 65 mph with the wind direction acting predominantly transverse to the ridge of the structure when the structure failed (NIST, 2010).

It was determined that there were large demands on the structure that exceeded the structural capacity for the wind speed at failure which was much lower than the design wind speed. This indicates that there was a design issue with this structure. This was especially true for the inner chord on the leeward side of the structure in the straight section and around the knee (NIST, 2010). Figure 2.3-1 shows a cross-sectional view of the steel frames in the practice facility, along with labels of the wind direction and important sections in the frame.

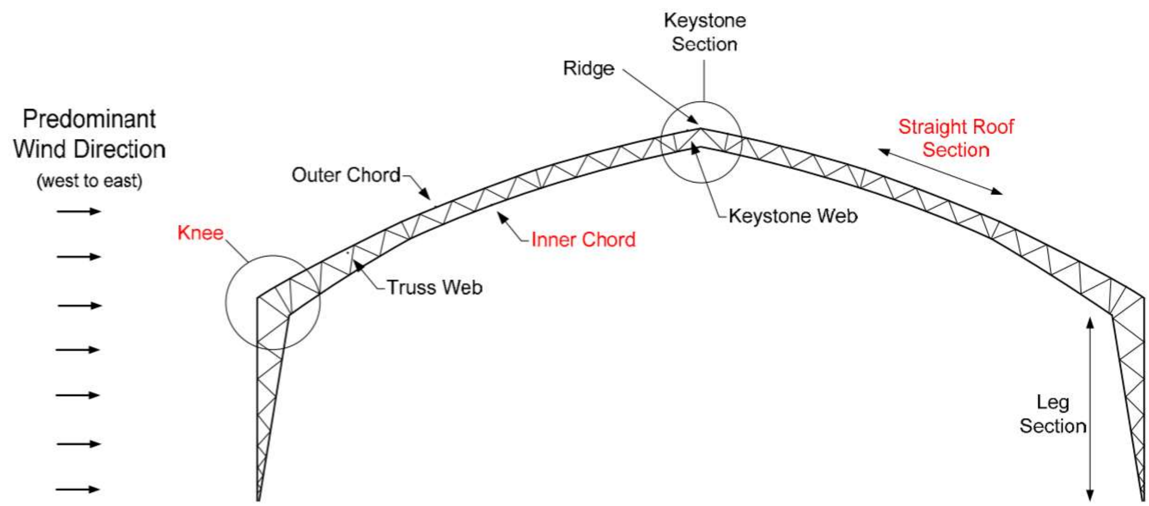

Figure 2.3-1. Dallas Cowboys practice facility steel frame cross-section (NIST, 2010).

In their findings, Gross et al. (2010) found that the wind loads used for the design of both the original 2003 structure and the 2008 upgrade were different than the loads calculated using the ASCE Standard. The calculations for the wind loads were made using a mean height of fewer than 60 feet when it should have been 67 feet. The calculations were also only made for a frame in the center of the structure when it should have been made for one of the frames near the end walls where the loads were larger. No internal wind pressure was used for the calculations and the roof slope was assumed to be 11 degrees when it was 21 degrees. The capacities of the frame members were also reported to be larger than what was calculated using the AISC specifications. At the joints, and more specifically the knees of the frames, large bending moments and shear forces were generated that were not taken into consideration in the design process. The reinforcements made in 2008 did not affect the critical members since they focused on compressive capacity reinforcements. When calculating the member capacities, it was incorrectly assumed that the exterior fabric provided lateral bracing to the framing. Incorrect effective length factors and incorrect unbraced lengths were considered in calculations (NIST, 2010).

The Building and Fire Research Laboratory determined the collapse likely occurred from the buckling of the inner chord in the straight section of the roof on the leeward side. This in turn caused failures in the knees on both the windward and leeward sides which then allowed the building to sway. The ridge of the roof was the next point of failure. From there, the redistribution of forces in the structure caused it to continue to collapse until it had fallen to the ground. Figure 2.3-2 shows a visual representation of how the collapse of the practice facility occurred.

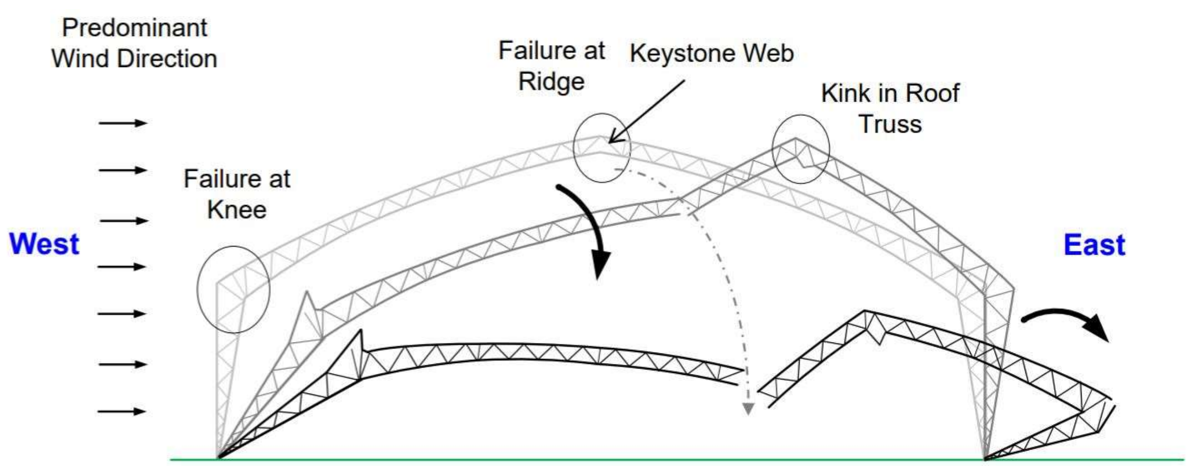

Figure 2.3-2. Dallas Cowboys practice facility collapse sequence (NIST, 2010).

2.3.2 Collapse of the Minneapolis Metrodome, 2010

On December 12th, 2010, the fabric roof of the Minneapolis Hubert H. Humphrey Metrodome was overloaded and tore apart. Seventeen inches of snow covered the Metrodome on that day. The Metrodome was erected using mostly a fabric roof, with a truss system to support the fabric. The dome was inflated to put the fabric in tension using inflation fans. The dome was designed so that the inflation fans would keep the internal pressure greater than or equal to the external pressure on the roof. The roof was designed to withstand pressures from wind, snow, and even earthquakes (Wiegler, 2011).

The fans in the Metrodome were designed to be able to increase the internal pressure of the dome when the external pressure is increased due to snow, wind, or rain. Based on the amount of snow on the dome, the weight of the roof increased five to seven times the weight of the roof alone. If the load on the roof is close to the maximum load it can hold, the weight has to be removed. On December 11th, 2010, a group of workers got on the roof of the dome and used fire hoses to try to wash the snow off the roof (Wiegler, 2011).

At 5 A.M. on December 12th, a triangular panel on the west side of the dome tore apart. Once this happened, the dome began to lose its internal pressure. With the internal pressure decreasing, quickly after the first tear, 2 of the panels adjacent to the ripped one also tore. Three days later, another panel tore, due to the lack of inflation in the dome. Once the dome was deflated, there was no way to get the snow to drain off once it was melted. In detail, the first tear in the roof was caused by an overload of snow. This shifted the weight of the dome, which caused the subsequent 2 panels to tear (Wiegler, 2011). Overall, the failure of the fabric panels in this roof dome was caused by extreme loads. While this is not a common occurrence, it demonstrates the importance of monitoring loads on fabric structures. The difficulty of this is the maintenance that must be done when these structures are overloaded. Unloading these structures can be complicated and if done incorrectly, can have dangerous outcomes.

2.3.3 Large Area Maintenance Shelter Failures

There are 4 documented instances in recent history of failures in Air Force large area maintenance shelters or similar structures. These occurred in February 2014, February 2015, April 2016, and August 2017 (Stiles, 2021). The failures in 2014, 2016, and 2017 occurred on the same LAMS studied in this research, while the 2015 failure occurred on a similar structure designed by a different manufacturer with slightly different dimensions.

Considering the 2014, 2016, and 2017 failures, in two of these instances the doors were not secured to the foundation due to broken parts. In the third event (2017), a shelter failed while maintenance on an aircraft was ongoing in the shelter and a door was in a partially open position. Two of the shelters failed during wind speeds of 60 and 70 mph. The third failure occurred on a shelter that did not have the high wind kit installed. Although these structures were not properly secured to the foundation, the failures did not occur at the supports. All three failures occurred on the retractable door frames. Peak gust wind speeds in this case were estimated to be 51 mph. Three additional shelters were damaged in the 2016 event, however, there is little knowledge of the damage. The only information on these shelters is an estimated wind speed of between 60 and 70 mph that caused the damage (Stiles, 2021).

The 2015 failure occurred in a frame supported fabric membrane structure similar to the type studied in this research. It was installed in October of 2014 and had dimensions of 90 ft wide, 130 ft long, and a peak height of 32 ft. The shelter was designed for a 100-mph wind speed. The failure initiation point for this structure was in the base plates. Several base plates in the structure were lifted out of the ground approximately 6-7 feet. The reason for the base plate failure was due to anchor pins being installed in sandy, non-cohesive soil. Helical anchors should have been installed in this type of soil to prevent uplift.

2.4 Tension Fabric Structure Failures

With the failures occurring in LAMS, it is important to understand any potential systemic causes beyond the specific structural failure mechanisms highlighted in the previous section. This section will provide a review of common mistakes in fabric structure design and construction that can potentially lead to failure. This section also focuses on how these issues could be the reason for failure issues in LAMS.

The first common mistake is a mono-cover fabric membrane (Legacy Building Solutions, 2015). Mono-cover fabric membranes are fabric covers that come in a singular large piece that is draped over the top of the framework of the structure. With this type of cover, the membrane is only attached to the end frames. This causes most of the forces and pressures to be transferred to the end frames and not uniformly to all the frames. When the fabric is not connected to the members, buckling of the interior members is not restrained by the tension in the fabric. Allowing these members to rotate and move freely can lead to failure or damage due to loads below what they are designed to withstand. This can lead to rips in the fabric or even the collapse of the frames. Individual membrane panels are suggested to be attached between each frame member to help distribute pressures evenly and alleviate this problem. The main framing systems are usually designed so that the fabric attaches to the flanges of the members. Kedered connections, the connections used in LAMS, are one of the most common types of these connections.

Relying on fabric tension to provide stability to the structure is the second common mistake (Legacy Building Solutions, 2015). In fabric building construction, it is common to design the structures under the assumption that the fabric is assembled so that it is a tight fit and in tension. The majority of the time, fabrics are designed to be prestressed to prevent any slack in the fabric from occurring (Huntington, 2013). This allows the designers to assume that the fabric will provide lateral support to the rigid frame top flange (Legacy Building Solutions, 2015). In reality, lateral support must be designed for the structure. The fabric does give the structure some lateral support, but the structure should be designed under the assumption that the purlins and cables are the only source of lateral support.

Third, allowing inexperienced crews to install fabric buildings can be a common mistake (Legacy Building Solutions, 2015). Although fabric-type structures can be easier to install, it is still important to have an installation crew that is trained and fully equipped to install the structure. In the Air Force, LAMS are installed by different crews nearly every time. This makes it extremely important to have these individuals trained to be able to professionally install the shelters. The stability of supporting members during the erection of a fabric structure must be carefully designed (Huntington, 2013). During the erection of the structure, a small wind event could cause the structure to collapse if the supporting members are not designed to withstand the erection of the structure. While installing the structures, it is important that the fabric is taken care of properly. The fabric should not be placed on the ground or stored anywhere before that surface has been cleared or cleaned. Along with the installation of fabric structures, careful packaging and shipment is critical to prevent weakening and tearing (Huntington, 2013). LAMS are designed to have a lifetime of several different cycles of deployment, so the packaging and shipment of the structures is important, as well as proper setup. Impacting members with steel hammers or mallets to correct misalignments can damage members when done over multiple installations. Improper installation and maintenance can put undue stress on damaged elements of the LAMS and compromise the structural capacity.

Improper foundations are another common mistake (Legacy Building Solutions, 2015). Foundations for tensile fabric structures are designed for large uplift forces (Huntington, 2013).

Due to the lightweight fabric and framing members, the foundations can experience small compressive forces and large uplift forces. This makes foundation designs critical for temporary structures. LAMS are designed to be installed both on concrete foundations and bare ground. Foundational supports can become complicated when a structure is designed for different types of foundations. This is the case for LAMS in the Air Force. The LAMS they use are designed and constructed all over the world with several different types of foundations. For the specific LAMS studied in this research, the foundation is a concrete structure. For this type of foundation, anchor bolts are used to connect the exterior high wind kit cables to the foundation. For other foundation conditions, duckbills and below ground T-barriers are used depending on the type of soil. It can sometimes be difficult determine if the soil conditions at a military base, whether a permanent facility or an expeditionary location, are adequate to support the shelters being built.

When looking more specifically at the failure of the fabric in tensile fabric structures, there are several common reasons that failure occurs. The first is ultraviolet radiation (Wilson, 2016). When exposed to the sun, over time UV rays damage the fabric (Huntington, 2013). It wears down and deteriorates the coating which can expose the fibers that give the fabric its strength. As these fibers start to deteriorate, the fabric loses its tensile strength and is more susceptible to failure. Figure 2.4-1 displays the cross-section of a typical tensile fabric and how UV rays can cause damage and deterioration to the fabric. For the LAMS used by the Air Force, this is important, because the degree of UV exposure can vary for the different environments where the shelters are employed.

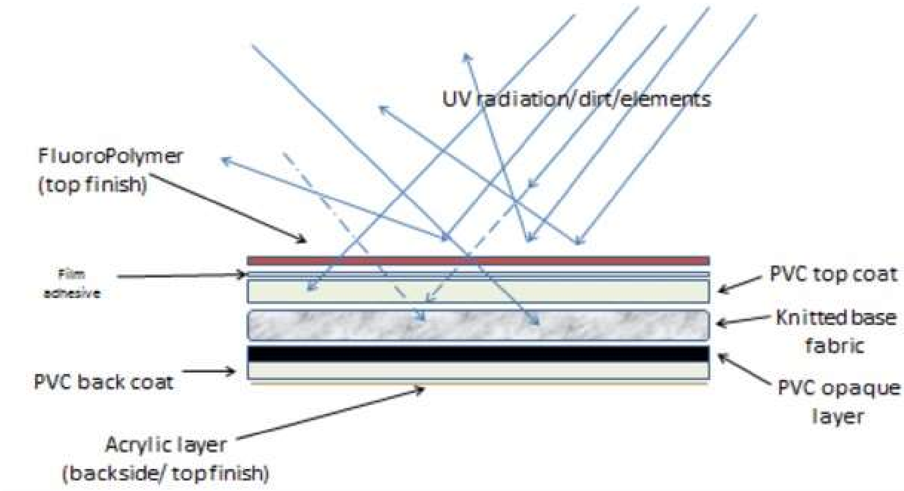

Figure 2.4-1. Cross-section of UV damage to tensile fabric (Wilson, 2016)

Besides UV rays, other forms of weathering can damage the fabric (Wilson, 2016). Wind, rain, and snow are the most common causes of weathering. Over time, these forms of weathering can deteriorate the fabric (Wang, Wood, Abdul-Rahman, & Mohd-Rahim, 2015). This is common and is the reason the fabric will have a reduced life expectancy. This can become an issue when the fabric is in use for longer than initially designated. Due to the variety of locations LAMS are installed by the Air Force, the weather conditions that affect the weathering of the fabric can be drastically different. In the desert, high winds and sandstorms can be a major cause of weathering and cause weathering to occur quicker. In a cold-weather environment, continual snow loads could be the main reason for weathering and deterioration.

The use and design of the fabric can also affect its lifespan and effectiveness. The lifespan can be different based on the environment. The usage of retractable doors on structures, like those used in LAMS, can also affect the lifespan. If a LAMS is heavily used and the doors are opened often, it can cause the fabric to fold or scratch and wear out in a shorter period (Wang, et al. 2015)

Tearing of the fabric is another reason that the structure could fail. The fabric should be designed to withstand tearing due to the loads it will experience. However, over time as the fabric is damaged through weathering or deterioration from UV rays, the structural capacity of the fabric may also decrease. This can lead to tears in worn-out fabrics. Tears can also occur by accidents or vandalism (Huntington, 2013). Tears are a major issue for several reasons. They could be holding certain members together, and the whole structure could collapse due to a tear (Wang et al., 2015) A tear can also alter any wind loads on the structure and cause the structure to react differently than it was designed to. This can quickly lead to failure and the collapse of a structure. Failures in tensile fabric structures can occur due to tears in the fabric, so factors of safety for the tear strength of fabric can be anywhere between 5 to 8 (Huntington, 2013). This is important for the Air Force because with the different structures being used several times at different locations, tears could easily occur. From the setup, take down, or packaging and shipping of the structures, small tears could occur without being noticed that can cause severe damage.

Loose fabric is a complex flaw that can lead to damage or failure of tensile fabric structures. To prevent loose fabric, it is often uniformly prestressed to stretch the fabric out to its proper tensioning (Bridgens, Gosling, & Birchall, 2004). When fabrics are not prestressed and not in complete tension, several issues can occur. First, when the fabric is slacked, it essentially acts as a mono-cover membrane. As discussed previously, when this occurs, the fabric does not provide any lateral stability to the frames. Second, when the fabric is relaxed, any loading on the fabric can cause bearing on any members that the fabric is draped over. This bearing can cause large stresses that may not have been accounted for in the design of structural members. Third, rain or snow can accumulate on the fabric, which can create large loads over small areas on the structure that can lead to forces on certain members in the structure to exceed the design demands. Finally, flutter can occur in the fabric during wind events (Huntington, 2013). Flutter can produce impact load effects on members directly beneath the loose fabric and could also introduce resonant load effects.

Along with the enhanced wind loads, flutter can also cause the fabric to be weathered at a much higher rate than if it were tensioned appropriately. To reduce the impacts of flutter, it is important to pre-tension the fabric, although optimal pre-tensioning levels are not available. PVC-coated polyester fabric members are known to have a higher level of creep (Bridgens et al., 2004) that can cause the tension to decrease over time, therefore, regular checks on the tension of the fabric are required.

Another potential cause for failure in the LAMS is the positioning of the bay doors. The large retractable doors on the structure affect how the structure handles wind loads based on their positioning. Fabric structures with these types of doors are designed to be used in both open and closed positions (Liew & Tran, 2006). With both doors closed, one open, or both open, the structure experiences and transfers loads differently, changing the demands. When both doors are closed, the LAMS is nominally enclosed from a wind perspective, minimizing internal pressurization, and benefits from the longitudinal stiffness provided by the door frames and fabric. When one door is open, the interior will be pressurized either positively or negatively depending on the wind angle of attack, potentially causing wind loads to differ from design levels and cases. With both doors open, the stiffness provided by the doors is lost. Internal pressurization is not much of a concern, but the surface area presented by the bundled fabric in the roof from the retracted doors will catch wind and contribute to wind loads in the longitudinal direction. The LAMS manufacturer specifies maximum wind speeds for the scenarios of both doors closed, one door open, and both doors open. If the doors are not closed during large wind events, failure could occur.

2.5 Chapter Summary

This chapter provided background information on tensile fabric structures along with two examples of commonly fabricated fabric structures that experienced some forms of failure were presented to give a better understanding of how fabric structures could experience failure. four examples of failures that have occurred in LAMS were presented and a synopsis of explanations for typical failure in fabric structures was listed along with descriptions of why these issues could occur in the LAMS used by the Air Force. The main takeaways from this chapter are that there are several variables in tensile fabric structure design and construction that can lead to damage or failure of the structures. The study of the LAMS failures provided evidence that many of the failures occurred in the door frames.

Chapter 3 Modeling Analysis and Procedure and Load Application

This chapter provides the details of the LAMS studied in this research. Along with these specifics, the design of the model is presented. The wind load calculations and applications are also provided.

3.1 Large Area Maintenance Shelter Specifics

The requirement of the LAMS by the Air Force is to have a "relocatable tension fabric building consisting of parallel structural aluminum arches with high-strength architectural fabric panels connecting the arches to form the walls, roof and aircraft doors of the shelter" (Clamshell Buildings, 2019). The design of these structures in the United States should be in accordance with ASCE/SEI Standard 55-16 (ASCE, 2016). Figure 3.1-1 shows a picture of the LAMS setup and Figure 3.1-2 shows the LAMS framing in a 3-D isometric view.

Figure 3.1-1. Setup at in-service LAMS

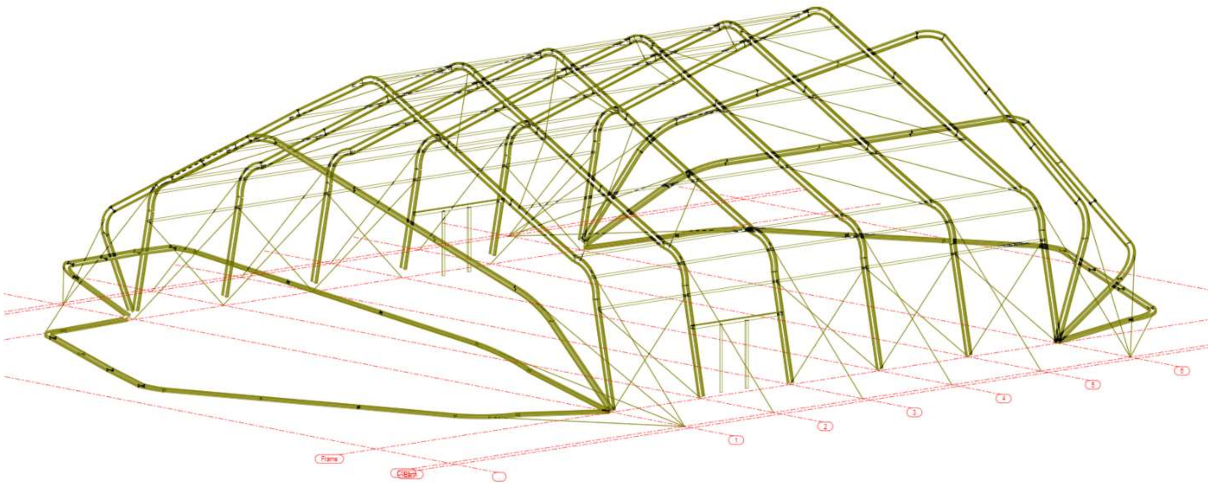

Figure 3.1-2. 3-D isometric view of the LAMS.

There are six vertical arches on the shelter. On both ends of the building, there are 3 additional arches that are the same size and shape as the vertical arches. However, the doors are positioned at angles of 60, 30, and 0 degrees from the ground. All the frames have a pinned connection to baseplates installed on a concrete slab foundation. The angled frames are connected to a cable system in the roof that allows them to be winched into an open position. Figure 3.1-3 shows the shelter with one end in the open position. Figure 3.1-4 shows the shelter with both ends in the open position.

Figure 3.1-3. LAMS configuration with one end in the open position

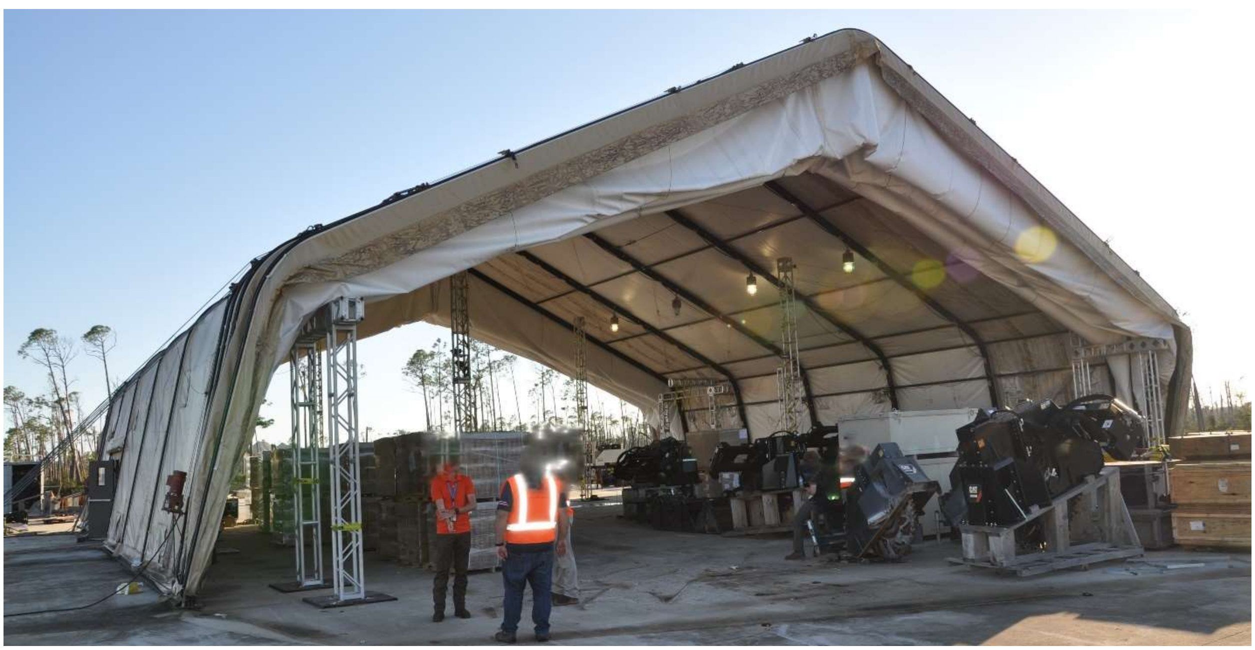

Figure 3.1-4. LAMS configuration with both ends in the open position

The product description of the shelter specifies that the total length of the shelter, with both ends in the closed position, is 128.72 feet. The width of the shelter is specified as the distance between the arch supports, which is 75.65 feet (Clamshell Buildings, 2019). The sidewalls of the frames are not completely vertical but have a slight angle inward. This causes the width of the shelter at the eave to be 70 feet, instead of the 75.65-foot width at the supports. The height of the ridge is 30.9 feet, and the height of the eaves is 14.4 feet. The roof slope is 26 degrees. The shelter was "designed to be installed on existing parking ramps or soil by a nine-person crew in less than five working days with minimal heavy equipment support" (Stiles, 2021). The manufacturer's technical order specifies the doors are only safe to operate in the winds up to 20 mph, and a maximum of 30 mph during an emergency.

The product description defines the shelter frame as "a clear-span, frame-supported, tension fabric structure of modular design with no internal posts or supports." The shelter is a "pre-engineered kit requiring no on-site fabrication, welding or gluing to install or relocate" (Clamshell Buildings, 2019). The shelter was designed so that it can be disassembled, with all the components being able to be reused so that it can be fully relocatable. The components were designed so that they can be exchanged within the structure or between like structures. Along with the frames, the shelter includes purlins and cables on the inside of the structure that holds the shelter together. These members can be seen in both Figure 3.1-3 and Figure 3.1-4.

The round channels on the frame members were designed for the kedered connection of fabric to the frames. The shape of the flange was designed to allow the splice members to connect the frames. A splice member is attached to the top and bottom flange. Six aluminum spiral pins are then used to connect each splice member to the frame members. The arches are spliced together on the ground using the frame members. The dimensions of the frame members are shown in Figure 3.1-5. Figure 3.1-6 shows the cross-section of the splice member. Figure 3.1-7 shows a side view of the splice member. The frame members are then attached to the base plates using pin connections. The arches are then raised into the appropriate position. Figure 3.1-8 displays the connection of the arches to the base plates.

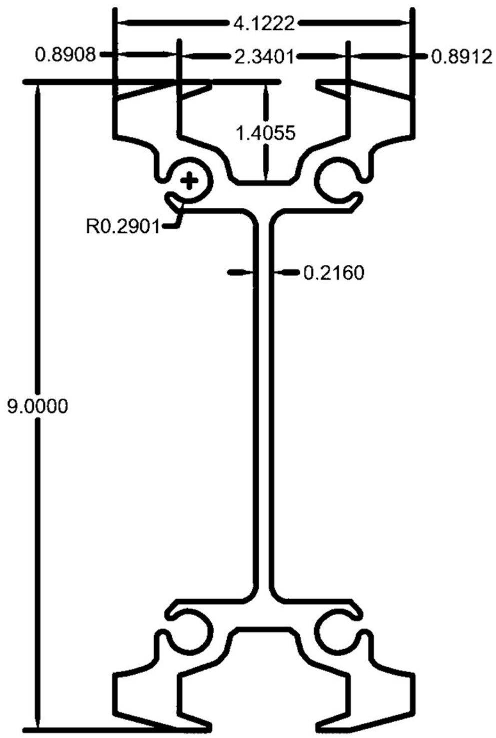

Figure 3.1-5. Cross-section of the framing members. Units are in inches.

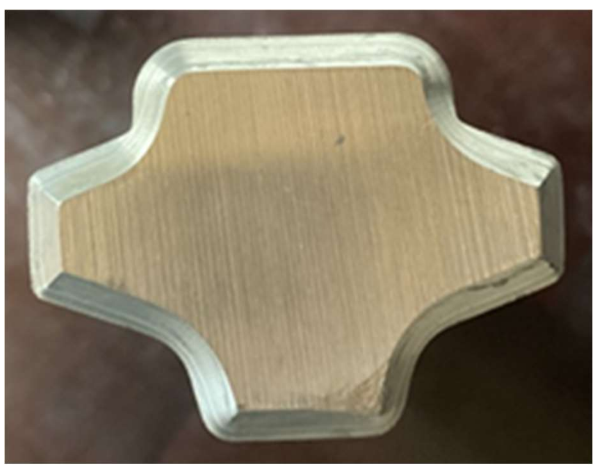

Figure 3.1-6. Cross-section of the splice

Figure 3.1-7. Side view of splice member

Figure 3.1-8. Base plate connections

There are 13 purlin lines in the shelter that connect the six vertical arches. Each line consists of 5 purlins, for a total of 65 purlins. The purlins are connected to arches by a pin connection system. Figure 3.1-9 shows the connection of the purlins to the arches.

There are 24 roof cables and 16 wall cables in the shelter that connect the vertical arches. The roof cables consist of ¼-in diameter, 7x19 steel cables that are connected to the arches with a pin connection. The cables are attached between each frame line. The wall cables are also ¼-in diameter steel cables; however, they are connected to turnbuckles that connect to the arches. The distance between the cable and purlin connections along the frames is 8 inches. This is also the same distance between the baseplate connections and the wall cables. Figure 3.1-10 shows the connection of the purlins to the arches, along with the connection of the roof cables and arches. Figure 3.1-11 shows the connection of the arches to the wall cables. The interior configuration, including the vertical arches and purlins, can be seen in Figure 3.1-12. Figure 3.1-13 highlights the configuration of the wall and roof cables.

Figure 3.1-9. Purlin connection

Figure 3.1-10. Purlin, roof, and wall cable connection

Figure 3.1-11. Wall cable connection to columns.

Figure 3.1-12. LAMS interior configuration.

Figure 3.1-13. LAMS wall and roof cable configuration.

An exterior high wind kit is supplied along with the shelter. This kit includes (20) ½-in. diameter steel cables that attach to the arches near the eave and attach to base plates on each side of the shelter. The base plates are 10.73 feet away from the arch base plates and produce an angle of 45 degrees (Stiles, 2021). Without the high wind kit attached, the shelter is designed for 3-sec gust wind speeds up to 70 mph, and with the high wind kit, the shelter is designed for 90 mph gust wind speeds. Figure 3.1-14 shows the high wind kit attached to the LAMS at the in-service LAMS.

The fabric is described in the product description as a "weathershell (exterior) fabric that must be a PVC-coated/laminated polyester reinforced membrane with a clear topcoat for UV protection. The exterior color must be desert tan, the interior color must be white, and the fabric must be opaque (“blackout”) rather than translucent” (Clamshell Buildings, 2019). The reported typical fabric lifespans range from 15 to 25 years. Channels are designed in the aluminum rigid frame members that allow the fabric to be connected to the frames with a kedered attachment method. Inflatable chambers are present in the fabric to provide tensioning, with two in between each frame on the main framing system. The chambers are oriented in the same direction as the frames. When looking at the LAMS, it is clear to see that each fabric panel is relaxed, and not in total, uniform tension. An example of the kedered attachment of the fabric to the frames is shown in Figure 3.1-15.

Figure 3.1-14. LAMS exterior high wind kit

Figure 3.1-15. Kedered fabric attachment to the framing members.

3.2 Material Properties of LAMS Structural Elements

The material properties and section properties used in the design of the LAMS are shown in Table 3.2-1 and Table 3.2-2. “HR_AL-OUT” refers to hot-rolled aluminum material properties that are used in the design of the “BEAM” section. This section refers to the arched frame members (S50BEAM) that make up the largest portion of the structural members. “HR_AL” is the hot-rolled aluminum used to design the purlins (S50PURLIN) in the structure. “HR_CBL_STL” refers to the material properties used to design all cables in the structure. “1-4 Cable” is the section property of the ¼ inch diameter cables used for the wall and roof cables. "1-2 Cable" is the section property of the ½ inch diameter cables used for the exterior high wind kit.

Table 3.2-1. Material properties of LAMS members (Clamshell Buildings, 2019)

	Label	E [psi]	G [psi]	Nu	Density [lb/in^3]	Yield [ksi]	Fu [ksi]
1	HR_AL-OUT	1.01E+07	3.8E+06	0.33	0.2	35	58
2	HR_AL	1.01E+07	3.8E+06	0.33	0.098	35	58
3	HR_CBL_STL	4.8E+06	1.8E+06	0.3	0	36	58

Table 3.2-2. Section properties of LAMS members (Clamshell Buildings, 2019)

	Label	Shape	Material	A [in2]	Iyy [in^4]	Izz [in^4]	J [in^4]
1	BEAM	S50BEAM	HR_AL-OUT	6.944	8.37	78.559	5
2	PURLIN	S50PURLIN	HR_AL	1.039	0.987	0.987	1.975
5	1-4 Cable	1-4_CABLE	HR_CBL_STL	0.049	0.000192	0.000192	0.000383
6	1-2 Cable	1-2-CABLE	HR_CBL_STL	0.196	0.003	0.003	0.006

A Safety Factor of 1.95 was used when comparing demands to capacities, as recommended by the Aluminum Association (2005), resulting in an allowable stress of 19 ksi. The high wind cables have a breaking strength of 22,800 lbs, and the ¼-in. diameter roof and wall cables have a breaking strength of 7,000 lbs (Clamshell Buildings, 2019). The 2006 International Building Code (IBC 2006) was used for the structural evaluation. The controlling load case was the dead and wind load combination, with a design wind speed set to 90 mph with Exposure C for the wind load calculations per IBC 2006. The stresses on the in-service LAMS in the frames are bending stresses at the top and bottom of flanges, and the purlin stresses were reported as axial stress.

3.3 Model Design

To gain a better understanding of the forces, stresses, and deformations that the LAMS experience, a finite element model was developed. The model was created using SAP2000 version 21 (CSI, 2017). The model was designed to replicate the in-service LAMS with a concrete foundation. The structure was created as a 3-D structure with non-linear analysis that does not include P-delta effects. If any limits set on members in the structure were met, the non-linear analysis allowed the software to remove the member from the analysis and run the loads again. P-delta effects were not included in the analysis of this model because they would have very little effect on the responses of the model. This is because the direction of the loads and the high wind kit cables prevent large deflections in the model. Figure 3.3-1 displays the finite element model.

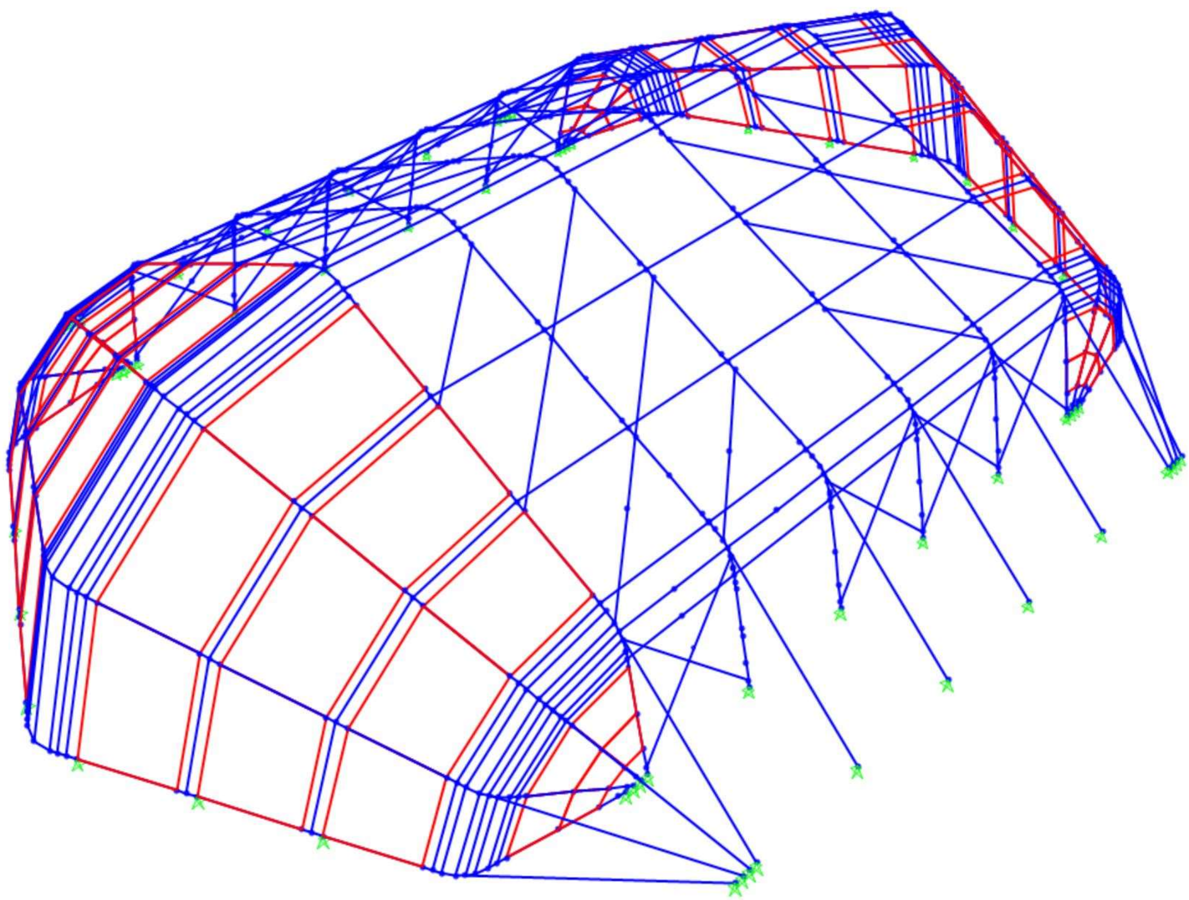

Figure 3.3-1. SAP 2000 3-D finite element model

The material and section properties used for the different members in the model primarily came from the properties listed by the manufacturer and were provided in Table 3.2-1 and Table 3.2-2.

The frame section “S50 BEAM” was used to model the arch frames in the model. These frames are the largest structural pieces in the structural system and are a critical component for resisting loads in the transverse direction. To reduce the computational complexity in the stress calculations, the exact cross-section of the S50 beams was simplified using the section designer tool in SAP2000. The round channels for the kedered fabric were slightly modified. The modified cross-section did not produce the exact correct section properties, so section modifiers were applied to the beam to correct the section properties. Modifiers were used to increase the cross-sectional area by less than one percent and decrease the moment of inertia about the y and z axis by five percent. There are 3 different types of frame members used in the design of the LAMS. There are two different curved members used for the eaves and the ridge of the roof. There are also eleven-foot straight members. There are ten splice connections and eleven frame members in each frame line. The appropriate section properties were listed in Table 3.2-2. The cross-section of the S50 BEAM is displayed in Figure 3.3-2.

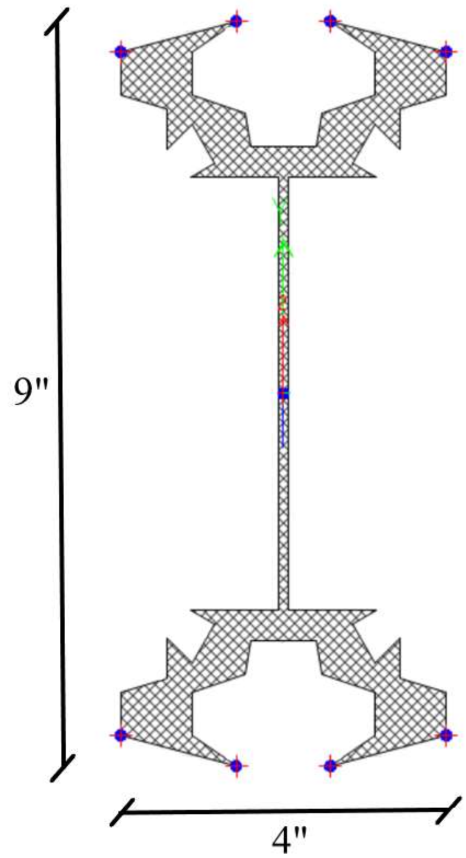

Figure 3.3-2. S50 BEAM cross-section

Purlins were modeled as an aluminum pipe. The outside diameter and wall thickness were measured to be 2.86 in and 0.12 in. The pin-to-pin purlin length was measured at 148 inches. The purlins were expected to provide lateral support for the frames and transfer loads throughout the different frame lines. The wall and roof cables were specified with a ¼-in diameter. These cables were modeled as a circular steel section with a height and width of ¼-in. The high wind kit cables were specified with a ½-in diameter. These cables were modeled as a circular steel section with a height and width of ½-in. Separate laboratory testing (outside the scope of this thesis) determined that an approximate modulus of elasticity for the cables was 15,000 ksi and the appropriate area of the ¼-in cables was 0.0339 in^2, and these values were used to define the cable material and section properties in the model. The change in the area is because the cables are not solid but made of stranded wire. These are the only properties that were changed from what the manufacturer provided. The cables provided lateral support to the frame member and assisted in minimizing deflection in the structure. The weight of the cables had very little effect on the responses on the structure, therefore they were given a density of 0 lb/in^3.

Frames were modeled at 12 feet 6 inches spacing center-to-center. This spacing was based on the provided dimensions of the structure and verified by a lidar scan of the interior of the structure. Pin supports were placed on the ends of the frames, where they are attached to the ground. The door frames were developed by replicating the end vertical frame 3 times. Each door frame was spaced at 8 inches, as verified by on-site measurements at the LAMS. The closest door frame to the end vertical frame was then rotated about the supports to give the frame an angle of 60 degrees above the ground. The second frame was rotated to 30 degrees, and the final door frame was rotated to be level with the ground. On the third door frame, pin supports were applied where there were tie-downs at the in-service LAMS that held the final door frame down to the foundation. All the support connections were modeled based on the in-service LAMS that has a concrete foundation. It should be noted that the foundation supports do vary depending on the type of foundation the LAMS is installed on.

The purlins were added to the model and the locations of the purlins were found using a lidar scan of the interior of the structure and measurements taken at the in-service LAMS. Major axis and minor axis moment releases were placed at the connections of the purlins to the arch frames to represent the pinned connections of the purlins in the structure. The purlins were designed with a tight connection to the frames that do not allow any deflection or movement in the at-rest state.

The locations of the wall cables and roof cables were determined using the lidar scan and measurements. The cables were modeled as frame elements and given a compression limit of 0 lbs to represent the tensile only cables in the shelters. Along with the compression limits, major axis and minor axis moment releases were placed at the connections of the cables to the frames. All cables were assumed to be taut but with no pre-tensioning.

The locations of the high wind kit anchors were measured at in-service LAMS to be 11.4 feet away from the frame base plates. The high wind kit cables were added for each frame line in the model. The cables are attached to the frame members at the eave of the structure, which is consistent with the product description. A compression limit of 0 lbs and major axis moment releases at each end is applied to the cables. These cables were also assumed to be taut but with no pre-tensioning. The connection to foundation was modeled after the anchor bolt connection of the in-service LAMS to the concrete foundation. Similar to the frames, it should be noted that the foundation supports do vary depending on the type of foundation the LAMS is installed on.

The fabric on the structure was slack, and therefore did not provide any structural support in the main framing system. Therefore, the fabric did not affect the load path on the main framing system of the structure and was not modeled over the vertical arches in the structure. However, for the door frames, the fabric helps hold the members in place and plays a role in the transfer of the loads. To model the fabric, both area sections and frame sections were created. Along the door frames, where the distance between the nodes was long, spanning eight feet four inches, the area fabric was applied. Where the nodes created short members, spanning one foot, frame members were used to represent the fabric. The area section used was modeled as a membrane with a thickness of 0.05 inches, matching the actual thickness of the fabric. The fabric was modeled with a modulus of elasticity of 14 ksi and Poisson’s ratio of 0.3. These values were approximated based on strip tensile tests conducted on PVC-coated polyester fabric (Fittro, 2018). The weight of the area section was taken as zero because the weight of the fabric was modeled as a dead load on the structure. Nine frame members were designed to represent the different tributary widths needed for the fabric attached to the short door frame members. The tributary widths were multiplied by the thickness (0.05 inches) of the fabric to calculate an appropriate cross-sectional area. These nine different cross-sectional areas were then attached to the door frames with the fabric material properties to correctly represent the fabric. This was done to minimize the aspect ratio of the membrane elements. These fabric frame sections were applied to the model and given a compression limit of zero. Figure 3.3-3 displays area membrane used to model the fabric in red and the frame sections used to model the membrane in blue.

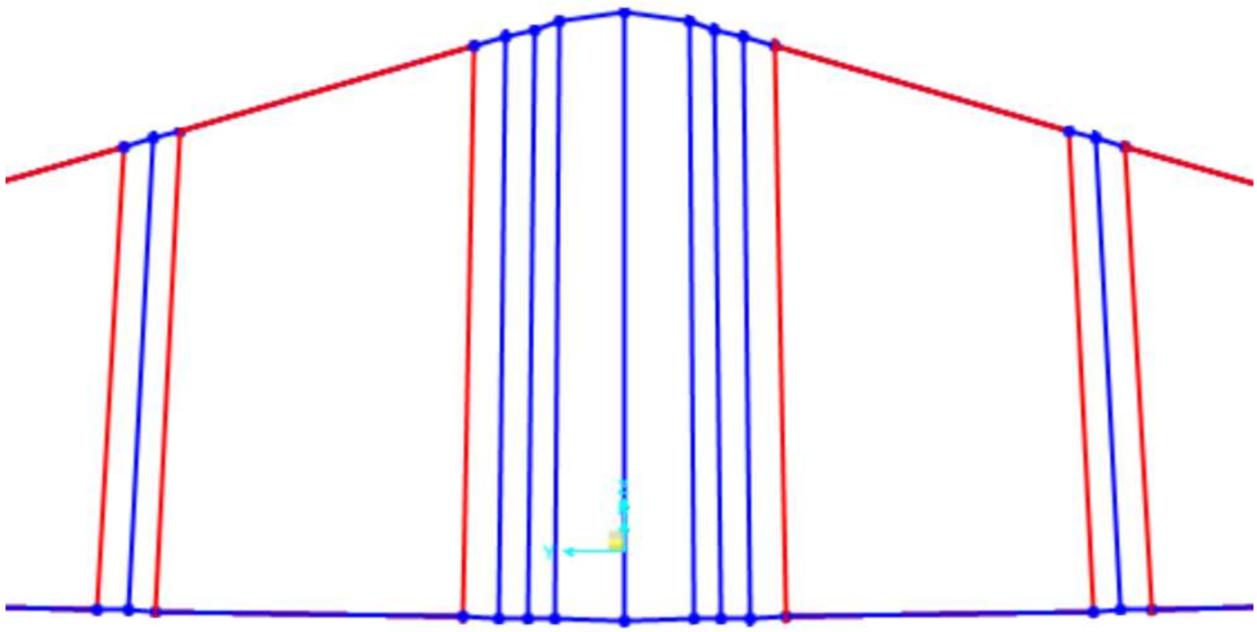

Figure 3.3-3. Connection of fabric to door frames. Blue lines represent fabric cables, while red lines represent the edges of the membrane area.

3.4 Wind Load Calculation and Application

Wind load cases for the LAMS were calculated using ASCE 7-05 (ASCE, 2005) and a design wind speed of 90 mph to match the parameters used in the original LAMS design. A total of 10 different wind conditions were used, as summarized in Table 3.4-1. Wind conditions 1-4 refer to winds that act perpendicular to the ridge (transverse orientation), and conditions 5,7,9, and 6,8,10 are wind loads acting parallel to the ridge (longitudinal orientation). Wind loads are identical for conditions 5,7,9 and identical for 6,8,10.

Load conditions 1 and 3 both have a positive internal pressure, and the only difference is a negative windward roof pressure on load condition 1 and a positive windward roof pressure on load condition 3. Load conditions 2 and 4 have the same conditions, except with negative internal pressure. Wind condition 5,7,9 has a positive internal pressure and a negative windward roof pressure while wind condition 6,8,10 has both negative internal pressure and windward roof pressure. This is summarized in Table 3.4-1.

Table 3.4-1. Summary of wind load conditions applied to the model

Wind Load Condition	Orientation	Internal Pressure	Windward Roof Pressure
1	Transverse	(+)	(-)
2	Transverse	(-)	(-)
3	Transverse	(+)	(+)
4	Transverse	(-)	(+)
5,7,9	Longitudinal	(+)	(-)
6,8,10	Longitudinal	(-)	(-)

For the wind load conditions, negative values represent pressures acting away from the structure, and positive values represent pressures acting inward on the structure. For conditions 1-4, the door frames were treated with the same loads as the windward and leeward walls and roofs. The windward and leeward wall and roof pressures were applied to the door frames, and no sidewall pressures were applied. For wind conditions 5,7,9 and 6,8,10 with the wind acting parallel to the ridge, the roofs of the door frames were treated as the windward and leeward walls. The sides of the door frames for all vertical frames were treated as sidewalls. For each condition, the wind pressures were multiplied by the tributary width of each frame and applied to the frame members as distributed loads. The wind loads were applied in the local 2 axis so that the load acted perpendicular to the frame angles. For loads applied to the frames attached to the door frames, the angle of the load was different than the angle of the frame. These loads were separated into two different vectors based on the angles. The orientations of the finite element load locations are shown in Figure 3.4-1. Figure 3.4-2 and Figure 3.4-3 show what type of load is being applied to which frame members for loads 1-4 and 5,7,9-6,8,10 respectively. Table 3.4-2 provides the wind load pressures for each wind load condition.

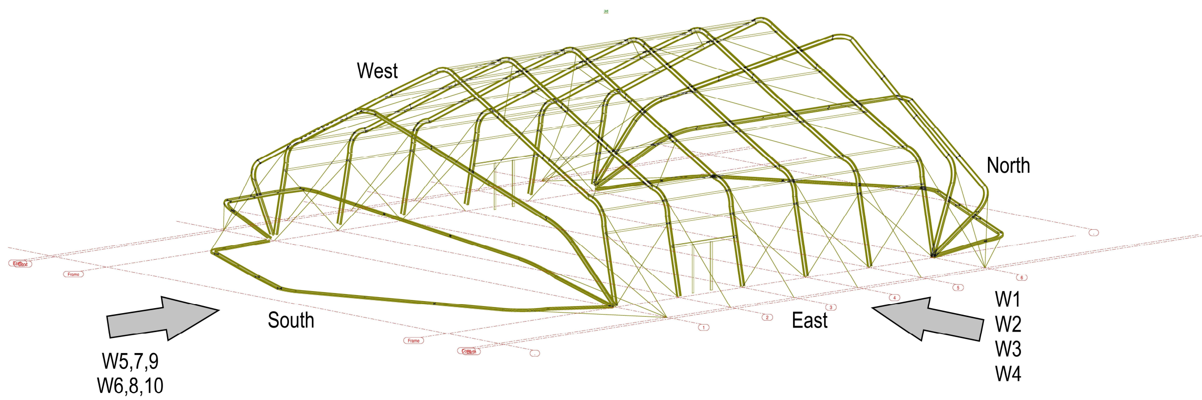

Figure 3.4-1. Finite element wind load directions

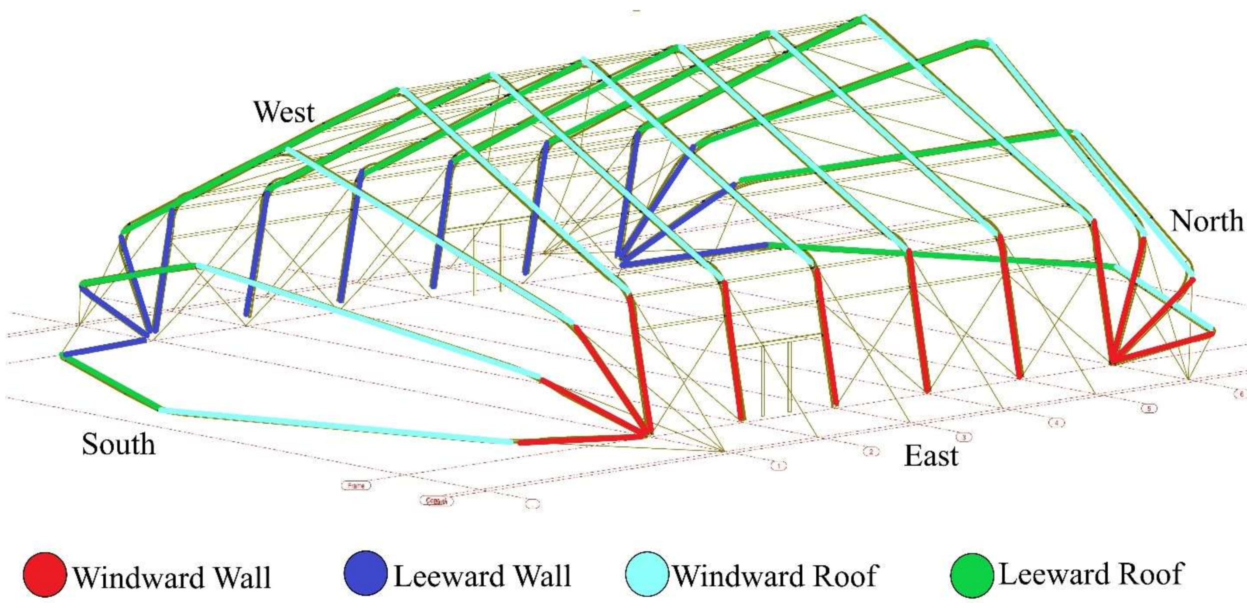

Figure 3.4-2. W4 load case frame loads

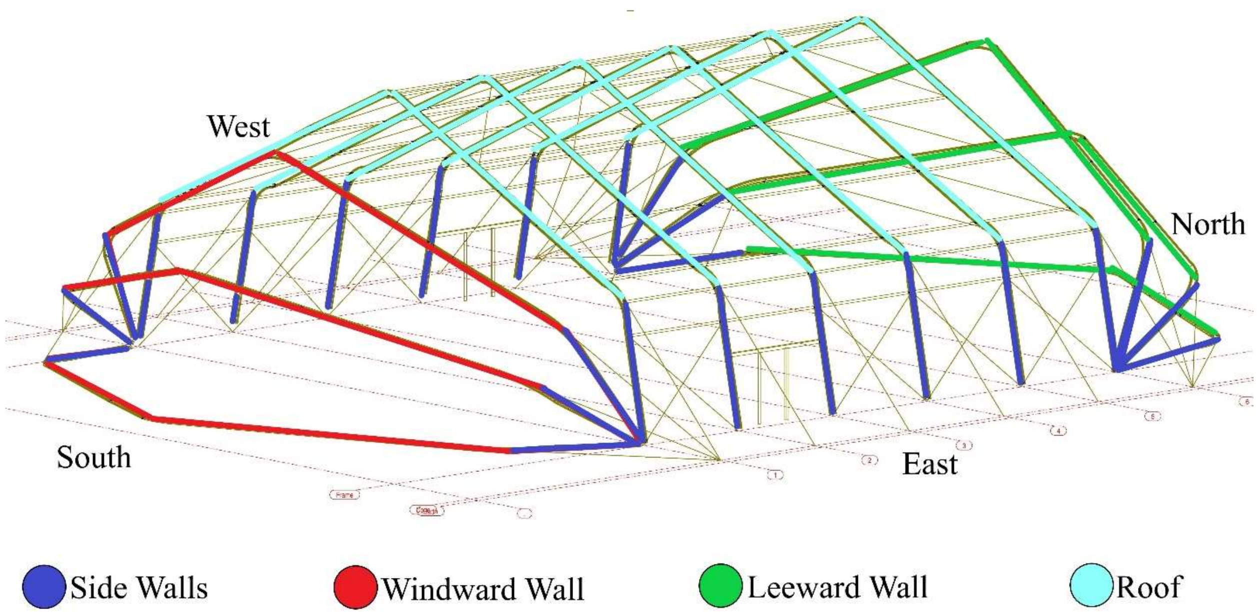

Figure 3.4-3. W5,7,9 load case frame loads

The loads applied to the model were all based on a 90-mph wind speed. To facilitate comparisons against the demands measured during the LAMS in-situ monitoring (which were typically obtained at wind speeds less than 40 mph), a separate load case was tested for a wind speed of 35 mph. Comparing the stresses, forces, and reactions for the 35 mph and 90 mph wind speed cases (without dead load applied) confirmed a linear response of the LAMS, despite the model being constructed to account for nonlinear effects. Thus, it is appropriate to take demands measured at one wind speed and scale them to different wind speeds using the squared ratio of the wind speeds as the scale factor.

For the wind calculations, K_d, K_z, K_h, G, I_w, K_{zt}, and GC_{pi}, were taken as 0.85, 0.85, 0.92, 0.85, 1, 1, and ±0.18 respectively. With these values, q_z and q_h were calculated using Equations (1) and (2). The directionality factor (K_d) was only used for the maximum demand calculations and not for the comparisons of the responses of the in-service LAMS to the model outputs, therefore, it was not used in the calculations of Equations (1) and (2). The wind pressures were then calculated using Equation (3).

$$q_z = 0.00256 K_d K_z K_{zt} I_w V^2 \quad (1)$$

$$q_h = 0.00256 K_d K_h K_{zt} I_w V^2 \quad (2)$$

$$p = qGC_p - q_i(GC_{pi}) \quad (3)$$

Where q_z/q_h is the velocity pressure, K_z/K_h is the velocity pressure exposure coefficient, K_{zt} is the topographic factor, V is the basic wind speed, G is the gust-effect factor (a rigid building is assumed), C_p is the external pressure coefficient, and GC_{pi} is the internal pressure coefficient. External pressure coefficients were determined using the all-heights method for Main Wind Force Resisting Systems (MWFRS) from ASCE 7 (ASCE 7, 2005).

Table 3.4-2. Pressures applied to the LAMS model for each wind load condition. (CP = pressure coefficient, P = wind pressure, WW = windward wall, WR = windward roof, LR = leeward roof, LW = leeward wall, SW = side wall, and h = mean roof height)

Calculated Wind Conditions				
	Condition 1		Condition 2	
	CP	P (psf)	CP	P (psf)
WW	0.8	8.55	0.8	15.42
WR	-0.22	-7.00	-0.22	-0.13
LR	-0.6	-13.16	-0.6	-6.30
LW	-0.5	-11.54	-0.5	-4.67
SW	-0.7	-14.78	-0.7	-7.92
	Condition 3		Condition 4	
	CP	P (psf)	CP	P (psf)
WW	0.8	8.55	0.8	15.42
WR	0.28	1.11	0.28	7.97
LR	-0.6	-13.16	-0.6	-6.30
LW	-0.5	-11.54	-0.5	-4.67
SW	-0.7	-14.78	-0.7	-7.92
	Condition 5/7/9		Condition 6/8/10	
	CP	P (psf)	CP	P (psf)
WW	0.8	9.54	0.8	16.41
WR 0<x<h	-0.9	-18.03	-0.9	-11.16
h<x<2h	-0.5	-11.54	-0.5	-4.67
x>2h	-0.3	-8.30	-0.3	-1.43
LW	-0.36	-9.27	-0.36	-2.40
SW	-0.7	-14.78	-0.7	-7.92

3.5 Chapter Summary

The details of the LAMS researched were presented in this chapter to provide a better understanding of the shelter and how the structure is designed and connected. The material properties and section properties were then listed for the structural elements in the shelter. A SAP2000 finite element model was created to model the LAMS. The different section properties along with the shape of the structure were modeled based on available drawings as well as field measurements and a lidar scanner. ASCE 7-05 was used to determine the wind loads to be applied to the model, assuming a rigid structure and using MWFRS provisions. The wind pressures were multiplied by the tributary widths of each arch frame and applied directly to the frames based on the different wind conditions and the locations of the structural elements.

Chapter 4 Finite Element Model Verification

This chapter includes the model verification that was performed using two methods. The first method used was a load path analysis study that focused on the distribution of loads when the wind is directed parallel and perpendicular to the ridge of the building. This load path is based on the purlins and roof cables acting as a truss system to carry the loads into the wall cable bracing. The second step in the model verification is the comparison of the preliminary demands measured on the instrumented LAMS to the finite element model in the transverse and longitudinal directions.

4.1 Load Path Analysis Study

The two primary load paths that are analyzed in this study are wind loads acting transverse and longitudinal to the length of the structure. A load path analysis was conducted on the main framing system of the structure to verify that simple loads are logically transferred through the structure. The primary focus of this analysis is to verify the transfer of loads through the purlins and cables.

The finite element model was adjusted for the load path analysis study. In an at-rest state, the weight of the doors puts the fabric in tension. The tensile forces are then transferred to the end vertical frames and throughout the main framing system. Because the focus of this study was on how load points are transferred through the system, the door frames were not included in the model to allow the main framing system to have no forces or stresses on them in the at-rest state. A series of different transverse and longitudinal loads were applied to the model for this analysis. A visual representation of where the loads were applied is shown in Figure 4.1-1. The exterior high wind kit is still attached in the model although it is not shown in Figure 4.1-1. Fourteen different tests were conducted with point loads at different locations acting in different directions and different placements on the structure. Table 4.1-1 presents this information.

Table 4.1-1. Load path analysis test locations

test	Load	Direction	Load Location	Frame Line
1	1 kip	-X	Ridge	1
2	1 kip	-Z	Ridge	1
3	1 kip	+Z	Ridge	1
4	1 kip	-X	Eave	1
5	1 kip	-Z	Eave	1
6	1 kip	+Z	Eave	1
7	1 kip	-Y	Ridge	1
8	1 kip	-Y	Eave	1
9	1 kip	-X	Ridge	2
10	1 kip	-X	Ridge	3
11	2 kips	-X	Roof Slope Midpoint and Ridge	1
12	2 kips	-X	Roof Slope Midpoint and Ridge	2
13	2 kips	-X	Roof Slope Midpoint and Ridge	3
14	2 kips	-X	Ridge	1 and 2
15	1 kip	+Y	Ridge	Center of the System

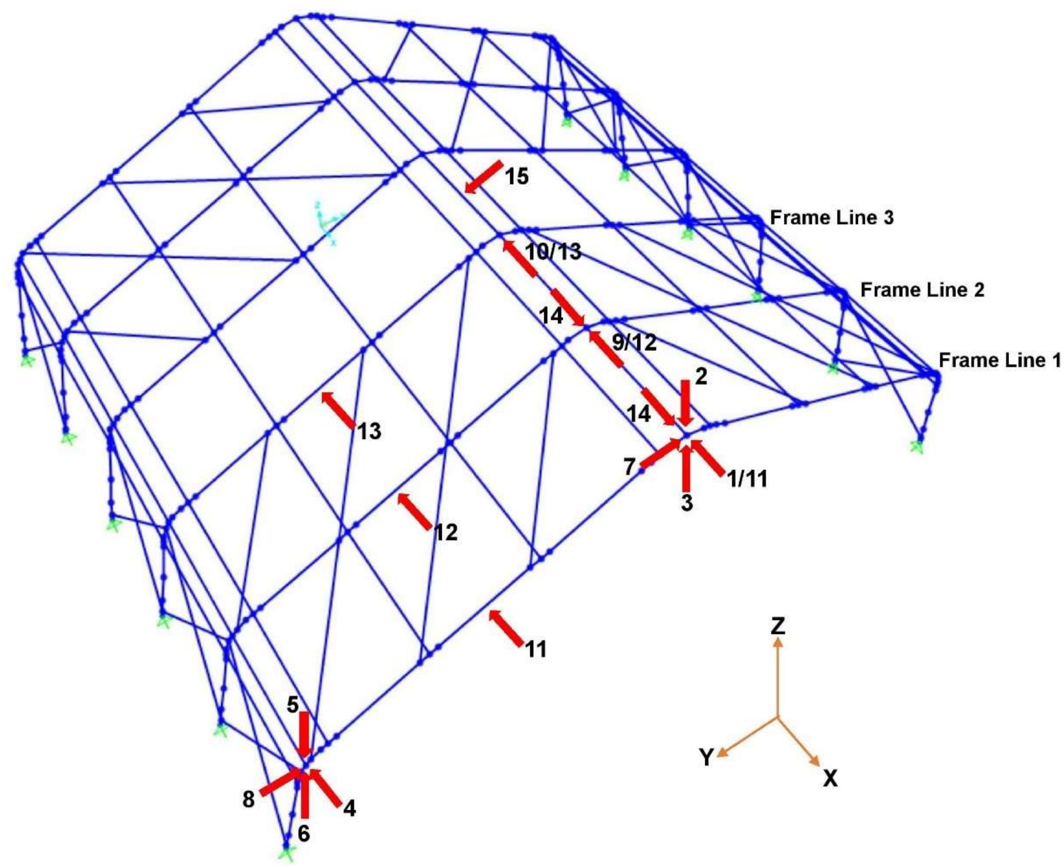

Figure 4.1-1. Load locations for tests 1-14.

A plan view of the roof was combined with a side view of the sidewalls to create a 2D visualization of the model. The axial forces are displayed next to each element. The coordinate system and direction of the load are shown at the top of each figure. The load placement and values are shown in the figures as well. The exterior high wind cables were present in each test, but are not depicted in the visualizations.

Figure 4.1-2 shows the member forces for test 1. Most of the load for test 1 was transferred through the ridge. As the load was transferred through the ridge, some of the force was shifted to the roof cables on the side of the model closest to the load. These tensile forces caused the purlins and frames attached to them to experience the compressive forces shown. Due to the placement and the direction of the roof cables on the right side, they experienced no tensile forces. As expected, the forces were symmetric on the roof with respect to the ridge. Two personnel doors are on either side of the shelter, causing asymmetry in the sidewalls. Due to the asymmetry of the sidewalls, the forces were not equivalent on the walls or the eaves. These slight differences were expected. Each column experienced a compressive force into the supports. The far-left columns experienced this force due to the angle of the wall frame and the location of the exterior cables. The tensile forces in the frames at the eave were transferred into the exterior cables. The exterior high wind kit cables experienced a tensile axial force of 623 lbs which produced a compressive force in the columns.

Figure 4.1-3 shows the analysis results for test 2. With the load for test 2 acting downward on the model, most of the load was transferred through the frame where the load was applied. As anticipated, tensile forces acted along the ridge, and on all the roof cables. These forces were due to the frame displacing outward from the ridge in the positive and negative y-direction along the frame. The displacement introduced tensile forces in the roof cables attached to the first frame. This caused the purlins and frames around the cables to experience compressive forces. Due to the load being placed in the negative z-direction, the wall cables experienced negligible forces. Based on the location of the load, the predicted load path was symmetric on each side of the ridge.

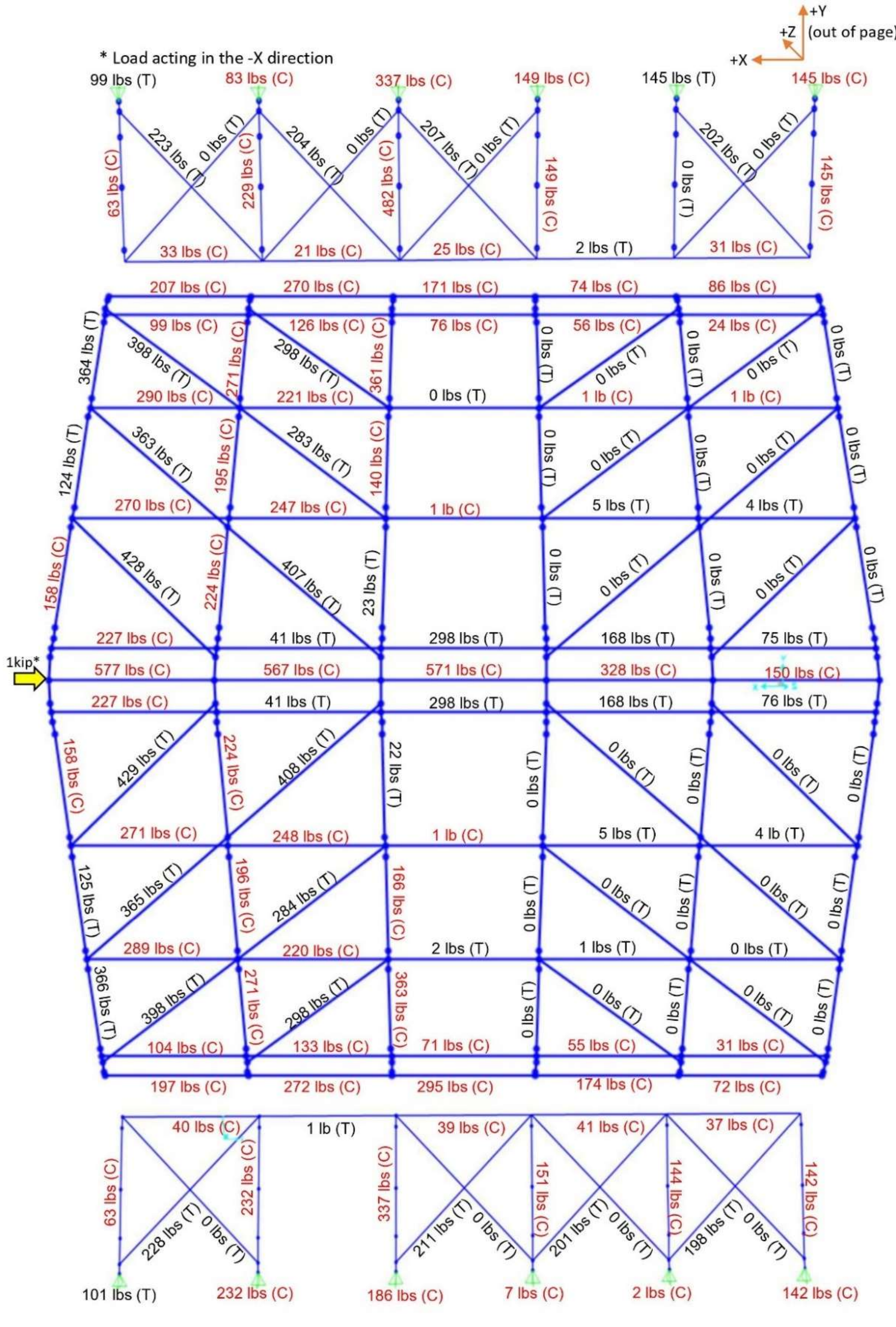

Figure 4.1-2. Test 1 element axial force analysis results

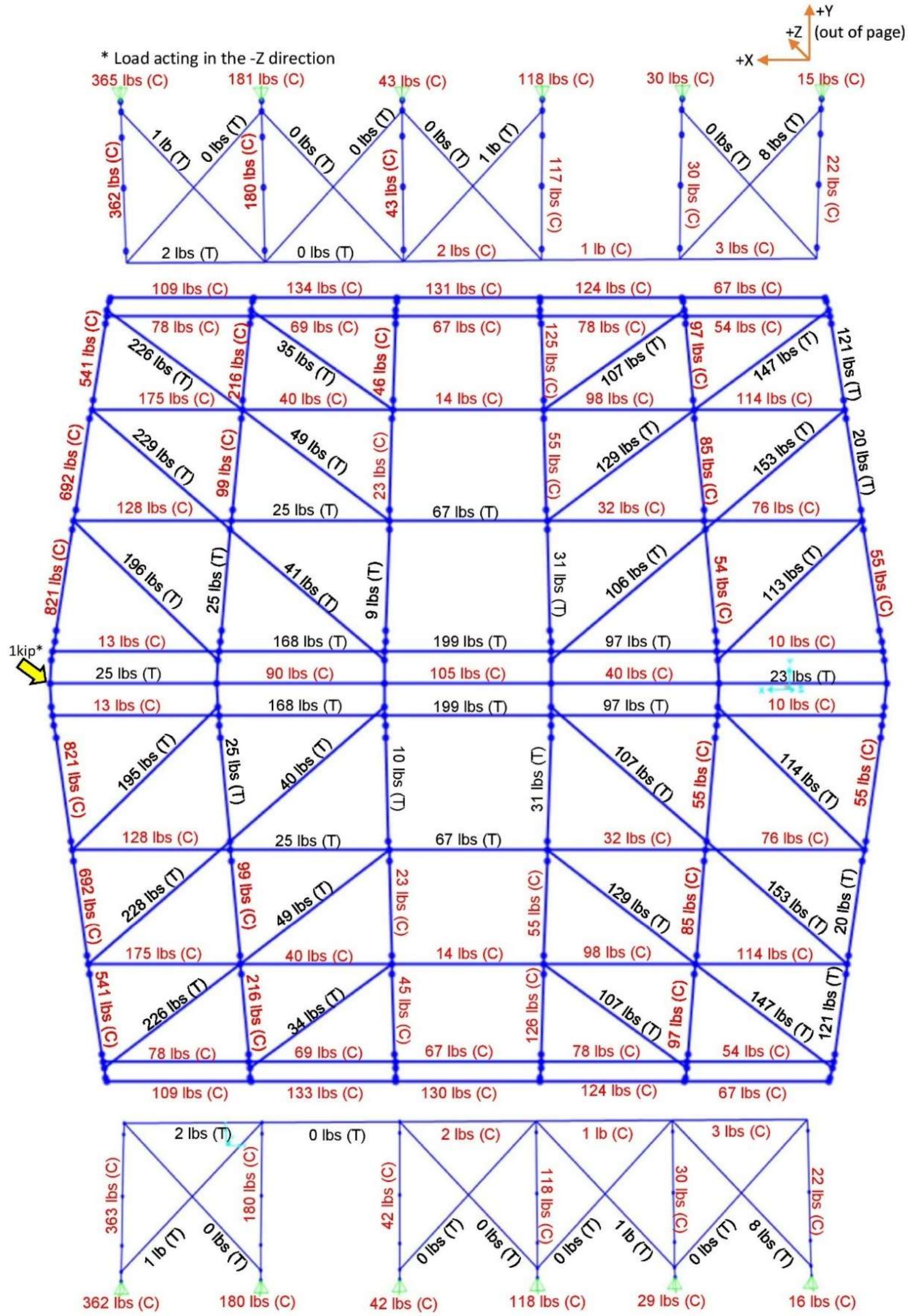

Figure 4.1-3. Test 2 element axial force analysis results

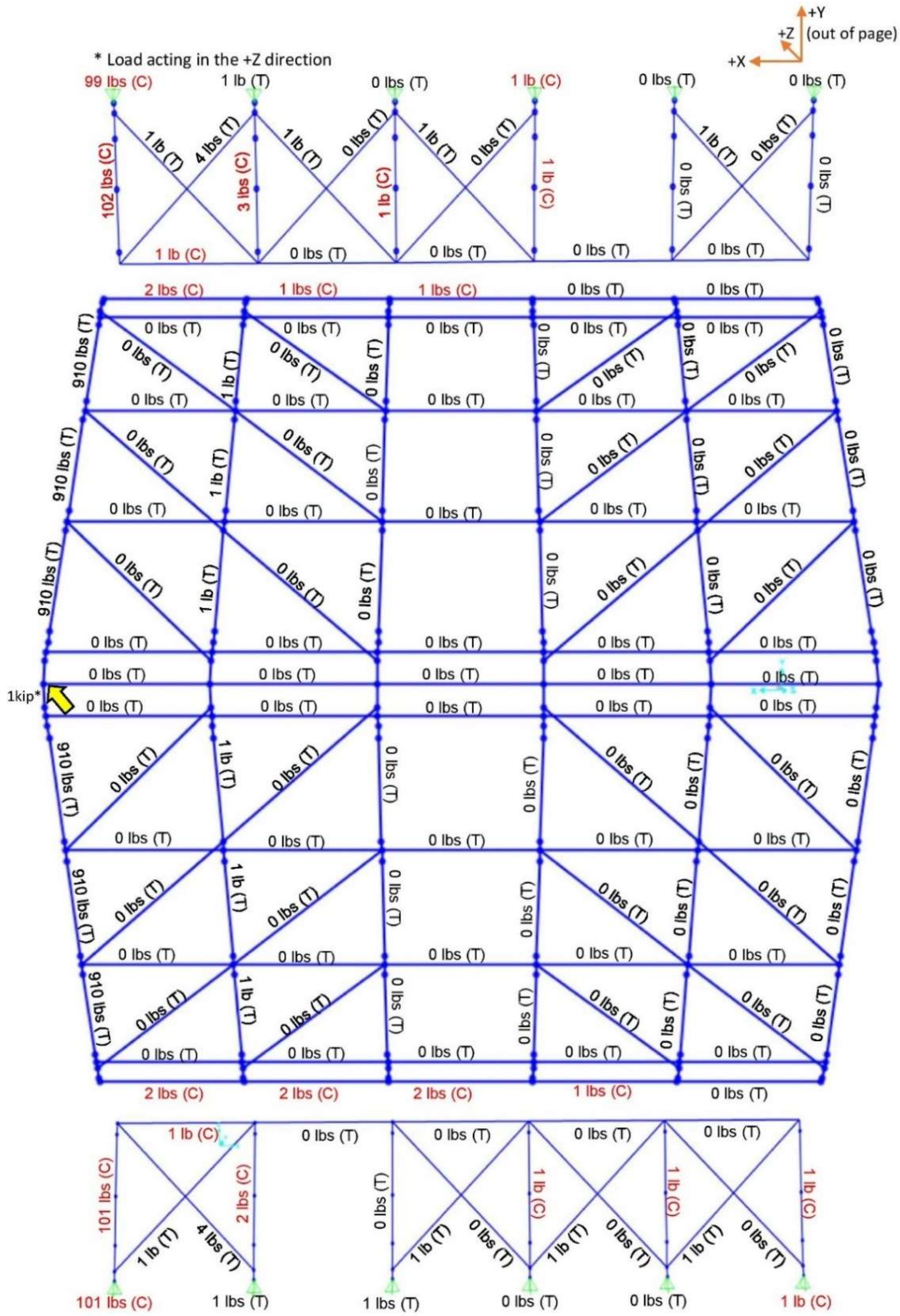

Figure 4.1-4 shows the analysis results for test 3.

The load for test 3 was in the same location as test 2 but acting in the positive z-direction. Like test 2, approximately all the load was transferred through the first frame. The upwards force produced negligible forces throughout the entire structure besides the first frame. Unlike test 2, the first frame displaced inward from the ridge in the positive and negative y-direction. With the geometry of the cables, they did not experience any tensile forces under these types of displacement. Therefore, no loads being transferred throughout the main framing system were seen. When the load reached the eave, the tensile force of 910 lbs was transferred to the exterior cable. Due to the geometry of the wall and column, this produced a compressive force in that first column. Based on the placement of the load, as expected, the load path was symmetric on each side of the ridge throughout the structure.

Figure 4.1-5 shows the analysis results for test 4. Test 4 consisted of a load on the eave of the roof in the negative x-direction. The majority of the load was transferred through the eave, down into the wall bracing. This created large compressive forces in the columns along the same path as the load. No tensile forces acted on the interior roof cables on the top left side of the model due to the direction of the cables. However, tensile loads were experienced by the interior cables on the top right and bottom left sides of the ridge. This produced compression forces in the members attached to those cables. As expected, much smaller loads existed on the wall opposite of the load.

Figure 4.1-6 shows the analysis results for test 5. The load for test 5 was in the same location as test 4, only acting in the negative z-direction. The first thing that stuck out was a compressive force larger than the load acting on the column where the load is placed. This was due to the angle of the wall frame. A tensile force of 300 lbs was experienced in the exterior cable, which added a compressive force to the column. Small forces were acted on the model, except where the load was placed, which produced confidence in the framing system. The tensile forces on the interior cables were larger on the opposite side of the ridge due to the displacement that wants to occur on the roof.

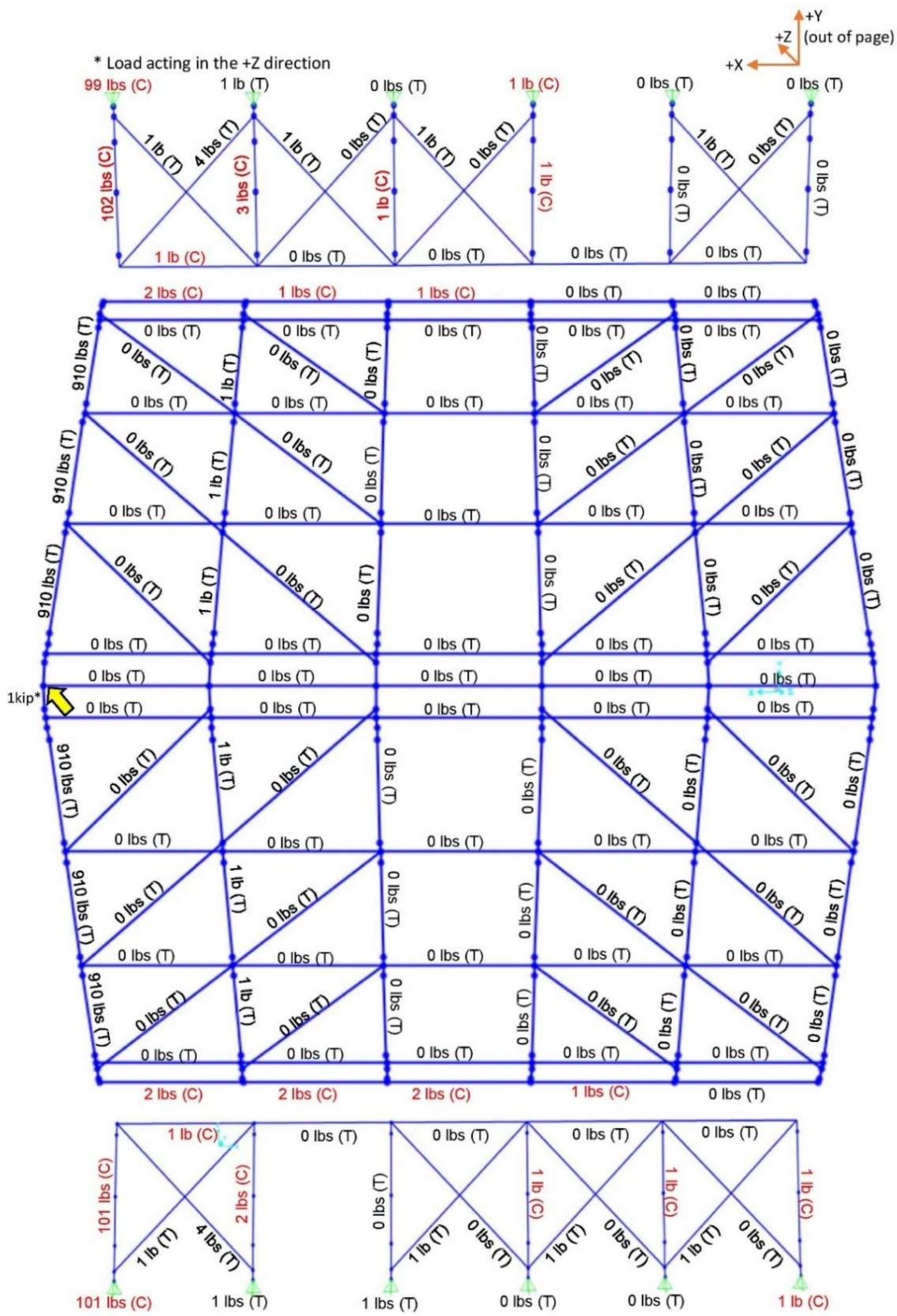

Figure 4.1-4. Test 3 element axial force analysis results

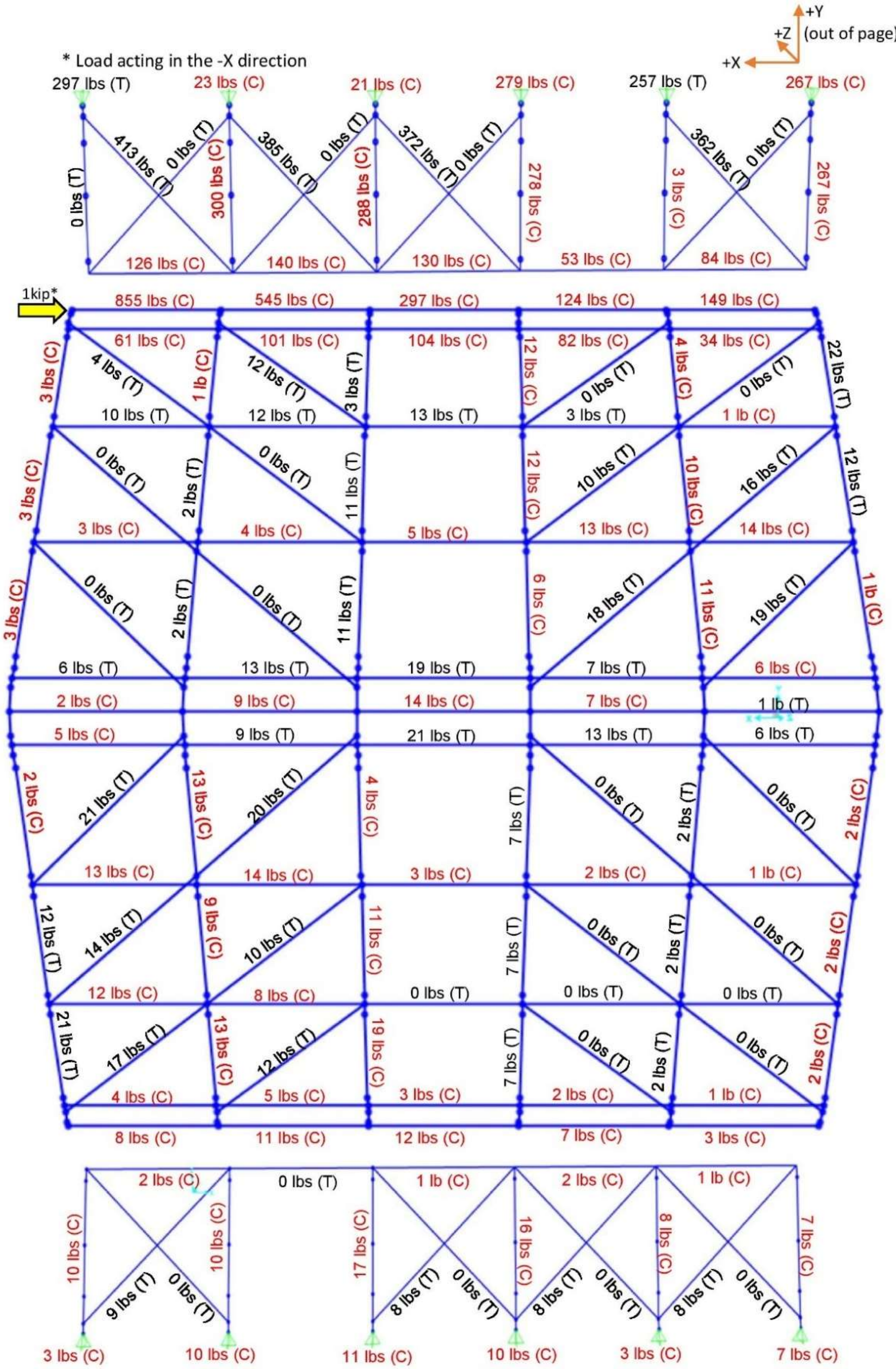

Figure 4.1-5. Test 4 element axial force analysis results

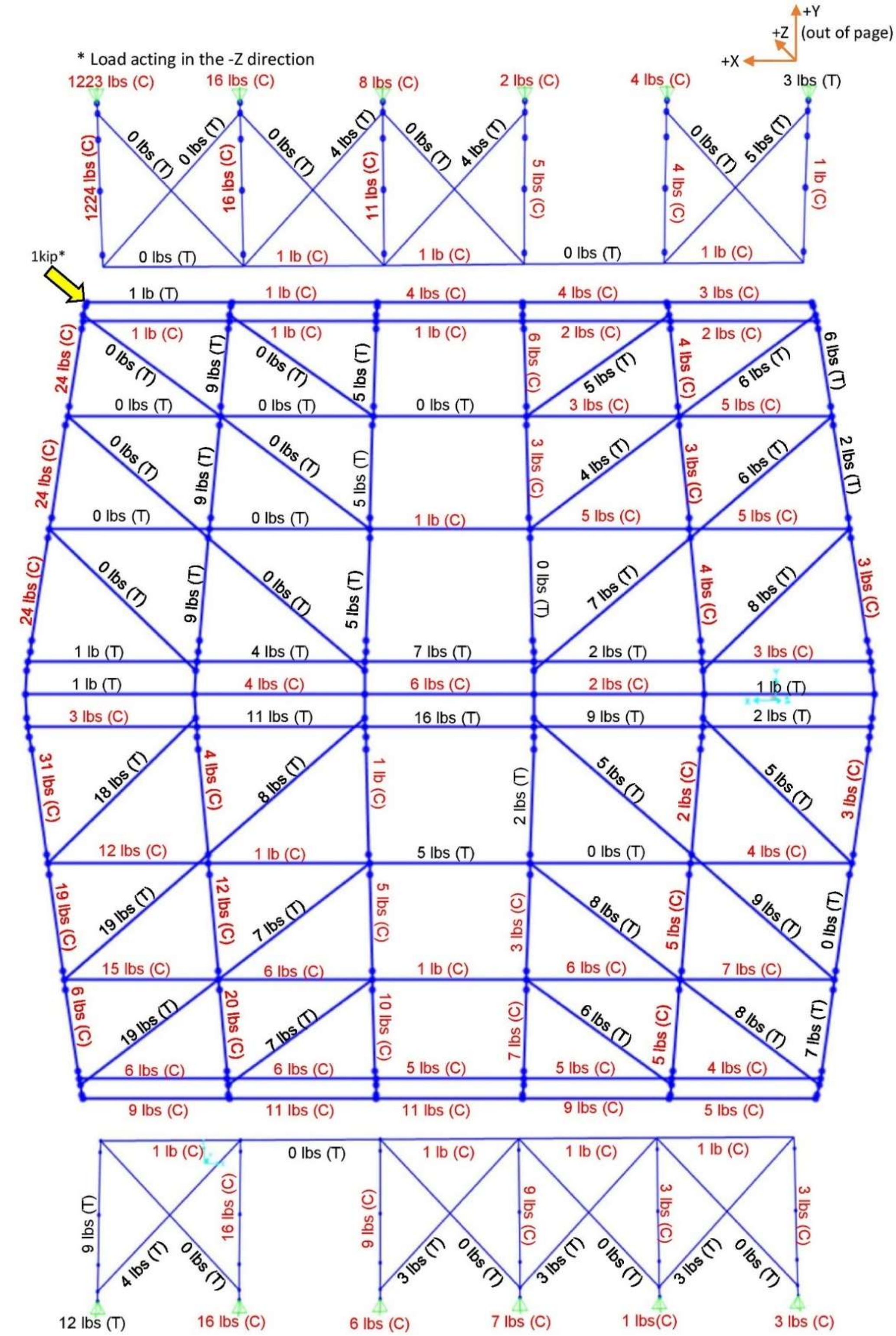

Figure 4.1-6. Test 5 element axial force analysis results

Figure 4.1-7 shows the member forces for test 6. Test 6 was the same as test 5, except the load was in the positive z-direction. As anticipated, there was a large tensile force on the top left column. The load produced a tensile force throughout the first frame. Tensile force reactions also occurred in the roof cables which resulted in compressive forces in the frames and purlins. There were small tensile forces in the wall cables and compressive forces in the columns, which are similar on either side of the ridge.

Figure 4.1-8 shows the analysis results for test 7. Test 7 consisted of a point load on the ridge of the far-left frame in the negative y-direction. Large compressive forces in the frame occurred below the ridge and tensile forces above the ridge, which was anticipated due to the load direction. The frames in compression caused the interior cables connected to them to experience tensile forces. The top left column was again experiencing compression due to the 835 lbs tensile force being transferred into the exterior cable which caused a compressive force to occur. The tensile forces along the ridge were due to the opposing forces in the roof cables.

Figure 4.1-9 shows the member forces for test 8. Test 8 had the same load direction as test 7, with the load applied to the eave. The exterior cable attached to where the load was placed experienced 1319 lbs in tension, which created a large compressive force on the top left column. The compressive force from the load was transferred through the far-left frame. Due to their direction, the top left roof cables did not experience any tension while the bottom left cables experienced the highest tensile forces. At the bottom left column, the tensile force of the roof cable was larger than the compressive force moving through the frame, therefore the column experienced a tensile force. Again, the tensile forces in the ridge were due to the opposing forces of the interior cables.

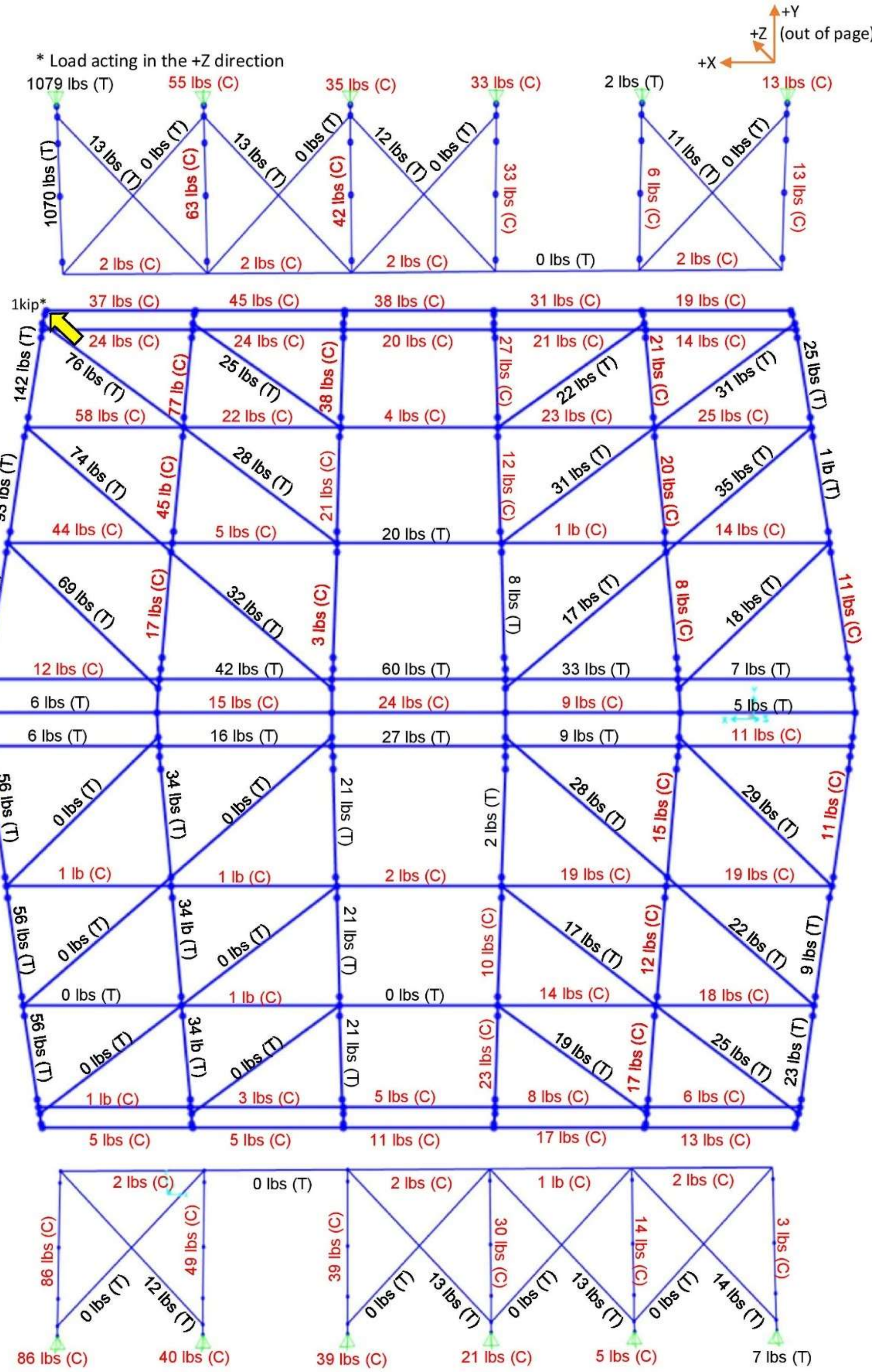

Figure 4.1-7. Test 6 element axial force analysis results

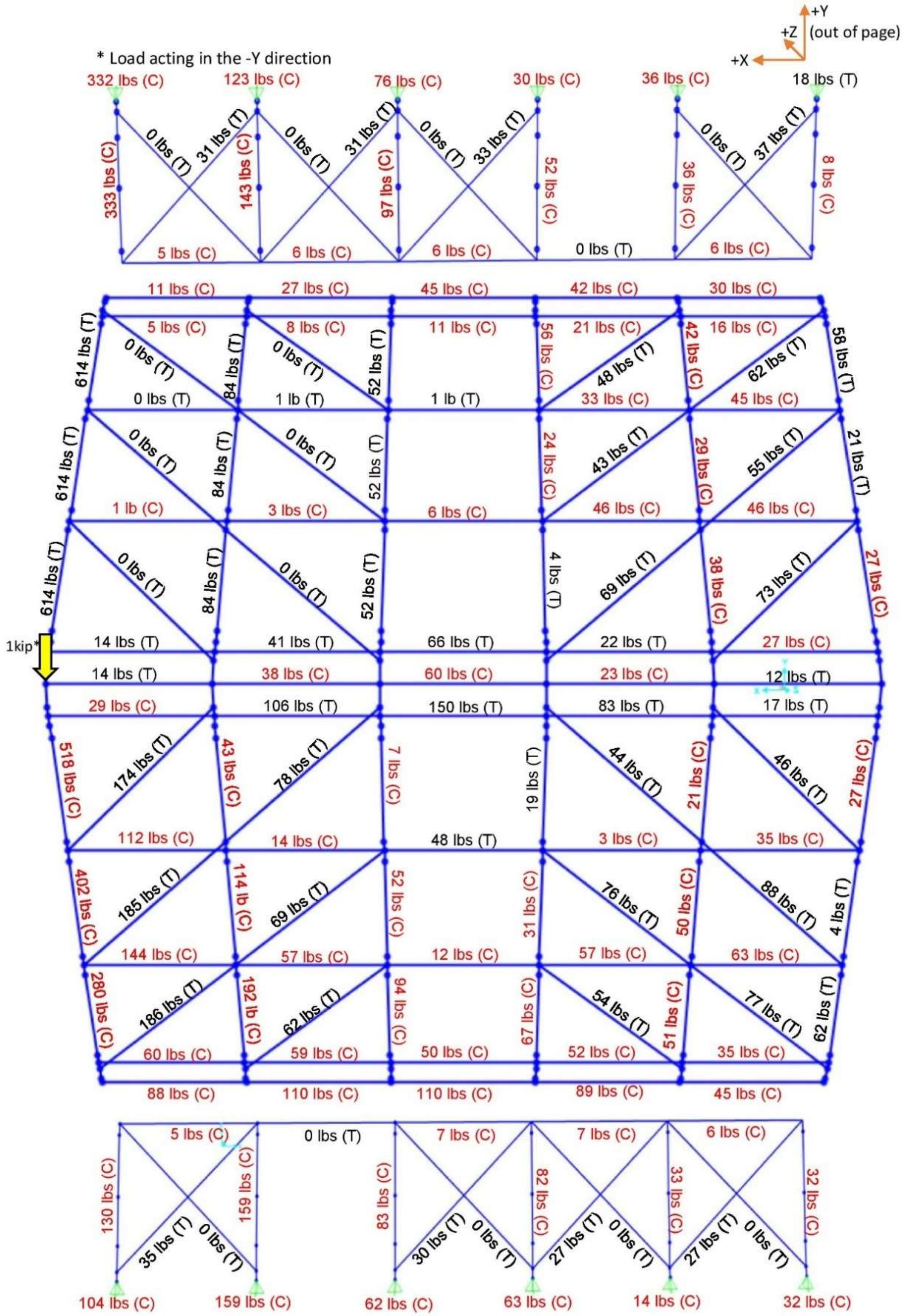

Figure 4.1-8. Test 7 element axial force analysis results

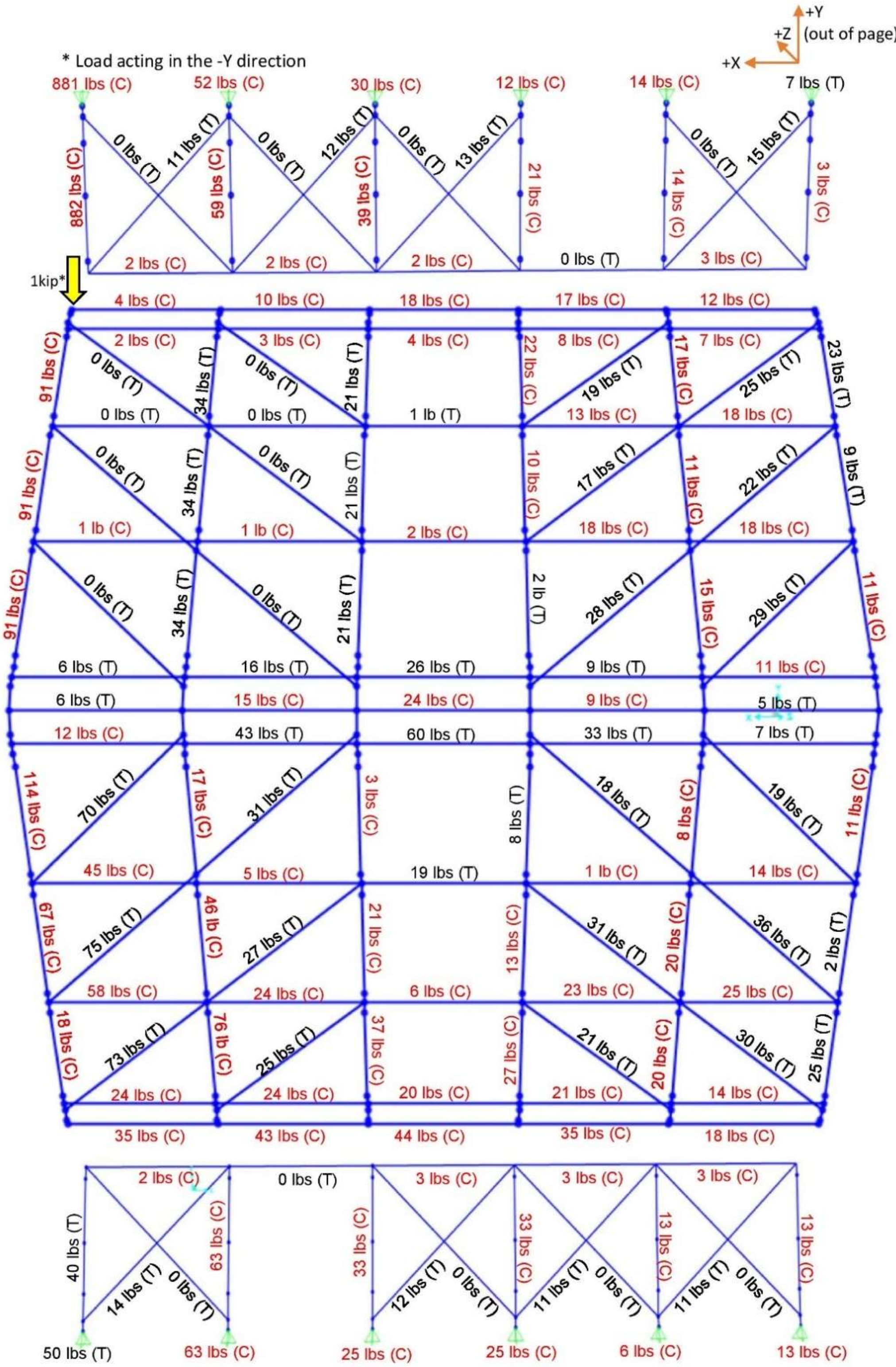

Figure 4.1-9. Test 8 element axial force analysis results

Figure 4.1-10 shows the analysis results for test 9. A load was placed at the ridge on the second frame from the left in the negative x-direction for test 9. A tensile force on the purlin to the left of the load and compressive forces through the ridge on the right side of the load was anticipated. The high tensile forces on the roof cables on the left of the model and no forces on the cables to the right are understandable due to their placement. Based on the load, the tensile and compressive forces experienced on each frame member is logical. The load direction creates high tensile forces in the wall cables, as expected. The symmetric load path on each side of the ridge is reassuring due to the location of the load.

Figure 4.1-11 shows the member forces for test 10. Test 10 is similar to test 9 in the direction of the load and the placement on the ridge, however, the load was placed on the third frame. This test showed similar results to test 9, as predicted. The tensile forces in the roof cables on the left side are reasonable, and the symmetry of the load path on either side of the ridge is accurate. It is also interesting to note that the wall brace forces were basically identical for cases 9 and 10.

Figure 4.1-12 shows the analysis results for test 11. Test 11 consisted of two points loads on the first frame. One load on the ridge and another at the midpoint between the ridge and the eave. The large tensile values on the roof cables on the left side of the model are understandable and contribute to the large compressive forces in the adjacent frames and purlins. The ridge and eaves experienced large compressive forces. The wall cables experienced high tensile values and each column experiences compression.

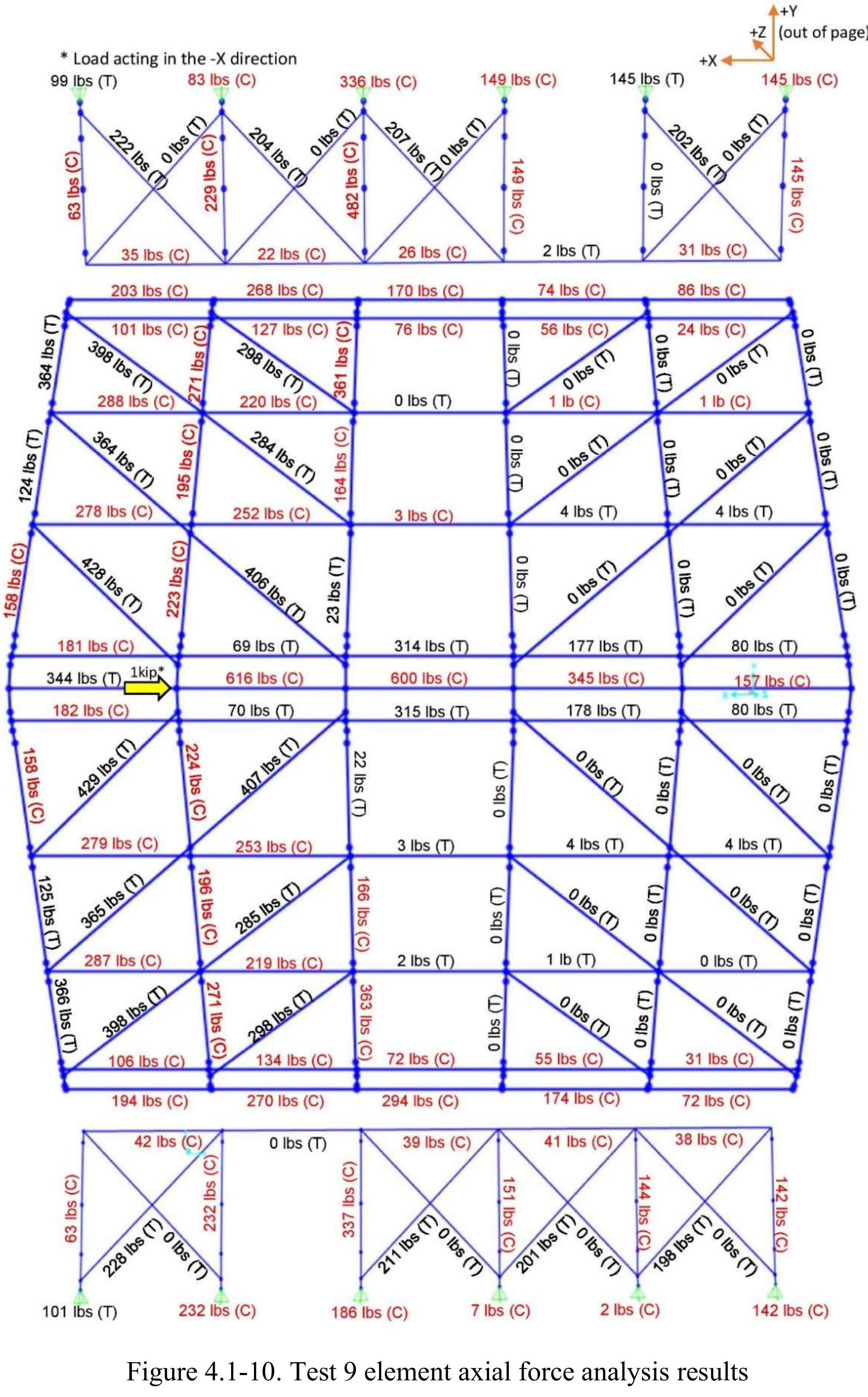

Figure 4.1-10. Test 9 element axial force analysis results

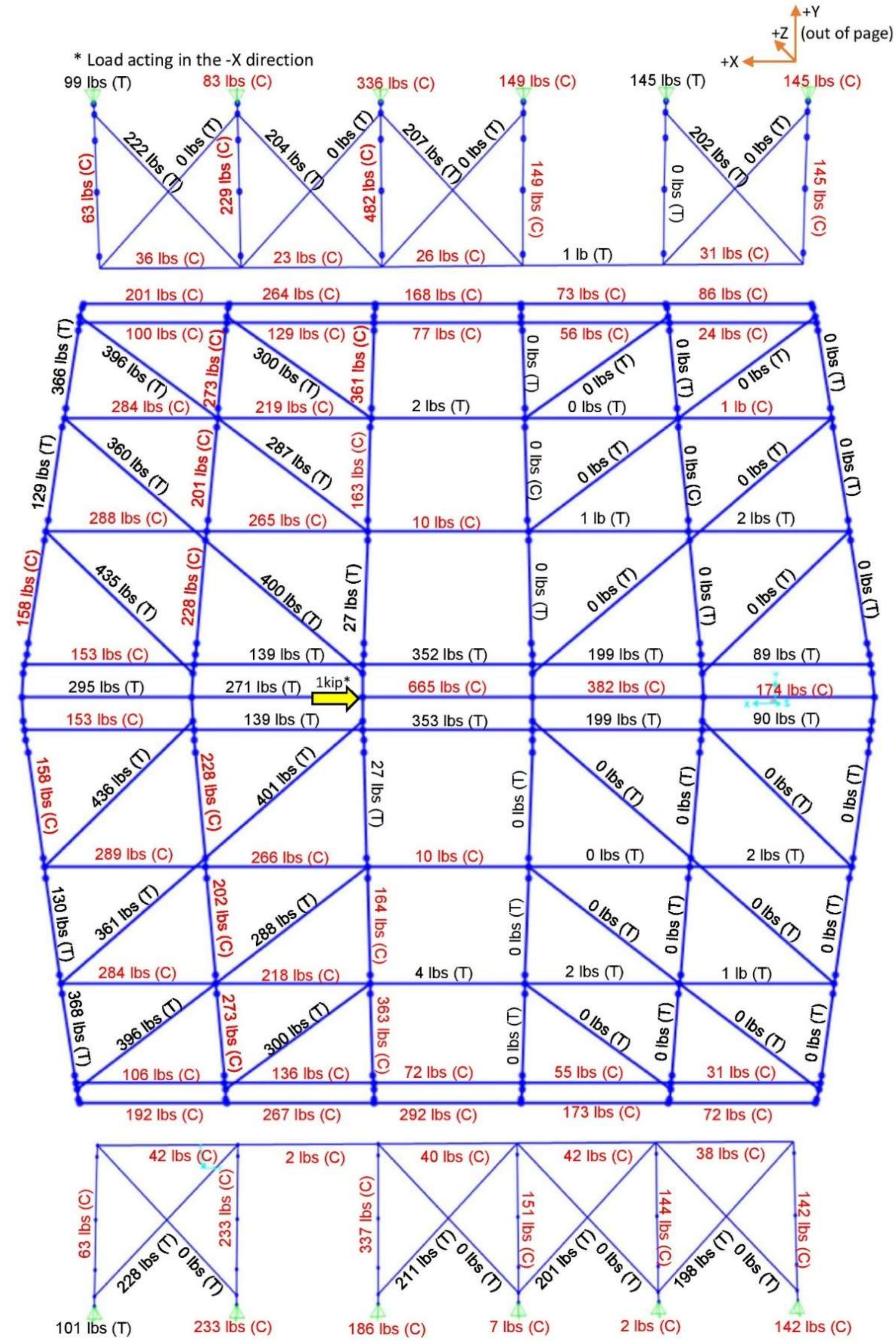

Figure 4.1-11. Test 10 element axial force analysis results

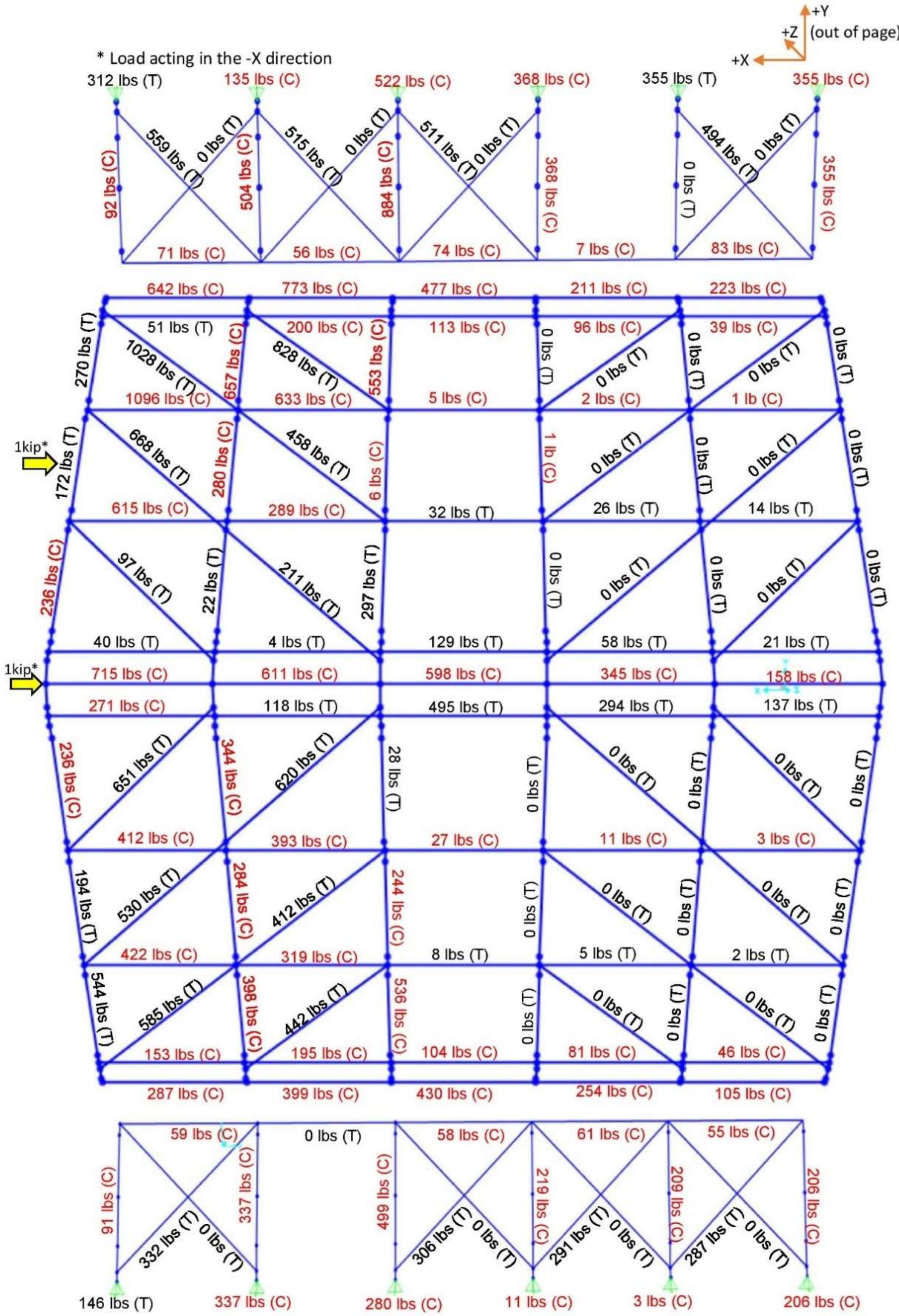

Figure 4.1-12. Test 11 element axial force analysis results

Figure 4.1-13 shows the analysis results for test 12. The only difference between tests 11 and 12 is the loads in test 12 were placed on the second frame from the left. A similar load path was seen as from the previous test, which was the expectation. The interior cables experienced a larger tensile force on the bottom side of the ridge because the load at the midpoint added some compression to the purlins which reduced the forces in the top interior cables. The wall cables experienced large tensile forces, and all columns were in compression. The frames and cables on the right side experienced negligible forces. The wall cable forces in cases 11 and 12 are again similar.

Figure 4.1-14 shows the member forces for test 13. Test 13 was the same as 11 and 12, but with the load on the third frame from the left. Again, the load path was similar to the previous two tests. One interesting observation is the wall cables experienced the same loads for each of these three tests. The ridge experienced compression on the right of the load and tension on the left. The roof cables on the left had large tensile forces and the ones on the right experienced no force. The frames on the right-side experienced negligible forces and each column were in compression.

Figure 4.1-15 shows the analysis results for test 14. Test 14 consisted of two-point loads, one each on the first and second frames along the ridge in the positive x-direction. Large tensile forces were felt along the ridge of the roof. The roof cables on the left side of the model experienced no forces, but large tensile forces were in the cables on the right side. The frames with the loads on them experienced no forces because the load was carried through the ridge to the right-side of the model, where the cables transferred the loads to the purlins and frames connected to them. The load path is symmetric on either side of the ridge due to the location of the loads. The wall cables experienced large tensile forces, and each column was in compression.

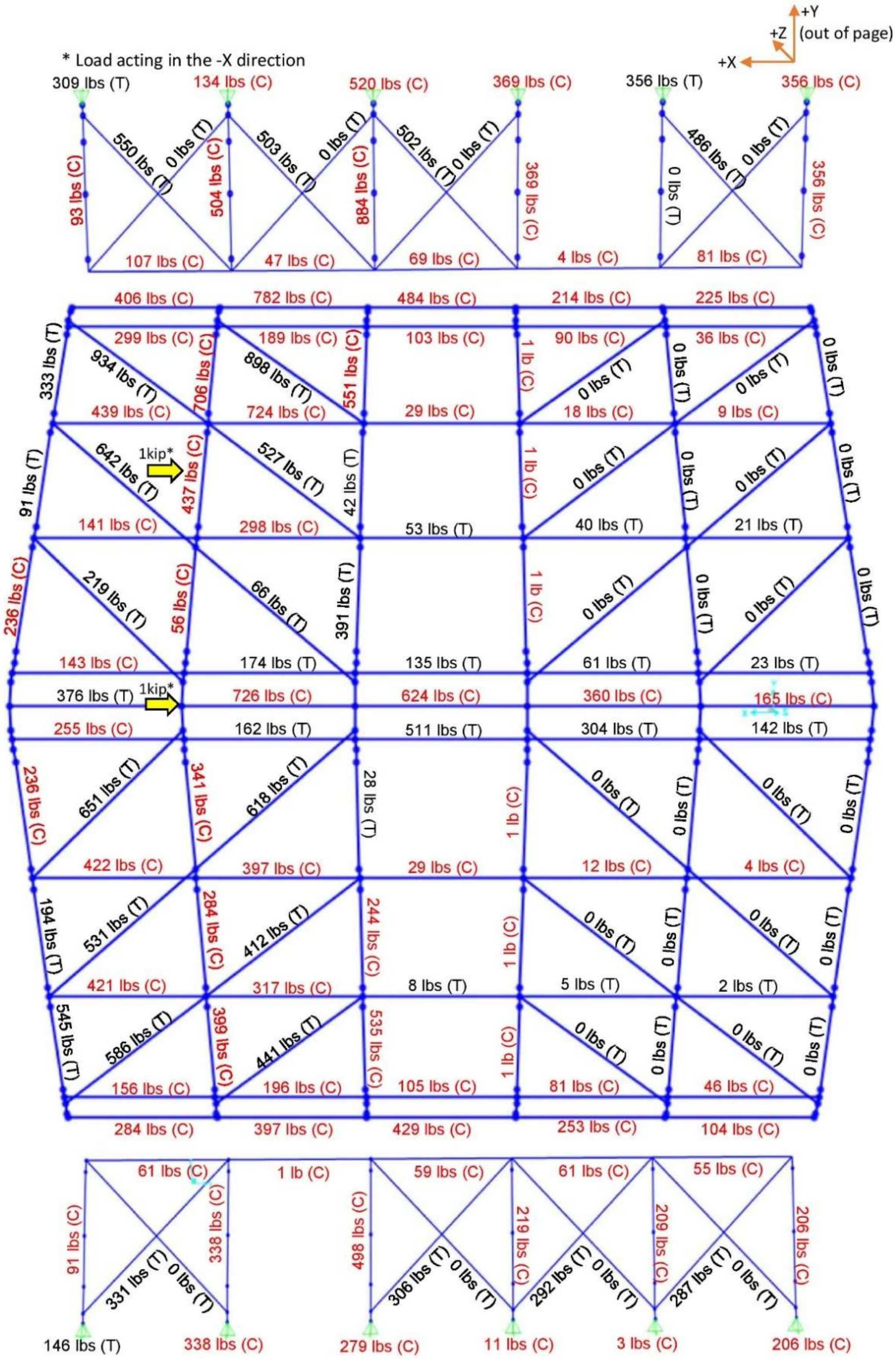

Figure 4.1-13. Test 12 element axial force analysis results

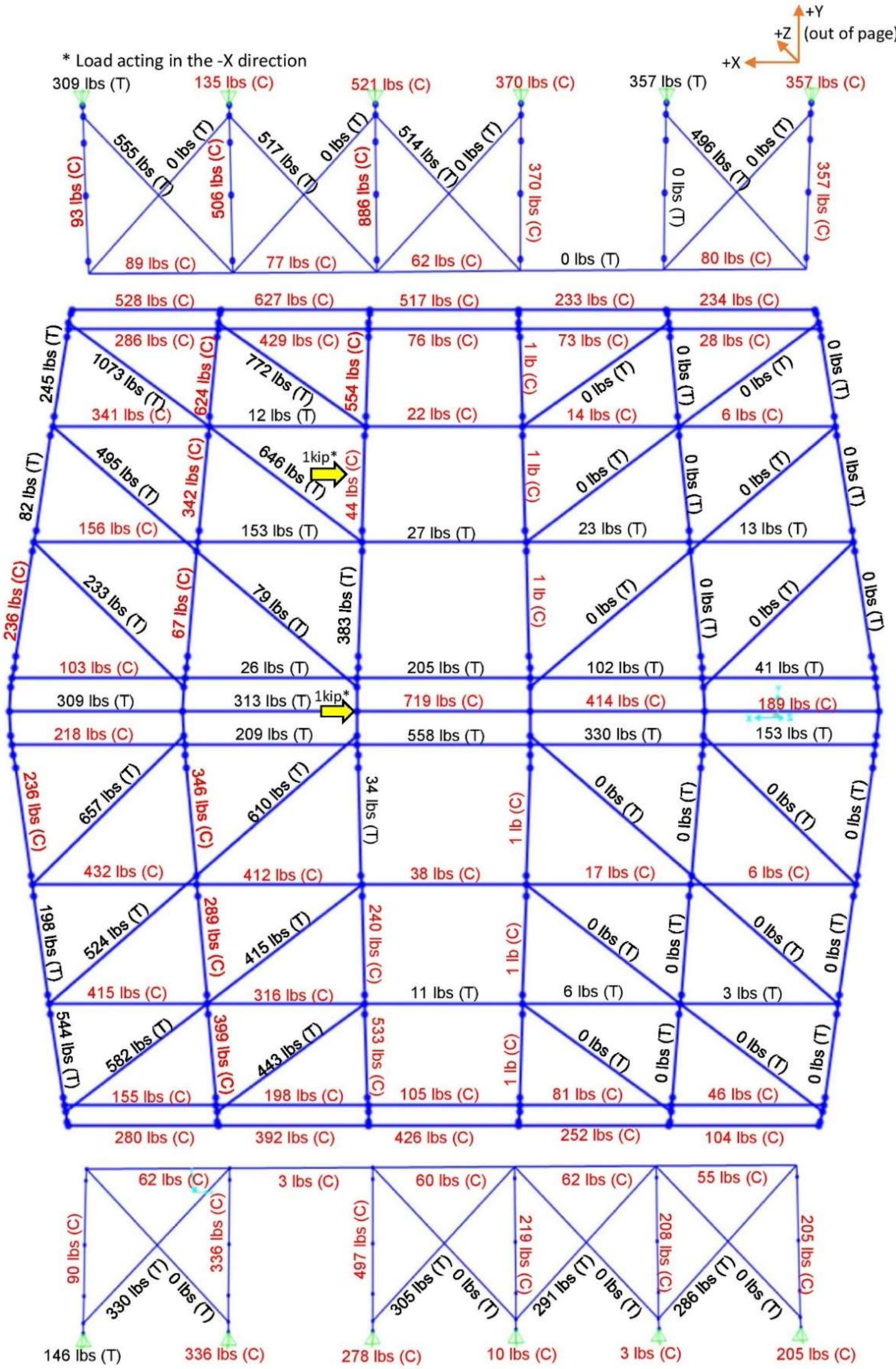

Figure 4.1-14. Test 13 element axial force analysis results

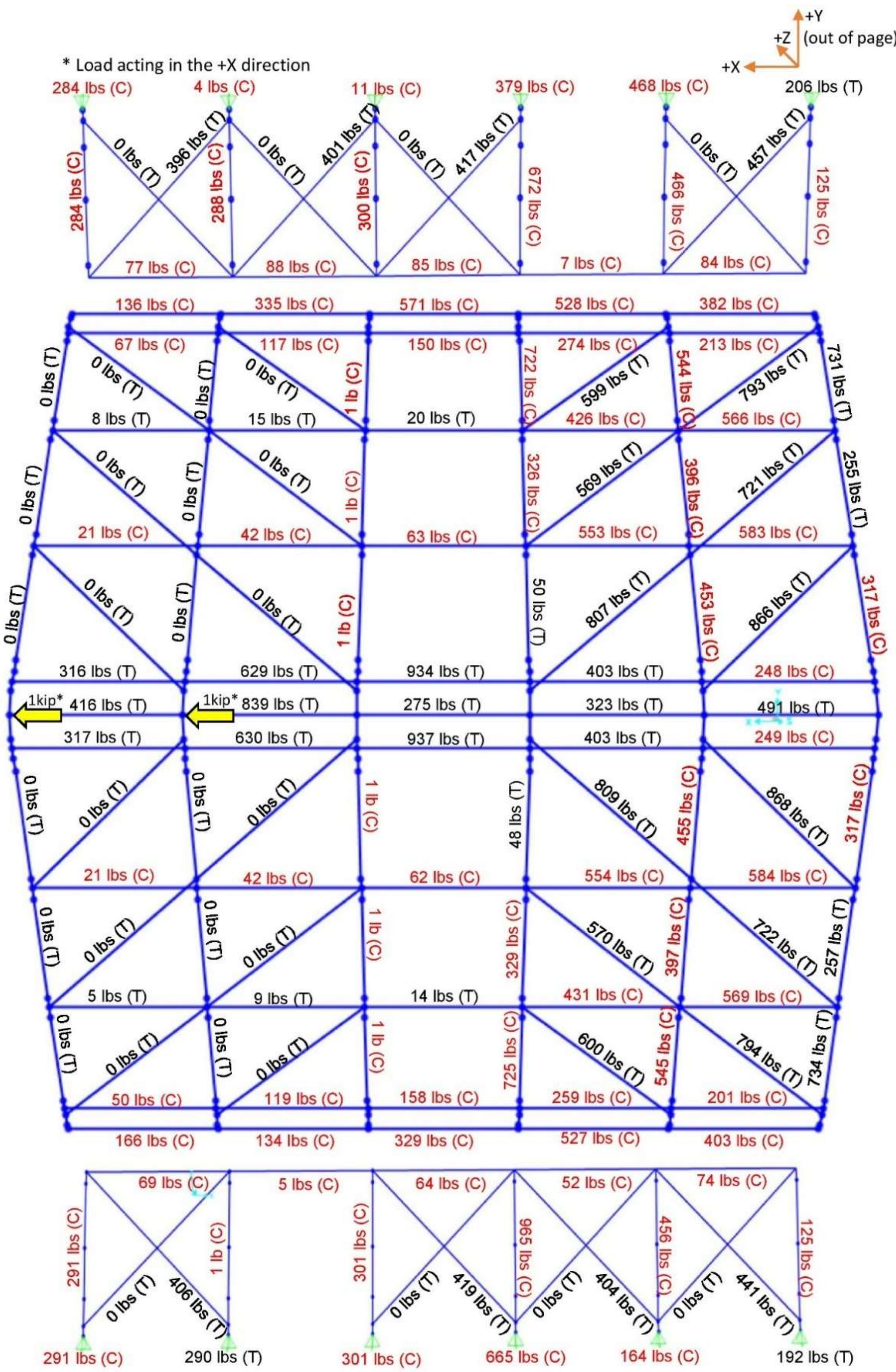

Figure 4.1-15. Test 14 element axial force analysis results

Figure 4.1-16 shows the member forces for test 15. The load was applied at the midpoint of the structure in the positive y-direction. On the side of the model below the load point, a large tensile force acted on the frames closest to the load and decreased as the frames got further away. These forces then put axial forces on the roof cables. The cables then put compressive forces in the purlins. The two most interior frames transferred the tensile forces into the cables, causing them to experience 288 lbs of force. On the side of the model above the load point, large compressive forces acted on the frames and the magnitude of the forces decreased as the frames got further from the load. Due to the direction of the interior cables, they did not experience any tensile forces on this side of the model. With no forces in the cables, there were negligible forces in the purlins. The compressive loads traveled through the frames and into the columns. The load path is symmetric on the left and right sides of the load point.

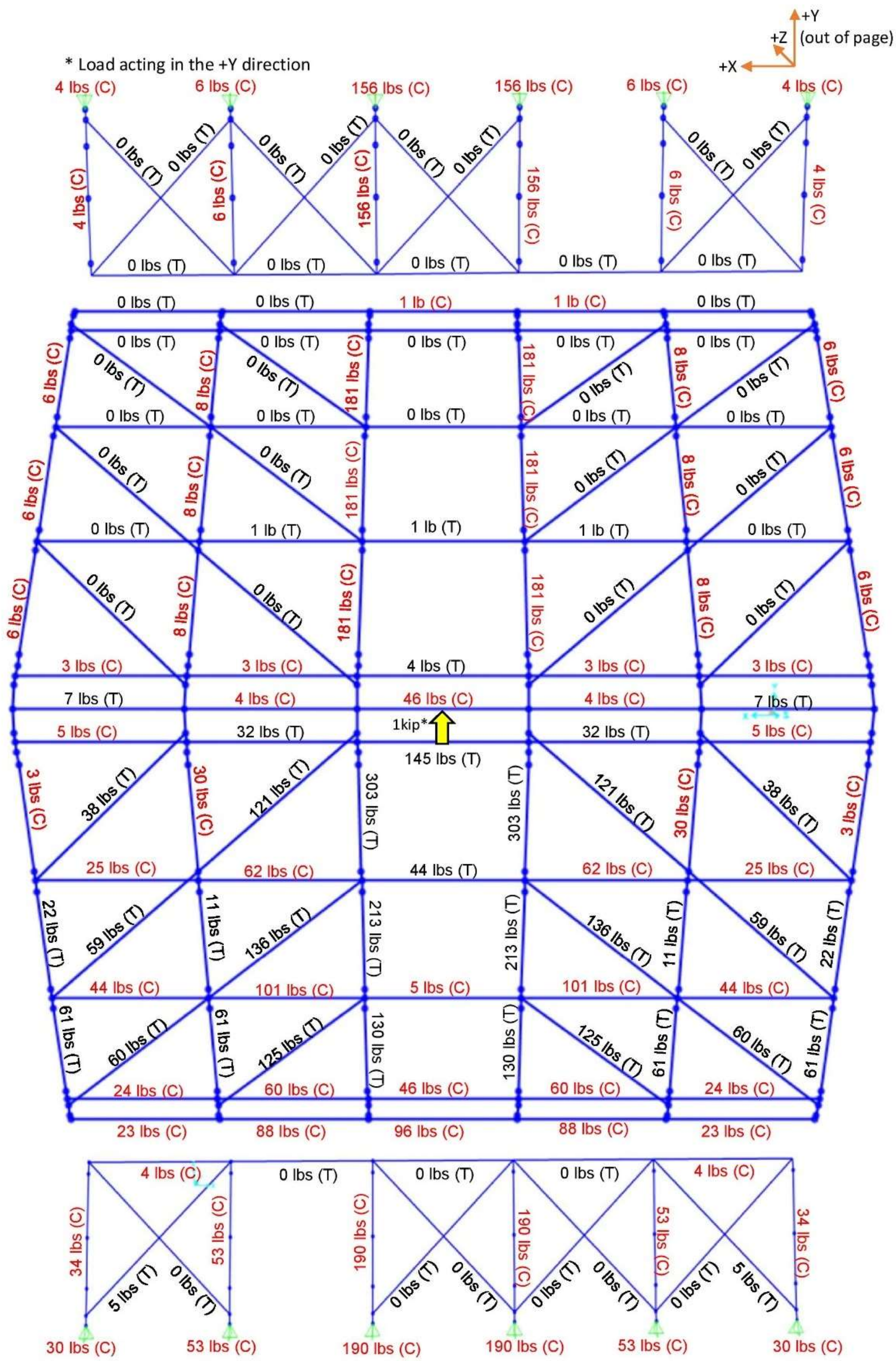

Figure 4.1-16. Test 15 element axial force analysis results

From this series of analyses, several general statements regarding the longitudinal and transverse load path can be made. In the longitudinal direction, with loads applied in the X direction on the ridge, most of the load was transferred through the ridge, into the roof bracing, and from there into the frames and purlins and down to the foundation. The load transferred through the ridge decreased as it got further from the load point. With loads applied in the positive and negative Z direction, the majority of the load was transferred through the frame where the load was applied and then into the supports. Consistently throughout the various tests, the axial loads in the ridge purlin were larger than in the purlins next to the ridge on either side. This was also found to be true on the eaves. The wall braces shared the load evenly independent of where along the ridge the load was applied. This is because the frames in the structure acted together in a system. As the loads were transferred throughout the different frames, the forces tended to decrease slightly in magnitude. These results all demonstrate that the cables and purlins in the model logically transfer loads in both directions throughout the entire framing system. In the longitudinal direction, the frames behind the load experience tensile forces, which transfer the loads to the supports, cables, and purlins. On the compressive side of the model, all the forces are transferred through the frames down to the columns and supports. The load path analysis also provided evidence that the structural members act together as a system. Loads applied to individual frames were transferred through that frame, into the purlins and cables throughout the other frames. This proves that the frames do not act individually but together as a system.

4.2 Model Comparison to the in-service LAMS Values

The purpose of this section is to compare preliminary demands on the members measured in an instrumented, in-service LAMS to demands obtained using the finite element model. This comparison serves as a validation that the model correctly represents the structure. The dead loads on the structure were not measured by the instrumentation because the instrumentation was attached to an existing structure. For this reason, dead loads were not measured in the model outputs. The directionality factor, K_d was set to a value of 1.0 in this comparison since only transverse and longitudinal wind directions were considered.

It is important to note that at the time of the submittal of this research, further analysis was ongoing for the comparisons of the model to the in-service LAMS. The values presented here are preliminary values.

4.2.1 Instrumentation of the LAMS

Instrumentation was installed on the in-service LAMS to record forces, strain, and displacements on the structure. The instrumentation that was installed is summarized in Table 4.2-1, and a visual representation of where on the structure the instrumentation was installed is shown in Figure 4.2-1. Instrumentation was installed throughout the structure, however, the second frame line from the south side of the structure was the most heavily instrumented. Several selected purlins and cables were also instrumented.

Table 4.2-1. Summary of installed instrumentation

Model	Manufacturer	Description	Quantity
BDI-ST350	Bridge Diagnostics	Bolt-on strain gages	43
WDS-1000-P60-CR-P	Micro-epsilon	String potentiometer	12
LCR-3K	Omega	S-beam load cell	6
		Total:	**61**

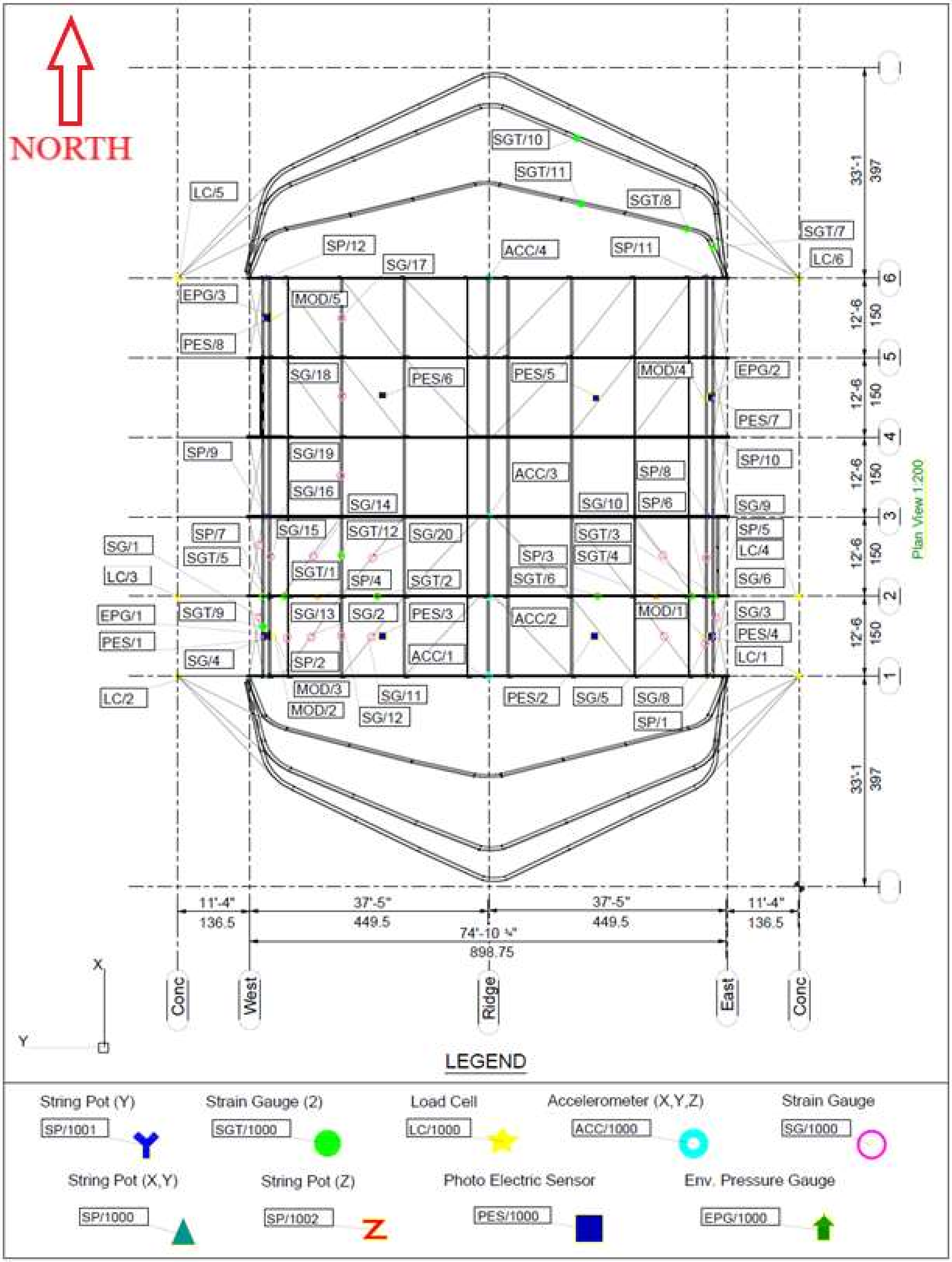

Figure 4.2-1. Instrumentation layout as of February 26, 2021. North is at the top of the figure.

With the recorded strain and the material and section properties provided in Table 3.2-1 and Table 3.2-2, data that could be compared to the model were calculated. For the frame members, the moment (M) and axial forces (P) were calculated. Equations (4)-(9) were used to make these calculations.

$$\sigma_1 = \varepsilon_1 E \tag{4}$$

$$\sigma_2 = \varepsilon_2 E \tag{5}$$

$$m = \frac{\sigma_1 - \sigma_2}{y_1 - y_2} \tag{6}$$

$$b = \sigma_1 - m \cdot y \tag{7}$$

$$M = -(\sigma_1 - b) * I/y \tag{8}$$

$$P = b * A \tag{9}$$

where ε and σ are the strain (measured by the strain gages) and stress respectively in the cross-section at a section distance from the neutral axis, y, and specifically $y_1 = 2.0$ inches and y_2 =-2.0 inches reflect the locations of the strain gages relative to the neutral axis. Based on the calculation, positive moments represent compression in the top flange and tension in the bottom flange. Negative axial forces represent compression.

For the purlins and cables, the axial force was calculated using equation (10).

$$P = \varepsilon E A \tag{10}$$

where ε is the measured strain; E is the modulus of elasticity.

A weather station was installed approximately 200 feet from the LAMS to monitor site conditions. The station recorded the temperature, barometric pressure, wind direction, and wind speeds approximately 30 feet above the ground. The wind direction and speed were measured every second with an accuracy of $\pm 3\%$ up to 40 m/s, resolution of 0.01 m/s, and 1° for wind speed and direction respectively.

4.2.2 Data Processing

This section provides the processing of full-scale data collected from the LAMS. Over a period between 1 August 2020 and 30 June 2021, at least 466 10-minute segments were measured at the LAMS site with peak 3-second wind gusts of 25 mph or higher. Storms impacting the LAMS included two nearby hurricane events, Hurricane Sally (2020) and Hurricane Zeta (2020) along with other convective and synoptic events. In total, the LAMS experienced wind speeds of at least 25 mph from all wind directions as shown in Figure 4.2-2.

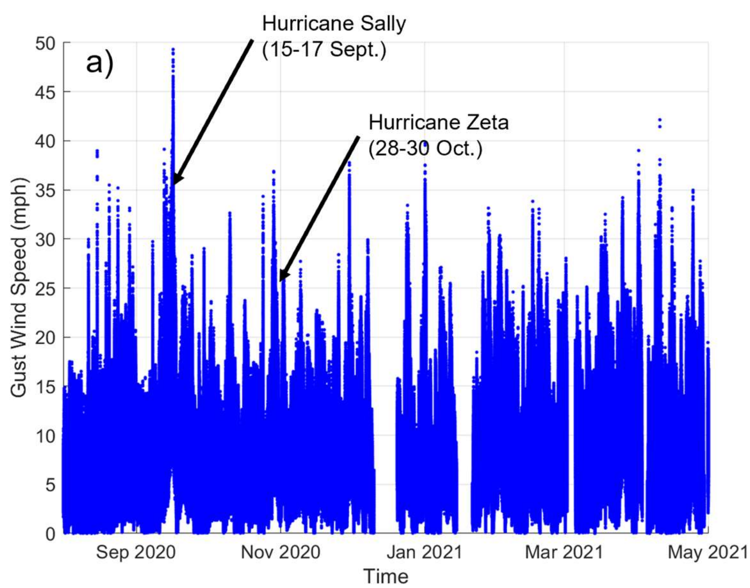

Figure 4.2-2. Gust wind speeds recorded at the LAMS site between August 2020 and April 2021 conditioned on (a) time, and (b) wind direction (where 0° represents winds out of the North and 90° represents winds out of the east).

4.2.3 Response of the LAMS to Transverse Wind Loads

The response of the LAMS to transverse wind loads was assessed by considering 10-minute segments of LAMS response data for which the wind velocity met the following criteria to be considered transverse, loosely stationary, and with sufficient magnitude to produce measurable demands in the structure:

- Average and peak wind angles between 70° and 110° (perpendicular to the ridge of the LAMS)
- 10-minute peak wind speed at least 10 m/s
- 10-minute gust factor (ratio of peak 3-second gust to 10-minute mean for the given segment) less than 2
- The difference between the maximum and minimum wind directions within the segment less than 45°

Fifty-eight 10-minute records met these criteria. The maximum, mean, and minimum reactions for each piece of instrumentation were then calculated relative to the demands in the at-rest condition after removing temperature effects. The values were then scaled to match the 90-mph design speed used in the model using Equation (11).

$$ScaleFactor_i = \left(\frac{90\text{ mph}}{\widehat{U}_{3sec,i}}\right)^2 \tag{11}$$

where $\widehat{U}_{3sec}$ is the peak 3-second gust wind speed that occurred during each segment, i. This approach assumes a linear-elastic response, which was confirmed to be a valid assumption using the finite element model. However, this approach does not account for compression limits to tension-only members. For example, in pre-tensioned elements (e.g., exterior high wind cables), compression relative to the at-rest condition can occur, which would result in a negative force in the data analysis. Scaling this value to an equivalent 90 mph event however ignores the non-linear compression limit. Thus, for tension-only elements, negative forces are ignored and set to 0. The locations of the instrumentation used for the transverse comparison are shown in Figure 4.2-3. The comparison included (1) axial forces measured by the load cells in the high wind kit; (2) internal moment and axial forces in frame members at 8 locations measured by strain gage pairs; (3) the displacement in the y-direction measured by five string potentiometers and (4) the displacement in the z-direction measured by seven string potentiometers.

Nodes, or joints, were created in the model at every location there was instrumentation on the structure. For the transverse wind comparison, wind conditions 1-4 were run in the model with the east side of the in-service LAMS treated as the windward wall. The appropriate demands at nodes matching that of the instrumented LAMS were then exported into a Microsoft Excel file. The maximum and minimum value of all the wind conditions at each node was presented for comparison. When comparing the internal moment, only the major axis moment was used.

The load cell values are shown in Table 4.2-2 for the instrumented structure and the finite element model. The in-service LAMS and finite element strain gage values are shown in Table 4.2-4 and Table 4.2-5. The string potentiometer values are shown in Table 4.2-5 for the in-service LAMS data and in Table 4.2-6 for the model results. The average of the maximum and minimum responses on the instrumented structure for each of the 37 recordings was calculated and then scaled to match the design wind speed. The output from the finite element model with the 90 mph-based wind loads was used for comparison. The 2-D deflection of frame line 2 can be seen in Figure 4.2-4.

When comparing the load cell values, the maximum model outputs were 3 times larger than the in-service LAMS data for LC1 and LC6. For LC4, however, the in-service LAMS data was more than twice as large as the model output. This discrepancy may have been because LC1 and LC6 were attached to the end vertical frame cables, and there are uncertainties about exactly how the wind loads should be applied to the door frames. All cables also may not have been equally pre-tensioned in the in-service LAMS. LC2, LC3, and LC5 were attached to the cables on the leeward side of the model. The model produced no outputs for these cables because the leeward eave displaced toward the cables supports, causing the cables to slack. The in-service LAMS, however, did produce tensile values for these locations, which may have been due to buffeting of the LAMS.

When looking at the internal moments for the in-service LAMS and model, the moments on SGT2 were negative for both the in-service LAMS and model outputs. The moments for SGT 1 and 5 had maximum values within an order of magnitude. SGT 3 produced the same maximum value for both the model output and in-service LAMS, and SGT 4 showed a difference within an order of magnitude. The moment for SGT 6 in the model was slightly more than twice the magnitude of the in-service LAMS. The positive and negative signs of the moments on the windward and leeward sides of the model and in-service LAMS respectively are reflective of a small positive wind pressure on the windward wall and roof and a negative wind pressure on the leeward wall and roof. SGT 7 and 8 were attached to one of the door frames and the comparisons of these values showed a difference in an order of magnitudes. The differences here could also have been due to the uncertainty in the wind loads that should be applied to the door frames.

When comparing the axial forces, SGT 2 and 6 showed comparisons of peak positive responses within a single order of magnitude. SGT 1,4, and 5 showed comparisons of responses larger than an order of magnitude. SGT 3 had a much larger magnitude response for the in-service LAMS, although both measured and modeled indicated compression dominated. For SGT 7 and 8, the axial comparisons were an order of magnitude different, however they showed similar patterns, with both having the largest response being negative for SGT 7 and positive for SGT8.

For the deflection in the Y-direction, almost identical responses were seen between the modeled and measured LAMS response at the location of SP1. SP6 showed comparisons within an order of magnitude. SP5 had a negligible deflection in the in-service LAMS, but a deflection of 1.68 inches in the model. SP 2 and 7 showed the largest difference, with the deflection in the model reaching nearly 7 inches. Both of these deflections occurred on the leeward side of the model. When looking at deflection in the Z-direction, SP3,4,9, and 12 were the locations with the most similar comparisons. The locations on the windward roof (SP 3,8,10, and 11) showed downward deflection in the model due to wind pressures acting downward on the windward roof, in agreement with the positive moment observed near the midspan of Frame Line 2 (SGT6). On the in-service LAMS, these locations also experienced downward deflection, indicating positive pressures dominated the external loading conditions on the windward side. The locations on the leeward roof (SP 4, 9, and 12) showed comparisons all within an order of magnitude.

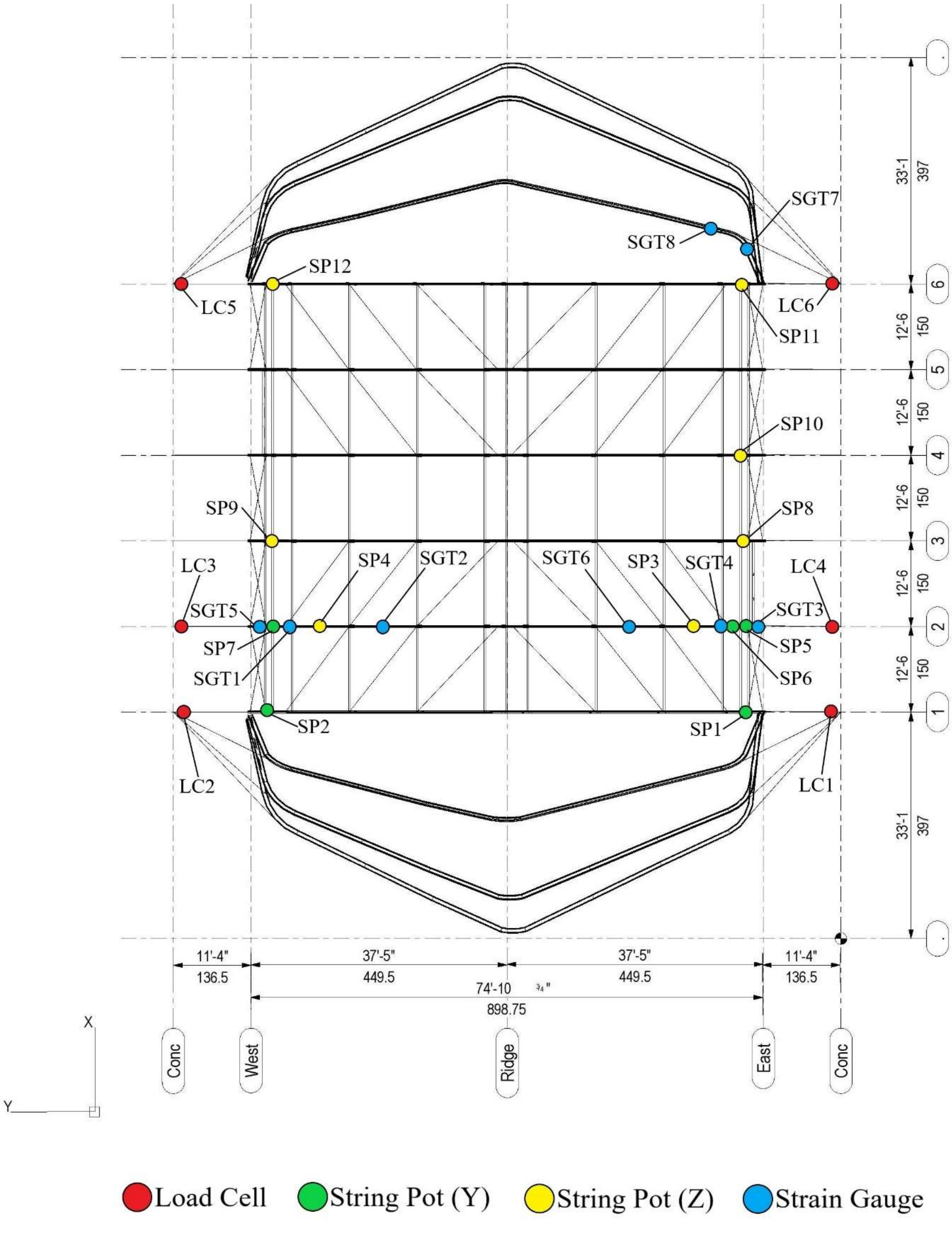

Figure 4.2-3. Layout of comparison instrumentation for transverse load cases

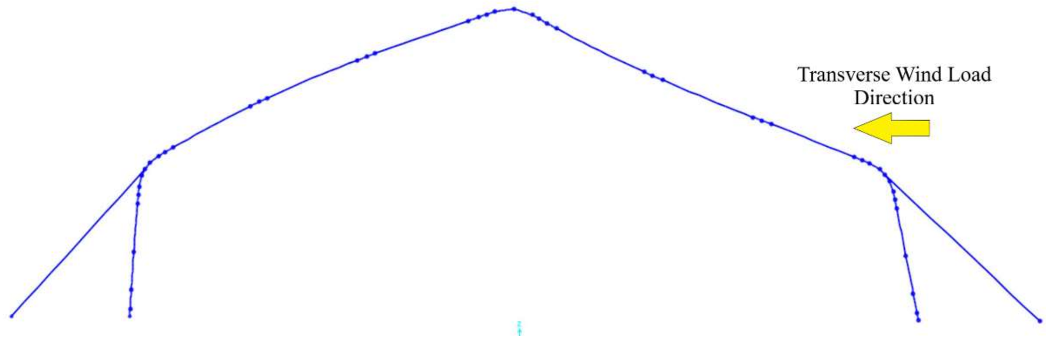

Figure 4.2-4. 2-D deflection of frame line 2 under transverse wind loads

Table 4.2-2. Modeled and observed axial forces in the high-wind cables under transverse wind loads (LC1, 4, 6 on the windward side).

	Observed Axial Force (lb)	
Sensor ID	Peak (-) Response	Peak (+) Response
LC1	286	3943
LC2	-254	278
LC3	-1305	2405
LC4	12134	19037
LC5	-1749	2271
LC6	51	3633

	Modeled Axial Force (lb)	
Sensor ID	Peak (-) Response	Peak (+) Response
LC1	6590	12172
LC2	0	0
LC3	0	0
LC4	5858	9577
LC5	0	0
LC6	6529	11492

Table 4.2-3. In-service LAMS strain gage internal moments and axial forces (SGT = strain gage)

	Moment (kip-in)	
Sensor ID	Peak (-) Response	Peak (+) Response
SGT1	-15	121
SGT2	-99	-15
SGT3	3	106
SGT4	28	138
SGT5	-10	120
SGT6	-4	91
SGT7	16	69
SGT8	2	61

	Axial Force (lb)	
Sensor ID	Peak (-) Response	Peak (+) Response
SGT1	-1485	1670
SGT2	-2065	7902
SGT3	-10212	-2543
SGT4	-2157	616
SGT5	-1552	2674
SGT6	-3302	4692
SGT7	-2233	1877
SGT8	793	4007

Table 4.2-4. Model output strain gage internal moments and axial forces (SGT = strain gage)

	Moment (kip-in)	
Sensor ID	Peak (-) Response	Peak (+) Response
SGT1	-213	62
SGT2	-264	-124
SGT3	-89	105
SGT4	-65	94
SGT5	-149	75
SGT6	-23	205
SGT7	-69	157
SGT8	-76	26

	Axial Force (lb)	
Sensor ID	Peak (-) Response	Peak (+) Response
SGT1	-219	4868
SGT2	-193	4866
SGT3	-873	-542
SGT4	1696	5532
SGT5	515	5382
SGT6	1695	5532
SGT7	-8580	749
SGT8	3194	8915

Table 4.2-5. In-service LAMS string potentiometer defections (SP = string potentiometer)

	Y-deflection (inch)	
Sensor ID	Peak (-) Response	Peak (+) Response
SP1	1.81	4.75
SP2	-1.08	3.32
SP5	0.06	0.07
SP6	2.44	5.72
SP7	-0.07	0.48

	Z-deflection (inch)	
Sensor ID	Peak (-) Response	Peak (+) Response
SP3	-3.74	-0.83
SP4	1.06	3.77
SP8	-5.57	-2.25
SP9	-2.03	3.66
SP10	-1.43	-3.83
SP11	-1.19	-2.98
SP12	-1.06	1.16

Table 4.2-6. Model output string potentiometer defections (SP = string potentiometer)

	Y-deflection (inch)	
Sensor ID	Peak (-) Response	Peak (+) Response
SP1	2.74	4.95
SP2	0.19	6.82
SP5	1.22	1.68
SP6	2.58	4.18
SP7	1.83	6.75

	Z-deflection (inch)	
Sensor ID	Peak (-) Response	Peak (+) Response
SP3	-4.31	-0.66
SP4	2.27	4.7
SP8	-0.83	-0.52
SP9	0.4	1.78
SP10	-0.82	-0.52
SP11	-0.99	-0.58
SP12	0.03	1.84

4.2.4 Response of the LAMS to Longitudinal Wind Loads

For the longitudinal direction, the same criteria for the structural monitoring of the in-service LAMS were used, except the angle of the wind had to be within 170° and 190° and between 350° and 10° (used for evaluating stresses in the door frames under a windward wall condition only). Within these criteria, there were 66 10-minute segments that met the criteria for the 180° condition and 17 for the 0° condition. The forces in the purlins, roof, and wall cables, along with the major axis moment and axial force on the first door frame were focused on for this comparison. The major axis moment and axial force in the door frames were calculated from the pairs of strain gages at each point as described in Section 4.3.1. For purlins and cables, the measured strains were converted to axial forces assuming all strains were due to compressive stresses, also described in Section 4.3.1. As noted previously, where compression values were present in the cables after scaling up to design-level conditions (due to uncertainties in the baseline value, or slight pre-tensioning), these were set to 0. Figure 4.2-5 shows the layout of the instrumentation used for the longitudinal load case comparisons.

For the longitudinal wind comparison, wind conditions 5,7,9 and 6,8,10 were run in the model. The model output corresponding to locations being reported from the instrumentation, at the appropriate nodes, were then exported into a Microsoft Excel file. The maximum and minimum value of all the wind conditions was then chosen for comparative analysis. When comparing the internal moment, the major axis moment was exported from the model.

The purlin axial forces for the in-service LAMS and the model data are presented in Figure 4.2-6. The in-service LAMS and modeled purlin axial forces are shown in Table 4.2-7. The in-service LAMS and modeled wall and roof cable axial forces are shown in Table 4.2-8. For the moments and axial forces in the windward and leeward door frames, the in-service LAMS values are shown in Table 4.2-9 and the model data are in Table 4.2-10. Figure 4.2-6 shows the 3-D deflection of the model under the longitudinal wind loads.

The comparisons these purlin axial forces show mixed results. SG9,12,13,15, and SGT12 all produced comparisons within an order of magnitude for the peak positive responses. SG4 produced a comparison within two orders of magnitude for the peak positive response. SG3,8,18,20 and SGT9 all produced responses for the in-service LAMS that were several orders of magnitude larger than the model outputs. The responses of the in-service LAMS were taken from wind events that had a variety of wind speeds. These responses were then scaled up to a 90-mph wind load. This explains why some of the responses on the purlins were larger than the expected capacity of the purlins.

The comparison of the roof cable responses also produced mixed results. SG10 showed comparisons well within an order of magnitude. SG2,5,11, and 14 produced peak positive responses for the model output values around 3 to 4 times larger than the responses of the in-service LAMS. SG20 produced a value for the 4 times larger for the in-service LAMS. The greater variation in cable forces of the in-service LAMS data was likely due to the difference in slackness/tension in the different cables.

The wall cable comparisons were well within an order of magnitude for SG16 in the positive peak responses. For SG1 and 6, the peak positive responses were orders of magnitude larger for the model output than the in-service LAMS. This difference could be attributed to the uncertainty of the application of the design wind loads.

For the internal moments on the leeward door frames, the moments of SGT10 produced comparisons within an order of magnitude. SGT7 and 8 produced moments orders of magnitude larger for the model than the in-services LAMS. Alternatively, SGT11 produced moments orders of magnitude larger for the in-service LAMS than the model. The axial forces did not provide good correlation. SGT7 (north door frame eave) produced compressive axial forces for the in-service LAMS, however, tensile forces are experienced in the model. The large uplift forces on the roof section of the door frames could have caused this tensile force reaction. These loads acted perpendicular to the frames, causing the tensile forces to not be transferred into the high wind kit cables. SGT10 showed similar comparisons, with the forces within an order of magnitude. SGT8 showed forces several times smaller for the in-service LAMS than what was experienced in the model. The uncertainty in the wind loads on the door frames could have contributed to these differences.

On the windward door frames, the model output and structural monitoring of the in-service LAMS produced similar results for the axial forces. The peak negative responses for SGT 7,8,10 and 11 produced comparisons within or around an order of magnitude. These were the most compatible comparisons in the longitudinal direction. Unfortunately, compatible comparisons for the moments were not seen. The model outputs were several orders of magnitude smaller than the structural monitoring of the in-service LAMS for SGT10 and SGT11. However, for SGT 7 and 8, the model outputs were orders of magnitude larger for the structural monitoring of the in-service LAMS. The windward door moments did, however, show similar patterns of increases and decreases between the three locations.

In the structural monitoring of the in-service LAMS, the forces in the cables were several times smaller than the forces experienced in the purlins. There are four potential reasons for the discrepancy between the modeled and in-situ observations. These are as follows:

(1) Uncertainties in the measurements from the strain gages. Under weak axis bending, the strain gauges could measure additional strain due to being mounted at a small offset from the web of the frames. This has not been accounted for in the analysis. Further, the strain gauges are sensitive to the temperature of the material, but do not directly compensate for these temperature effects. A statistical model was piloted to eliminate the temperature effects, but refinement and further analysis is ongoing and outside the scope of this thesis.

(2) Slack in the cables. The cables in the in-service LAMS were observed to not be fully tensioned on the structure, which could have caused the structure to not distribute forces through the cables properly.

(3) The purlins could have experienced out-of-plane bending, which could have affected the measurements of the strain gages. The lack of tension in the fabric of the instrumented in-service LAMS resulted in fabric bearing on the purlins when under positive pressure. Strain gages were installed along the approximate neutral axis of the purlins relative to the out-of-plane loading from the fabric, but some out-of-plane effects may have still been present. They were also installed near the midspan of the purlins, and therefore would begin to measure flexural strains if the purlins exhibited any out-of-plane deflections under the compression loading.

(4) The aerodynamics of the structure may not have been well enveloped by the ASCE load cases considered in this study due to the irregular geometry of the structure, particularly the clamshell doors. Subsequently, the wind loads being applied to the finite element model may have been substantially different from the true wind loads for the longitudinal wind direction.

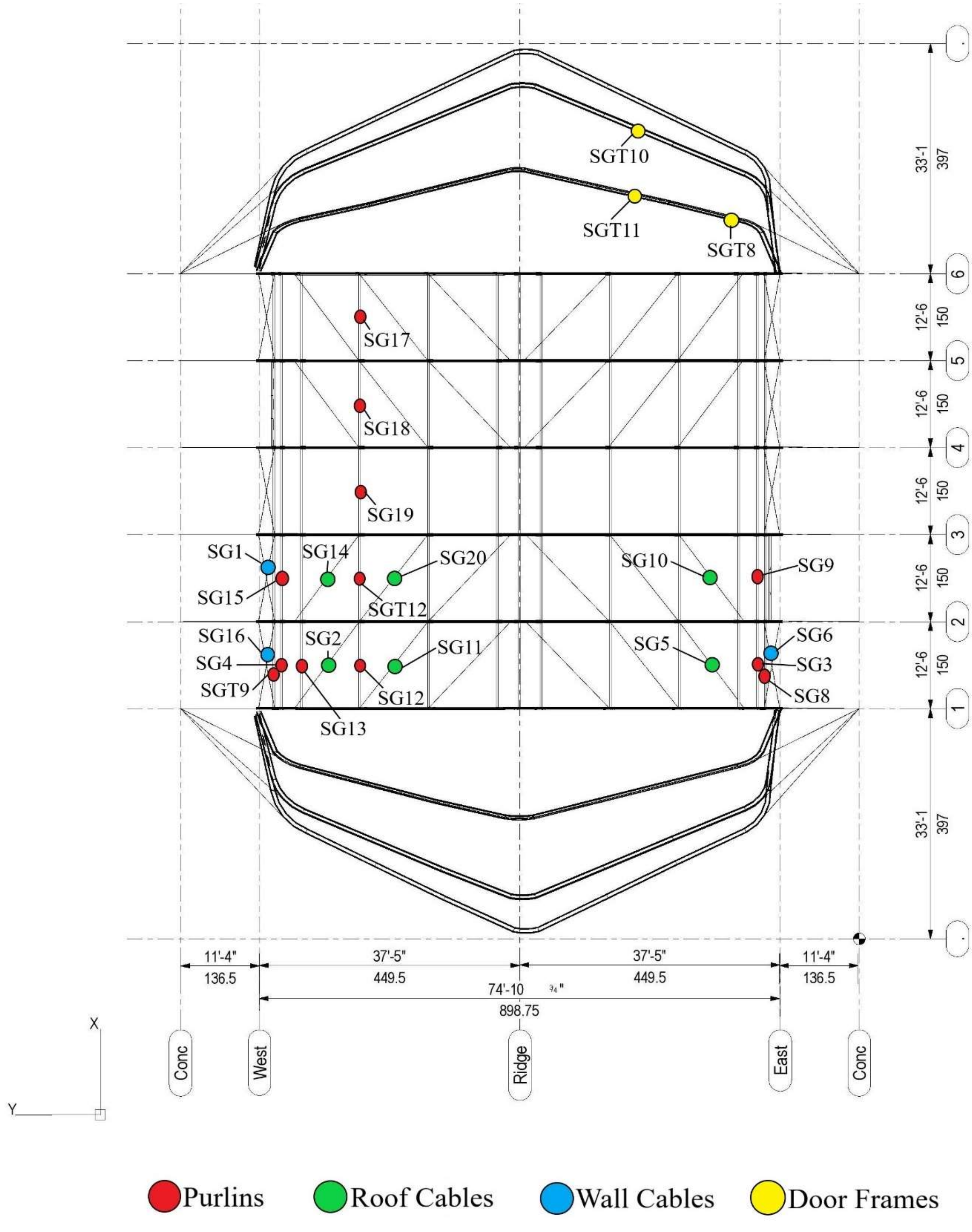

Figure 4.2-5. Layout of comparison instrumentation for longitudinal load cases

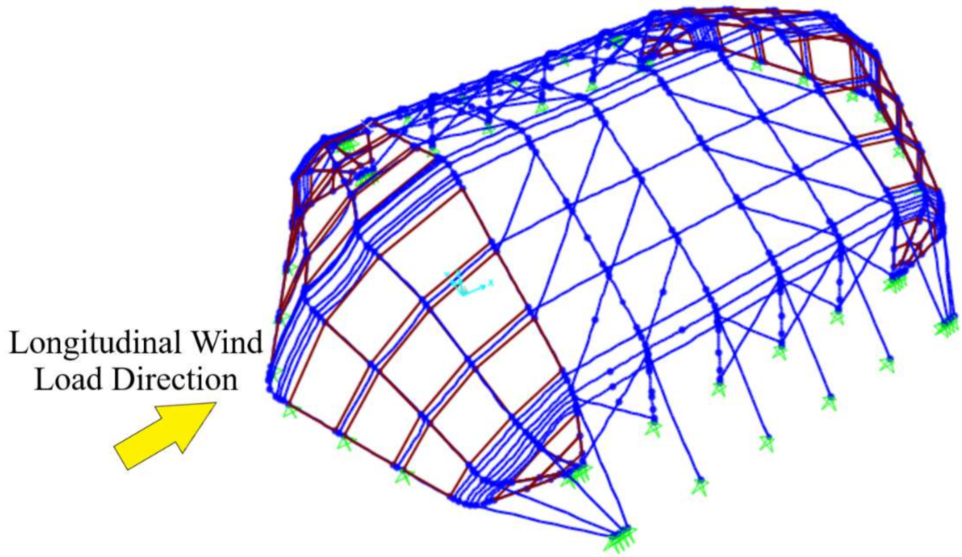

Figure 4.2-6. 3-D deflection under longitudinal wind loads

Table 4.2-7. Modeled and observed purlin axial forces

	Observed Purlin Axial Force (lbs)	
Sensor ID	Peak (-) Response	Peak (+) Response
SG3	-2069	3162
SG4	-3526	129
SG8	-1397	5417
SG9	-1949	720
SGT9	-5775	5305
SG12	-208	2115
SGT12	-579	1523
SG13	648	4454
SG15	-1156	2641
SG17	-4375	-272
SG18	-1721	1322
SG19	-1562	2020

	Modeled Purlin Axial Force (lbs)	
Sensor ID	Peak (-) Response	Peak (+) Response
SG3	235	371
SG4	204	343
SG8	624	629
SG9	1352	1445
SGT9	733	749
SG12	2211	3319
SGT12	608	1329
SG13	1685	2324
SG15	1424	1457
SG17	190	481
SG18	83	584
SG19	29	684

Table 4.2-8. Modeled and observed wall and roof cable axial forces

Sensor ID	Observed Roof Cable Axial Force (lbs) Peak (-) Response	Observed Roof Cable Axial Force (lbs) Peak (+) Response
SG2	0	1211
SG5	0	917
SG10	35	1827
SG11	0	745
SG14	0	546
SG20	1907	3971

Sensor ID	Model Roof Cable Axial Force (lbs) Peak (-) Response	Model Roof Cable Axial Force (lbs) Peak (+) Response
SG2	3060	3659
SG5	2990	3636
SG10	1799	1939
SG11	1814	2313
SG14	1853	1962
SG20	863	931

Sensor ID	Observed Wall Cable Axial Force (lbs) Peak (-) Response	Observed Wall Cable Axial Force (lbs) Peak (+) Response
SG1	0	182
SG6	0	595
SG16	36	1104

Sensor ID	Model Wall Cable Axial Force (lbs) Peak (-) Response	Model Wall Cable Axial Force (lbs) Peak (+) Response
SG1	1455	1609
SG6	1460	1617
SG16	1392	1525

Table 4.2-9. In-service LAMS moments and axial forces on windward and leeward door frames

Sensor ID	Windward Door Frame Moment (kip-in) Peak (-) Response	Windward Door Frame Moment (kip-in) Peak (+) Response
SGT7	-71	36
SGT8	-111	32
SGT10	-82	148
SGT11	-91	54

Sensor ID	Leeward Door Frame Moment (kip-in) Peak (-) Response	Leeward Door Frame Moment (kip-in) Peak (+) Response
SGT7	-37	3
SGT8	-42	15
SGT10	-6	48
SGT11	-26	33

Sensor ID	Windward Door Frame Axial Force (lbs) Peak (-) Response	Windward Door Frame Axial Force (lbs) Peak (+) Response
SGT7	-5595	528
SGT8	-5175	4221
SGT10	-9014	4273
SGT11	-8533	7480

Sensor ID	Leeward Door Frame Axial Force (lbs) Peak (-) Response	Leeward Door Frame Axial Force (lbs) Peak (+) Response
SGT7	-5804	-1669
SGT8	-2512	1136
SGT10	-2210	5165
SGT11	-2814	5396

Table 4.2-10. Model output moments and axial forces on windward and leeward door frames

	Windward Door Frame Moment (kip-in)	
Sensor ID	Peak (-) Response	Peak (+) Response
SGT7	-412	-277
SGT8	-378	-243
SGT10	-28	-16
SGT11	-15	-6

	Leeward Door Frame Moment (kip-in)	
Sensor ID	Peak (-) Response	Peak (+) Response
SGT7	29	102
SGT8	21	65
SGT10	11	35
SGT11	0	0

	Windward Door Frame Axial Force (lbs)	
Sensor ID	Peak (-) Response	Peak (+) Response
SGT7	-11411	-6432
SGT8	-9916	-5309
SGT10	-10645	-5968
SGT11	-10660	-5925

	Leeward Door Frame Axial Force (lbs)	
Sensor ID	Peak (-) Response	Peak (+) Response
SGT7	1672	4171
SGT8	3235	9386
SGT10	3190	9241
SGT11	-1329	-608

4.3 Chapter Summary

Overall, the modeled response of the LAMS matched the behavior of the in-service LAMS under transverse loads. When comparing the model outputs to the in-service LAMS data, there were differences in the data, however, it the overall patterns of the response compared reasonably well. The windward high wind cable forces, and the deflection of the leeward eave in the y-direction exhibited the most significant differences. The forces modeled on the windward exterior high wind kit cables were only slightly larger than half the size of the forces recorded on the structure. Alternatively, the deflection of the leeward eave in the model was multiple times larger than what is being experienced on the structure.

Agreement between modeled and observed response of the LAMS in the longitudinal direction was limited. This was not entirely unexpected, as there are non-linearities in the cable and purlin response due to the lack of pretensioning, and uncertainties as to the correct wind loads to apply in the longitudinal direction, both of which are coupled with the measurement uncertainties present due to temperature effects, installation variabilities, and other factors. Further analysis will seek to reduce the uncertainties in the measured values, and laboratory testing of LAMS components, quantifying the non-linearities, needs to be incorporated into future revisions of the numerical models.

Chapter 5 Finite Element Model Maximum Value Study

This chapter provides an analysis of the maximum demands that are experienced in the SAP2000 model under different wind conditions. The six wind conditions analyzed are defined in Table 3.4-2. The directionality factor, K_d, was applied to the wind loads by multiplying the wind loads by 0.85 in the load combination. An evaluation of these wind loads provides an in-depth analysis of locations on the structure that experience the largest demands. With this information, failure locations and mechanisms can be better defined, and the failures can be more correctly assessed. The maximum demands obtained from the SAP2000 model of the LAMS are presented in this section. Results are oriented based on the orientation of the LAMS, shown in Figure 5-1.

Figure 5-1. In-service LAMS configuration

5.1 Maximum Stresses

The bending stresses for each member of the structure were exported from the SAP2000 model for each of the six load cases. These stresses were reduced to the maximum absolute stress from the interior vertical frames (IVF), end vertical frames (EVF), south and north door frames

(SDF1-3, NDF1-3), and the purlins. In the model, each member was assigned a label. The label of the member that experienced the maximum stress is provided in the tables as the location. This data is shown in Table 5.1-1. Figure 5.1-1 and Figure 5.1-2 display where these maximum values occurred on the structure in the current study.

For the vertical frames, none of the load cases exceeded the allowable stress of 18.9 ksi. For the end vertical frames, none of the maximum stress under the longitudinal wind load cases exceeded the allowable stress. The largest stresses were found in the door frames under longitudinal wind load cases, with a maximum negative stress of -47.59 ksi exceeding the allowable stress by 150%.

To gain a better understanding of the large magnitudes in the door frames, the stresses were broken down into the major axis bending, minor axis bending, and axial stress. Roughly the same magnitude of bending stress was experienced in the major and minor axis. The axial stresses accounted for little stress in the door frames.

Table 5.1-1. Calculated maximum stresses

Vertical Frames (ksi)	
Load Case	Maximum
D+W1	9.77
D+W2	-5.58
D+W3	12.09
D+W4	-15.55
D+W5,7,9	17.03
D+W6,8,10	13.13

End Vertical Frames (ksi)	
Load Case	Maximum
D+W1	12.04
D+W2	6.16
D+W3	13.96
D+W4	-17.94
D+W5,7,9	11.71
D+W6,8,10	-18.44

Door Frames (ksi)	
Load Case	Maximum
D+W1	23.05
D+W2	9.55
D+W3	20.30
D+W4	-22.24
D+W5,7,9	-30.81
D+W6,8,10	-47.59

Purlins (ksi)	
Load Case	Maximum
D+W1	1.79
D+W2	1.32
D+W3	2.20
D+W4	-2.20
D+W5,7,9	-2.09
D+W6,8,10	-2.98

Door Frames – Major Axis (ksi)	
Load Case	Maximum
D+W1	10.17
D+W2	4.17
D+W3	9.24
D+W4	-12.06
D+W5,7,9	-17.38
D+W6,8,10	-26.56

Door Frames – Minor Axis (ksi)	
Load Case	Maximum
D+W1	12.26
D+W2	4.34
D+W3	10.61
D+W4	-9.09
D+W5,7,9	13.12
D+W6,8,10	20.39

Door Frames - Axial (ksi)	
Load Case	Maximum
D+W1	1.18
D+W2	0.45
D+W3	0.92
D+W4	-1.46
D+W5,7,9	-0.84
D+W6,8,10	-1.46

The maximum values for each load case in the purlins did not exceed the allowable stress; however, this is a pure compression and tension comparison. Under compression, the critical buckling stress would control. Using AISC provisions, the critical buckling stress for the purlins is calculated using Equations (12), (13), and (14), resulting in a critical buckling stress of 4 ksi.

$$r = \frac{I_{yy}}{A} \tag{12}$$

$$F_e = \frac{\pi^2 E}{(\frac{L_c}{r})^2} \tag{13}$$

$$F_{cr} = 0.877F_e \tag{14}$$

where I_{yy} was the moment of inertia and taken as 0.987 in^4, A was the cross-sectional area taken as 1.039 in^2. E was the modulus of elasticity and taken as 10100 ksi, L_c was the length of the purlin and was taken between 135 and 148 inches. This was because the total length of the purlins were 148 inches, however, not including the pinned connections, the length was 135 inches.

Potential flexural stresses may have also been experienced on the purlins in the structure from the fabric producing a load on the purlins. Due to the variability in how tightly tensioned the fabric was on the structures, it is not within the scope of this thesis to measure or model any out-of-plane loads that could have developed flexural stresses in the purlins due to the fabric.

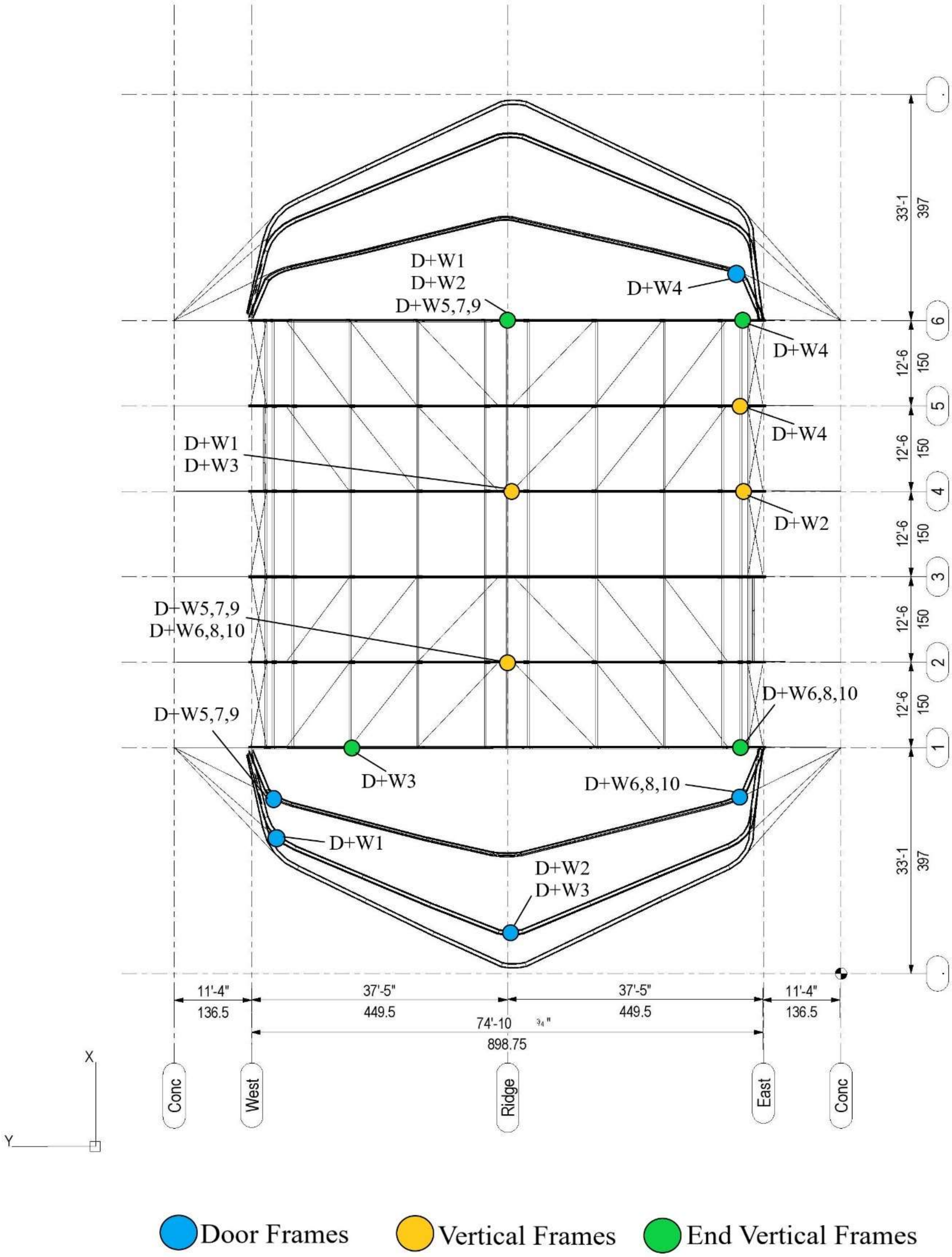

Figure 5.1-1. Calculated maximum frame stress locations

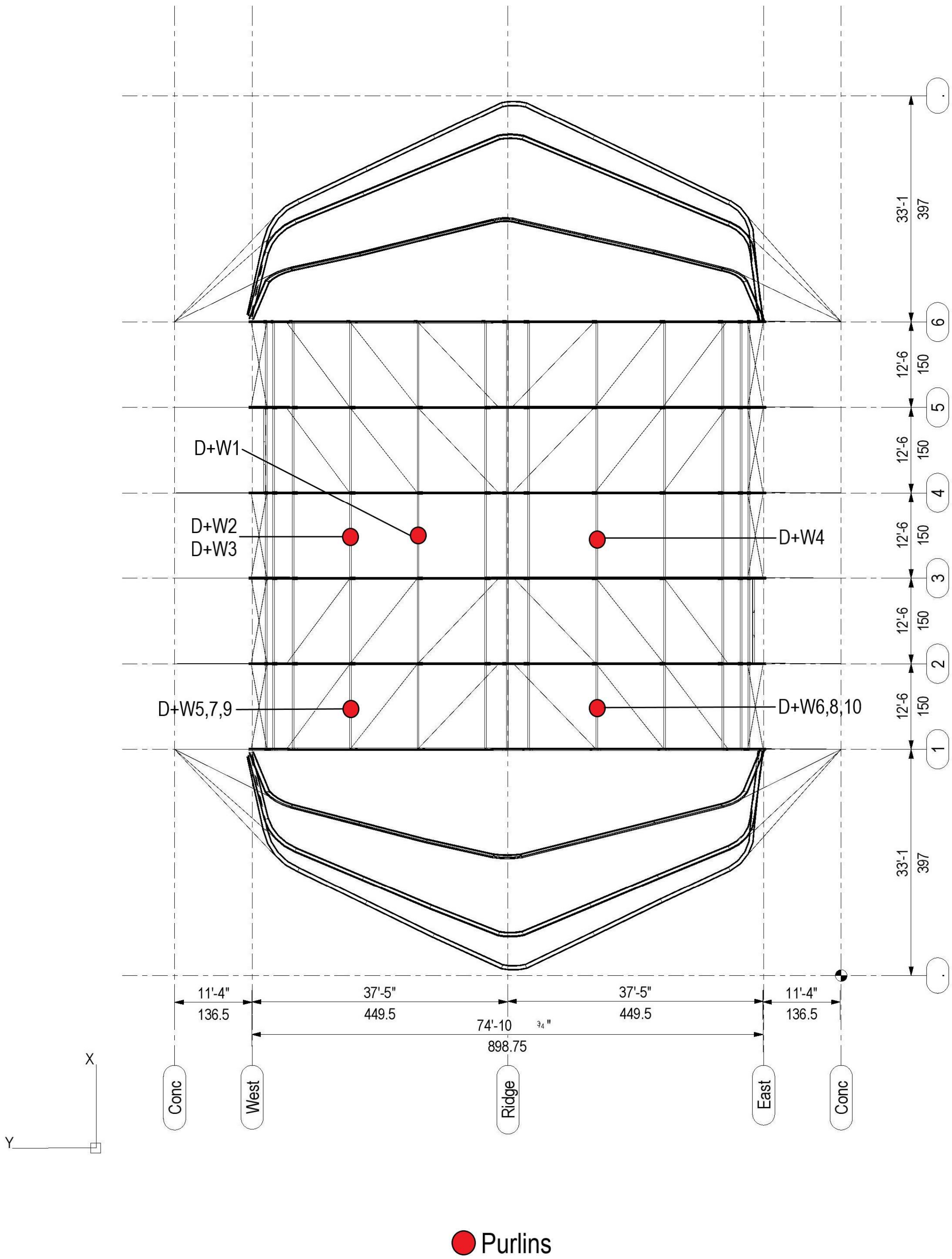

Figure 5.1-2. Calculated maximum purlin stress locations

5.2 High Wind, Wall, and Roof Cable Forces

The tensile force for the high wind cables, wall and roof cables were exported from the finite element model for each of the six wind conditions. For the high wind cables, these values were reduced to the maximum tensile force in cables attached to the vertical frames, end vertical frames, and door frames. For the roof and wall cables, the maximum tensile force was collected for each wind case. The values for the high wind cables are shown in Table 5.2-1. The maximum values in the wall and roof cables are shown in Table 5.2-2. Figure 5.2-1 displays the location of these maximum values in the model.

For the high wind cables, none of the maximum values from the model reached the breaking strength of the high wind cables. All the maximum values from the model were experienced on the windward side of the structure.

The maximum tensile forces on the wall cables for wind conditions 1-4 occurred on the leeward wall. For the longitudinal wind load cases, the cables were the primary bracing system, and therefore they experienced large forces. The maximum forces acted on the cable closest to the windward wall for wind conditions 5,7,9 and 6,8,10. None of the forces reached the breaking strength of the cables.

In the roof cables, the maximum force for load case 1 happened on the windward wall on the north side of the structure. Wind conditions 2, 3, and 4 had maximum tensile forces in the leeward wall on the north side. The maximum force for load cases 5,7,9 and 6,8,10 occurred on the west side of the ridge closest to the windward wall. The maximum tensile force in the roof cables was less than the breaking strength of the cables.

Table 5.2-1. High wind cable maximum tensile forces

Vertical Cables (lbs)		End Vertical Cables (lbs)		Door Cables (lbs)	
Load Case	Maximum	Load Case	Maximum	Load Case	Maximum
D+W1	6012	D+W1	8522	D+W1	9608
D+W2	5664	D+W2	6567	D+W2	7025
D+W3	9257	D+W3	12166	D+W3	12699
D+W4	9166	D+W4	10618	D+W4	10924
D+W5,7,9	1133	D+W5,7,9	2718	D+W5,7,9	4419
D+W6,8,10	148	D+W6,8,10	353	D+W6,8,10	1147

Table 5.2-2. Wall and roof cable maximum tensile forces

Wall Cables (lbs)	
Load Case	Maximum
D+W1	60
D+W2	44
D+W3	75
D+W4	70
D+W5,7,9	1284
D+W6,8,10	1400

Roof Cables (lbs)	
Load Case	Maximum
D+W1	26
D+W2	10
D+W3	19
D+W4	289
D+W5,7,9	2605
D+W6,8,10	3111

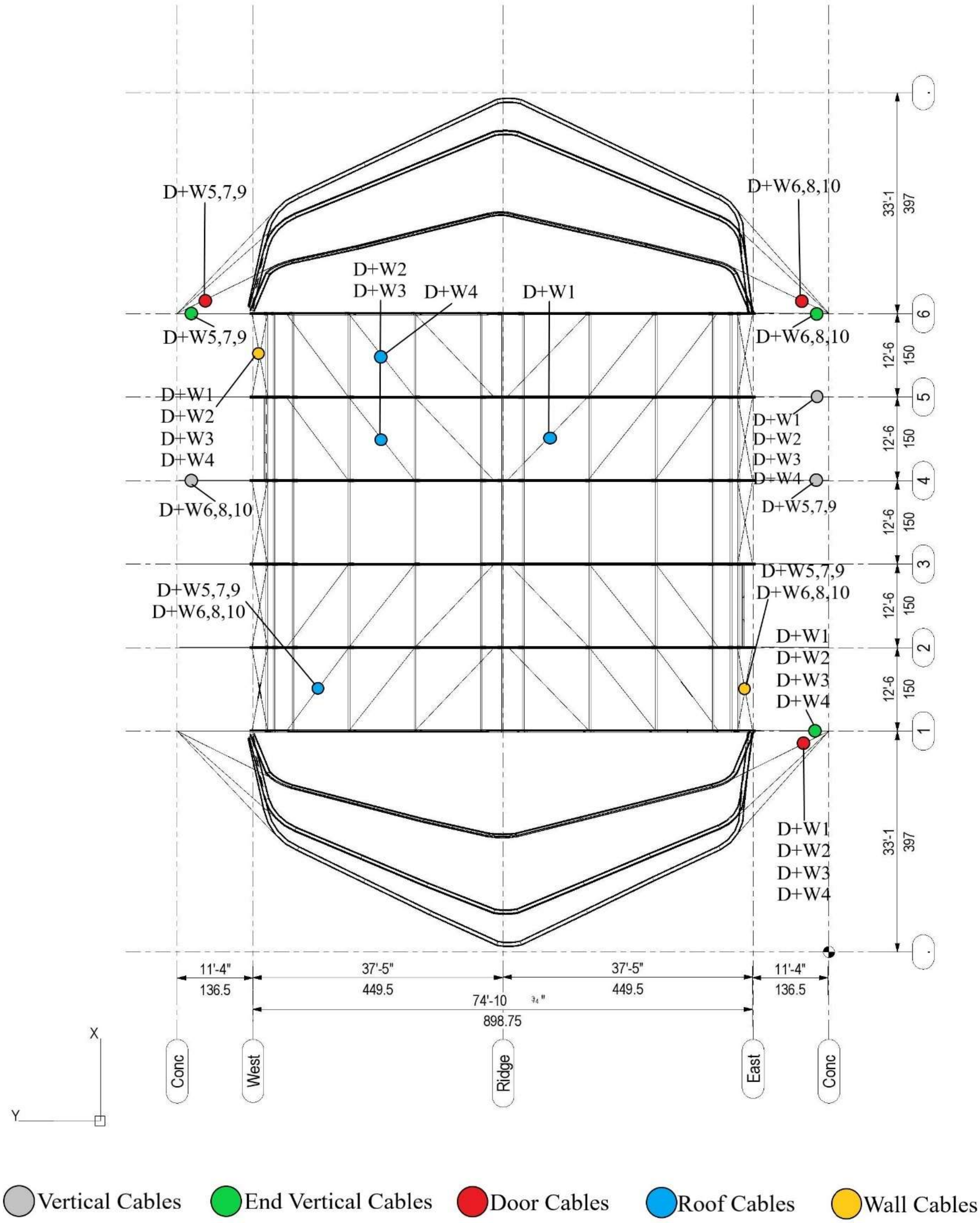

Figure 5.2-1. Calculated maximum cable force locations

5.3 Maximum Support Reactions

In the finite element model, pin supports were added at the support of each frame. Pin supports were also added on the door frames that lay flat on the ground, where the frames were tied down to the surface. For these supports, the reactions in the x, y, and z-direction were exported. The x-direction refers to the dimension that acts along the length of the structure. The y-direction refers to the dimension that acts along the width of the structure, and the z-direction is acting upwards in the model. The values were reduced to the maximum reaction force for the vertical frames, end vertical frames, and door frames for both the high wind cable supports and frame supports. The maximum reactions in the high wind cable supports are shown in Table 5.3-1, and the maximum reactions in the frame supports are in Table 5.3-2.

For the high wind cable supports, all the maximum reaction forces occurred in the y-direction. The largest force experienced on the cables attached to the vertical frames was 6,736 lb due to the D+W3 wind condition. For the cables attached to the end vertical frames, the D+W3 wind condition resulted in the largest force of 9,219 lbs. On the cables attached to the door frames, a force of 9,243 lbs was experienced due to the D+W3 wind condition. All maximum forces occurred on the windward side of the model.

The maximum reaction forces that occurred on the frame supports all acted in the z-direction except condition D+W1 on the door frames, which had a maximum force in the x-direction. For the vertical frames, the largest force on the structure was 9,293 lbs, acting downward which was due to the D+W4 wind condition and acted on the windward wall. At the end vertical frames, D+W4 resulted in the largest downward force of 10,204 that acted on the windward wall. D+W4 produced a downward force of 8,421 lbs, which was the largest force experienced on the door frame supports. This force occurred on the most vertical frame of the windward wall. The locations of the high wind kit cable supports, and frame supports are displayed in Figure 5.3-1.

Table 5.3-1. High wind cable support maximum reactions

X-Direction (lbs)		
Cable Attached to Door Frames		
Location	Maximum	Location
D+W1	5040	305
D+W2	3558	305
D+W3	6280	305
D+W4	5192	305
D+W5,7,9	-2360	299
D+W6,8,10	-608	302

Y-Direction (lbs)								
Cable Attached to Vertical Frames			Cable Attached to End Vertical Frames			Cable Attached to Door Frames		
Load Case	Maximum	Location	Load Case	Maximum	Location	Load Case	Maximum	Location
D+W1	-4375	287	D+W1	-6567	283	D+W1	-6993	304
D+W2	-4122	287	D+W2	-4779	283	D+W2	-5113	304
D+W3	-6736	287	D+W3	-9219	283	D+W3	-9243	304
D+W4	-6670	287	D+W4	-7727	283	D+W4	-7951	304
D+W5,7,9	-824	286	D+W5,7,9	1978	294	D+W5,7,9	3217	298
D+W6,8,10	108	292	D+W6,8,10	-257	288	D+W6,8,10	-835	301

Z-Direction (lbs)								
Cable Attached to Vertical Frames			Cable Attached to End Vertical Frames			Cable Attached to Door Frames		
Load Case	Maximum	Location	Load Case	Maximum	Location	Load Case	Maximum	Location
D+W1	-4124	287	D+W1	-5458	283	D+W1	-5711	304
D+W2	-3885	287	D+W2	-4504	283	D+W2	-4176	304
D+W3	-6349	287	D+W3	-7957	283	D+W3	-7548	304
D+W4	-6287	287	D+W4	-7282	283	D+W4	-6493	304
D+W5,7,9	-777	286	D+W5,7,9	-1864	294	D+W5,7,9	-2627	298
D+W6,8,10	-102	292	D+W6,8,10	-242	288	D+W6,8,10	-682	301

Table 5.3-2. Frame support maximum reactions

X-Direction (lbs)								
Vertical Frames			End Vertical Frames			Door Frames		
Load Case	Maximum	Location	Load Case	Maximum	Location	Load Case	Maximum	Location
D+W1	-19	235	D+W1	-49	236	D+W1	3959	918
D+W2	-7	235	D+W2	99	47	D+W2	-3073	912
D+W3	-11	235	D+W3	148	47	D+W3	-4592	912
D+W4	-12	235	D+W4	246	47	D+W4	-6665	912
D+W5,7,9	-746	189	D+W5,7,9	-601	1	D+W5,7,9	-4198	918
D+W6,8,10	-811	141	D+W6,8,10	-603	1	D+W6,8,10	-7293	918

Y-Direction (lbs)								
Vertical Frames			End Vertical Frames			Door Frames		
Load Case	Maximum	Location	Load Case	Maximum	Location	Load Case	Maximum	Location
D+W1	438	94	D+W1	1408	47	D+W1	1845	918
D+W2	442	48	D+W2	757	1	D+W2	816	904
D+W3	1812	48	D+W3	2297	1	D+W3	1916	904
D+W4	2462	189	D+W4	3188	1	D+W4	2979	874
D+W5,7,9	719	94	D+W5,7,9	-1233	47	D+W5,7,9	-3707	911
D+W6,8,10	742	189	D+W6,8,10	-2597	47	D+W6,8,10	-5351	911

Z-Direction (lbs)								
Vertical Frames			End Vertical Frames			Door Frames		
Load Case	Maximum	Location	Load Case	Maximum	Location	Load Case	Maximum	Location
D+W1	-3503	188	D+W1	-4311	47	D+W1	-3626	911
D+W2	4848	48	D+W2	5081	1	D+W2	4130	904
D+W3	6656	48	D+W3	8204	1	D+W3	6168	904
D+W4	9293	189	D+W4	10204	1	D+W4	8421	874
D+W5,7,9	-4561	94	D+W5,7,9	-2715	236	D+W5,7,9	4913	904
D+W6,8,10	-2079	94	D+W6,8,10	2342	47	D+W6,8,10	8193	911

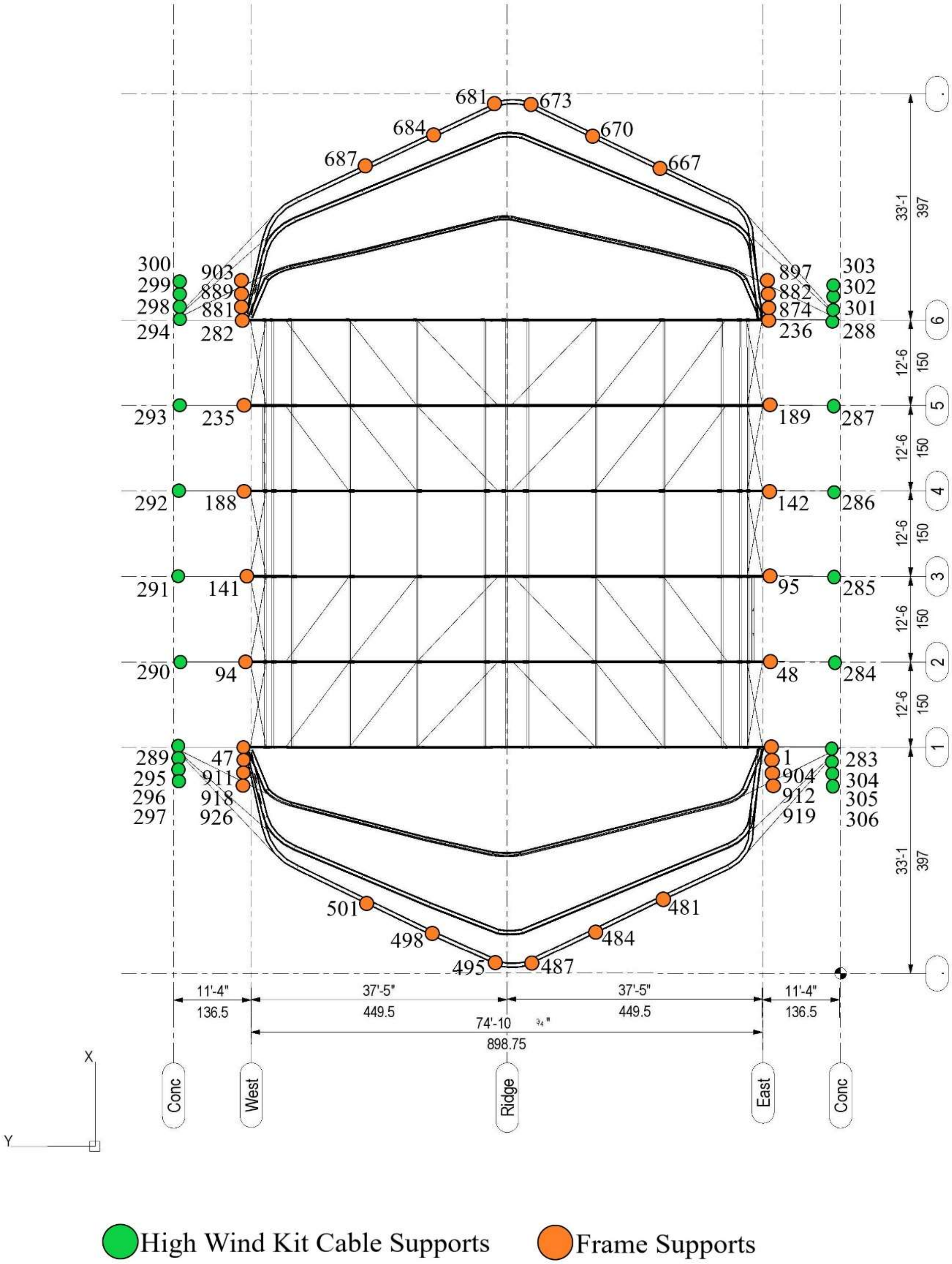

Figure 5.3-1. High wind kit and frame support locations

5.4 Support Reaction Summation

This section provides the summation of the reactions that occurred in all of the supports for the six load cases. This was conducted to validate and show the expected trends in the model based on the different load cases. The summations of the reactions at the supports were recorded for the x, y, and z-direction for all six wind conditions. The reaction summations for the high wind cable supports are represented in Table 5.4-1, and the reaction summations for the frame supports are represented in Table 5.4-2.

When looking at the high wind cable supports, the reactions in the x-direction were negligible for load cases 1-4. The reactions in the y-direction were larger than in the z-direction for the same load cases. Load conditions 1-4 are transverse wind loads, so large summations in the y-direction and small forces in the x-direction were expected. Alternatively, the summation in the x-direction was expected to be larger than in the y-direction for the longitudinal wind loads, D+W5,7,9 and D+W6,8,10. The summation of reactions in the y-direction was small for load cases D+W5,7,9 and D+W6,8,10. The largest summation in the x-direction was 7,710 lbs that occurred due to wind condition D+W5,7,9. The largest summation in the y-direction was 78,432 lbs that occurred due to wind condition D+W3. Similarly, the largest summation in the z-direction was 63,599 lbs that occurred due to wind condition D+W3.

Table 5.4-1. Summation of high wind cable support reactions

Load Case	Summation X (lbs)	Summation Y (lbs)	Summation Z (lbs)
D+W1	12	-49508	-49166
D+W2	0	-45068	-37026
D+W3	25	-78432	-63599
D+W4	6	-70691	-58623
D+W5,7,9	-7710	1384	-15175
D+W6,8,10	-1981	-69	-2694

For the frame supports, the summation of reactions in the x-direction was negligible for wind conditions D+W1-4. For these same load cases, the summation in the z-direction was significantly larger than in the y-direction. The largest summation in the x-direction was 33,883 lbs that occurred due to wind condition D+W6,8,10. The largest summation in the y-direction was 20,954 lbs that occurred due to wind condition D+W3. The largest summation in the z-direction was 83,722 lbs that occurred due to wind condition D+W4. Wind conditions 1-4 are transverse wind loads, while wind conditions 5,7,9 and 6,8,10 are longitudinal wind loads. For this reason, large summations in the y-direction for the transverse loads and large summations in the x-direction for the longitudinal loads were expected.

Table 5.4-2. Summation of frame support reactions

Load Case	Summation X (lbs)	Summation Y (lbs)	Summation Z (lbs)
D+W1	-12	9220	-13429
D+W2	-1	6154	32342
D+W3	-21	20954	31612
D+W4	13	15760	83722
D+W5,7,9	-28599	-353	-24404
D+W6,8,10	-33883	35	22872

5.5 Chapter Summary

The maximum demands study provided insight into possible systemic factors that could be contributing to premature failure. The model shows that the vertical and end vertical frames, and all purlins and cables, are expected to experience stresses within their design capacities. The strength of the door frames under longitudinal load cases was only concerning area on the structure based on the model output. The door frames experienced stresses that were larger than the allowable stress in certain areas. The largest area of concern in the door frames was at the eaves of the most vertical door frame on the windward side of the structure. The door frames have proven to be the cause of failure in some LAMS that have experienced failure. This analysis can provide a starting point on what corrections need to be made to the design of LAMS deployed by the military.

The support reactions were analyzed to provide research on the demands of the supports on the structure. Although this is not expanded upon in this paper, it provided outputs that can be compared to the design demands to understand if the supports are a potential area of concern in the structure. The support reaction summations validated the trends expected to occur in the model.

Chapter 6 Alternative Model Analysis Scenarios

This chapter provides an analysis of alternative scenarios on the model. There were two different cases studied. The first provided a change in the supports, and the second provided a change in the wind loads.

The base plates were designed for a LAMS connected to a concrete foundation, however, often the foundation is soil, which may be highly variable. When this is the case, the base plate connections are a large area of concern, and have failed, leading to damage on the shelters (Stiles, 2021). To gain a better understand of how a base plate allowed to deform can change the response of the structure, a spring was attached to one of the pinned supports on the frames to allow translation in all 3 directions.

The design of the wind loads on the door frames is the largest area of uncertainty in the model. The door frames are also the locations where the largest stresses are seen that are a possible failure initiation point. To gain a better understanding of how the wind loads affect the door frames, two different wind load scenarios were chosen for the longitudinal load cases.

6.1 Alternative Frame Support

For this alternative scenario, a spring was applied to the support on the windward side of the model for the second vertical frame line. The personnel door between frame lines 2 and 3 did not provide any additional rigidity. The location of the altered support is shown in Figure 6.1-1. A simple spring was added to this support with 1000 lbs/in stiffness in the x and y-direction, and a 5000 lbs/in stiffness in the z-direction. Once the spring was added, all 6 load cases were run for the model. The maximum stresses in the frames and purlins were then computed. The maximum reactions at the supports were also computed. All of the responses calculated were found at the same location as the responses in the maximum demand study. The maximum stresses are in Table

6.1-1. The maximum support reactions for the high wind kit cables and frame supports are in Table 6.1-2 and Table 6.1-3 respectively. The deflection of the spring support is shown in Table 6.1-4.

When comparing the stresses of the primary model to the model with the altered frame support, there was only one wind condition where the stress in the frame changes. The stress in the door frame for D+W2 decreased from 9.55 ksi to 8.78 ksi. The stress was identical for both models for every other stress. This provides evidence that if there is movement in on of the baseplates, it would have very minimal effects on the stresses experienced throughout the structure.

The comparisons of the high wind kit cable maximum reactions resulted in identical values for the high wind kit cables attached to the vertical frames in the y and z-direction. The high wind kit cables attached to the end vertical frames also resulted in the same values for the y and z-direction. Similarly, the high wind kit cables attached to the door frames resulted in the same values for both models. Like the stresses in the frames, this also provides evidence that if one of the baseplates failed, it would have very minimal effects on the reactions experienced in the high wind kit cables throughout the structure.

There were very small deflections on the spring support. The largest deflection in the x-direction was 0.71 inches. In the y-direction, the largest deflection was 1.37 inches, and 1.4 inches was the largest deflection in the z direction. These deflections were all due to D+W4.

The maximum reaction in the frame supports resulted in the same values for both models. These comparisons show that having a more flexible support reaction does not appreciably affect the maximum reactions experienced in the frame supports.

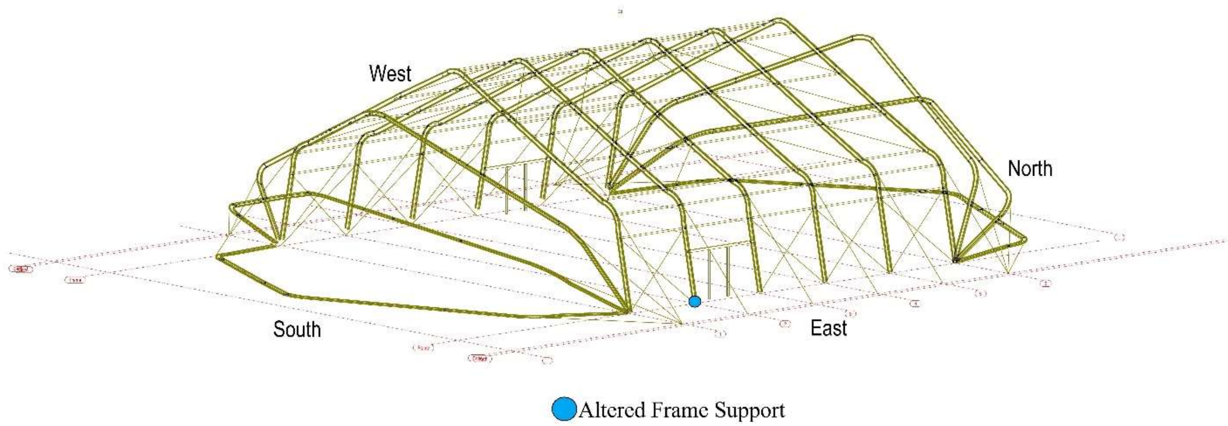

Figure 6.1-1. Altered frame support location

Table 6.1-1. Calculated maximum stresses in the alternative frame support condition for the altered frame support

Vertical Frames (ksi)	
Load Case	Maximum
D+W1	9.77
D+W2	-5.58
D+W3	12.09
D+W4	-15.55

End Vertical Frames (ksi)	
Load Case	Maximum
D+W1	12.04
D+W2	6.16
D+W3	13.96
D+W4	-17.94

Door Frames (ksi)	
Load Case	Maximum
D+W1	23.05
D+W2	8.78
D+W3	20.30
D+W4	-22.24

Purlins (ksi)	
Load Case	Maximum
D+W1	1.79
D+W2	1.32
D+W3	2.20
D+W4	-2.20

Table 6.1-2. High wind kit cable maximum support reactions for the altered frame support

X-Direction (lbs)		
Cable Attached to Door Frames		
Load Case	Maximum	Location
D+W1	5043	305
D+W2	3558	305
D+W3	6280	305
D+W4	5192	305
D+W5,7,9	-2360	299
D+W6,8,10	-608	302

Y-Direction (lbs)								
Cable Attached to Vertical Frames			Cable Attached to End Vertical Frames			Cable Attached to Door Frames		
Load Case	Maximum	Location	Load Case	Maximum	Location	Load Case	Maximum	Location
D+W1	-4375	287	D+W1	-6567	283	D+W1	-6993	304
D+W2	-4122	287	D+W2	4779	283	D+W2	-5113	304
D+W3	-6736	287	D+W3	-9219	283	D+W3	-9243	304
D+W4	-6670	287	D+W4	-7727	283	D+W4	-7951	304
D+W5,7,9	-824	286	D+W5,7,9	1978	294	D+W5,7,9	3217	298
D+W6,8,10	108	292	D+W6,8,10	-257	288	D+W6,8,10	-835	301

Z-Direction (lbs)								
Cable Attached to Vertical Frames			Cable Attached to End Vertical Frames			Cable Attached to Door Frames		
Load Case	Maximum	Location	Load Case	Maximum	Location	Load Case	Maximum	Location
D+W1	-4124	287	D+W1	-5458	283	D+W1	-5711	304
D+W2	-3885	287	D+W2	-4504	283	D+W2	-4176	304
D+W3	-6349	287	D+W3	-7957	283	D+W3	-7548	304
D+W4	-6287	287	D+W4	-7282	283	D+W4	-6493	304
D+W5,7,9	-777	286	D+W5,7,9	-1864	294	D+W5,7,9	-2627	298
D+W6,8,10	-102	292	D+W6,8,10	-242	288	D+W6,8,10	-682	301

Table 6.1-3. Frame support maximum reactions for the altered frame support

X-Direction (lbs)								
Vertical Frames			End Vertical Frames			Door Frames		
Load Case	Maximum	Location	Load Case	Maximum	Location	Load Case	Maximum	Location
D+W1	-19	235	D+W1	-49	236	D+W1	3959	918
D+W2	-7	235	D+W2	99	47	D+W2	-3073	912
D+W3	-11	235	D+W3	148	47	D+W3	-4592	912
D+W4	-12	235	D+W4	246	47	D+W4	-6665	912
D+W5,7,9	-746	189	D+W5,7,9	-602	1	D+W5,7,9	-4198	918
D+W6,8,10	-811	141	D+W6,8,10	-603	1	D+W6,8,10	-7293	918

Y-Direction (lbs)								
Vertical Frames			End Vertical Frames			Door Frames		
Load Case	Maximum	Location	Load Case	Maximum	Location	Load Case	Maximum	Location
D+W1	438	94	D+W1	1408	47	D+W1	1845	918
D+W2	442	48	D+W2	757	1	D+W2	816	904
D+W3	1812	48	D+W3	2297	1	D+W3	1916	904
D+W4	2462	189	D+W4	3188	1	D+W4	2979	874
D+W5,7,9	719	94	D+W5,7,9	-1233	47	D+W5,7,9	-3707	911
D+W6,8,10	742	189	D+W6,8,10	-2597	47	D+W6,8,10	-5351	911

Z-Direction (lbs)								
Vertical Frames			End Vertical Frames			Door Frames		
Load Case	Maximum	Location	Load Case	Maximum	Location	Load Case	Maximum	Location
D+W1	-3503	188	D+W1	-4311	47	D+W1	-3626	911
D+W2	4848	48	D+W2	5081	1	D+W2	4130	904
D+W3	6656	48	D+W3	8204	1	D+W3	6168	904
D+W4	9293	189	D+W4	10204	1	D+W4	8421	874
D+W5,7,9	-4561	94	D+W5,7,9	-2715	236	D+W5,7,9	4913	904
D+W6,8,10	-2079	94	D+W6,8,10	2342	47	D+W6,8,10	8193	911

Table 6.1-4. Spring support deflections for the altered frame support

	X-direction	Y-direction	Z-direction
D+W1	-0.17	0.17	-0.44
D+W2	-0.35	-0.12	-0.81
D+W3	-0.54	-1.08	-1.04
D+W4	-0.71	-1.37	-1.40
D+W5,7,9	-0.12	0.00	0.49
D+W6,8,10	-0.12	-0.28	0.18

6.2 Alternative Longitudinal Wind Load Cases

This section provides two alternative longitudinal wind load cases on the model. The first case applied the roof load on the most vertical door frame on either side of the model and windward and leeward wall loads on the other door frames. The second case applied the roof load on all the door frames. This study was done because it is uncertain how the wind loads should be applied to the door frames. To determine a better pressure distribution, a wind tunnel study should be conducted.

6.2.1 Alternative Longitudinal Wind Load Case 1

For the first alternative longitudinal wind load case, the columns of all the frames were assigned the sidewall wind pressures. The roof span of all the vertical frames were assigned the roof loads. The roof span of the most vertical door frame was also assigned the roof loads for both the windward and leeward sides of the structure. The roof span of the other two door frames were assigned as the windward and leeward walls. Figure 6.2-1 shows the layout of the loads assigned to the frame members. The calculated stresses are shown in Table 6.2-1.

The comparisons of the stresses in the vertical frames showed slightly smaller values in the first alternative longitudinal load case than the original load case. In the end vertical frames, the stress due to wind condition 5,7,9 decreased slightly from the original load case, however, for load condition 6,8,10 the stress was reduced nearly 50%. For the door frames, a similar pattern was seen. The stress due to condition 5,7,9 was reduced by around 20% while the stress under condition 6,8,10 was reduced by nearly 75%. This reduced the stress such that it became within the allowable stress. The reduction was so large for wind condition 6,8,10 because the load was changed from the windward force that acted downward on the frame to the negative roof pressure that switched the direction of the load. With this switch, the loads at the eave of the door frame were both outward forces, reducing the amount of stress at the eave. The purlin stresses were reduced by around 75%. The compressive forces in the purlin were reduced when the load on the most vertical door frame became a negative force on either side instead of a positive force on the windward side and negative force on the leeward side. The purlin stress for wind condition 5,7,9 became a tensile stress under this alternative longitudinal load case.

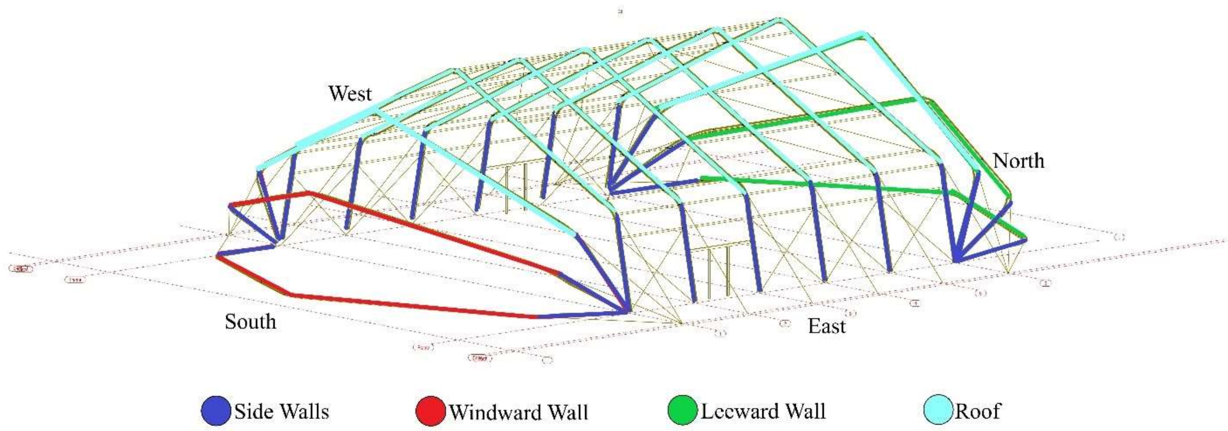

Figure 6.2-1. Layout of the first alternative longitudinal wind load case

Table 6.2-1. Calculated maximum stresses

Vertical Frames (ksi)	
Load Case	Maximum
D+W5,7,9	15.68
D+W6,8,10	9.85

End Vertical Frames (ksi)	
Load Case	Maximum
D+W5,7,9	10.87
D+W6,8,10	10.18

Door Frames (ksi)	
Load Case	Maximum
D+W5,7,9	25.04
D+W6,8,10	13.41

Purlins (ksi)	
Load Case	Maximum
D+W5,7,9	0.47
D+W6,8,10	-0.87

6.2.2 Alternative Longitudinal Wind Load Case 2

For the second alternative longitudinal wind load case, the columns of all the frames were assigned as the sidewall. The roof span of all the vertical frames were assigned the roof loads. The roof spans of all the door frames were also assigned the roof loads. In this load case, there are no windward or leeward wall loads. Figure 6.2-2 shows the layout of the loads assigned to the frame members. The calculated stresses are shown in Table 6.2-2.

The comparisons of the stresses in the vertical frames showed slightly smaller values in the second alternative longitudinal load case than the original load case. Compared to the first alternative longitudinal load case, the stresses were marginally larger. In the end vertical frames, the stress due to wind condition 5,7,9 decreased slightly from the original load case, however, for load condition 6,8,10 the stress was reduced by more than 50%. The stress in the end vertical frame due to load condition 5,7,9 was marginally smaller for the second alternative longitudinal load case compared to the first alternative longitudinal load case. However, the stress in the end vertical frame due to load condition 6,8,10 was around 20% smaller for the second alternative longitudinal load case than the first. For the door frames, the stress due to condition 5,7,9 was reduced by around 20% while the stress under condition 6,8,10 was reduced by nearly 75%. The stress under load condition 6,8,10 was below the allowable stress. The reduction was so large for wind condition 6,8,10 for the same reasons as the first alternative longitudinal load case. The stresses in the door frame were around 1 ksi larger for the second alternative longitudinal load case than the first. The purlins experienced tensile stresses for both wind conditions under the second alternative loads case. Both stresses were larger than the first alternative longitudinal load case. This change is due to the same reasons as the first alternative longitudinal load case, however they were more prominent because all the loads act outward on the door frames for this load case.

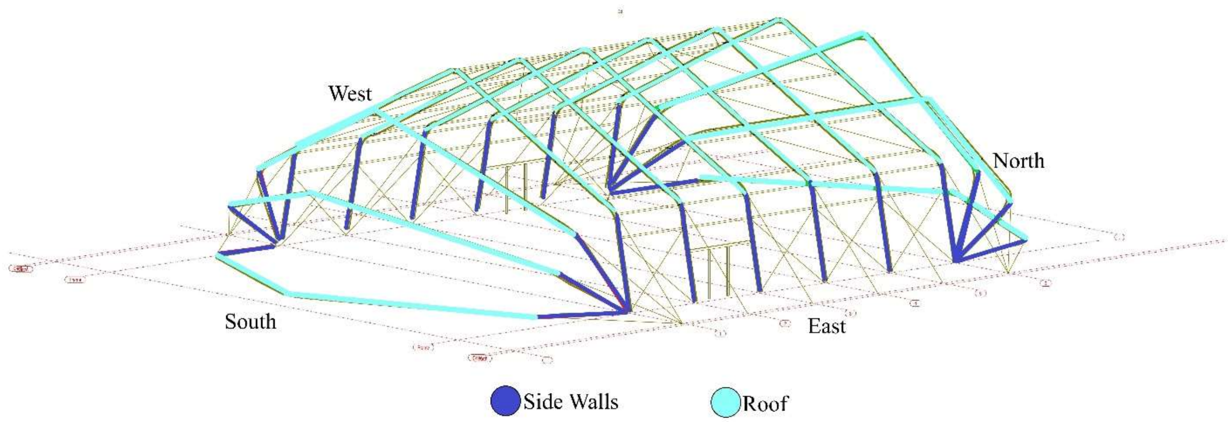

Figure 6.2-2. Layout of the second alternative longitudinal wind load case

Table 6.2-2. Calculated maximum stresses

Vertical Frames (ksi)	
Load Case	Maximum
D+W5,7,9	15.94
D+W6,8,10	9.91

End Vertical Frames (ksi)	
Load Case	Maximum
D+W5,7,9	10.39
D+W6,8,10	8.47

Door Frames (ksi)	
Load Case	Maximum
D+W5,7,9	26.36
D+W6,8,10	15.03

Purlins (ksi)	
Load Case	Maximum
D+W5,7,9	1.44
D+W6,8,10	1.08

6.3 Chapter Summary

The objective of the alternative frame support study was to determine how the responses of the structure would change if there was movement in one of the baseplates. Based on the comparison of the stresses in the frames and purlins, there were no changes except for one load condition in the transverse direction for the door frame. Similarly, there were no changes in the reaction of the exterior high wind kit cables, or the frame supports. There was very minimal deflection of the spring support. A change in the stresses of the frames and purlins along with the reactions of the supports were expected, however this shows that the failure of one base plate has a minimal effect on how the wind loads are transferred throughout the structure. A more detailed study of greater foundation movements should be considered to better understand how the structure would reacts when movements occur in the baseplates.

The first alternative longitudinal wind load case showed that if the most vertical door frame experiences roof forces instead of windward wall forces, it reduces the stresses experienced in the structure. The stresses were largely reduced in the purlins for both the wind conditions and largely reduced in the end vertical frames and door frames for wind condition 6,8,10. Under this load case, the maximum door frame stress under wind condition 5,7,9 was the only stress larger than the allowable stress.

The second alternative longitudinal wind load case showed the same results as the first alternative longitudinal wind load case with slightly different values. For the vertical frames, the stresses were marginally larger for the second alternative longitudinal wind load case than the first. Similarly, the purlins experienced larger tensile stresses in the second alternative longitudinal wind load case. The end vertical frame experienced slightly larger stresses in the first alternative longitudinal wind load case. For the door frames, the stresses were larger for the second alternative longitudinal wind load case than the first.

The alternative longitudinal wind load cases provide evidence that the uncertainty in the longitudinal wind loads is crucial. Based on the longitudinal wind load cases used, the stresses in the model experienced significant change. This was especially true for the door frames under wind condition 6,8,10. This was the location of the largest stresses in the model. Based on this study, to have confidence in the maximum demands on the model, it is vital to gain a better understanding of how wind loads in the longitudinal direction are applied to the structure.

Chapter 7 Summary, Conclusions, and Future Work

7.1 Summary

The objective of this study was to investigate the structural response of a typical LAMS to design wind load cases and identify any systemic factors that may be contributing to premature failure. A literature review was presented to provide insight on the background of these large-area maintenance shelters, along with a better understanding of the failures that have occurred. On multiple occasions, LAMS that were erected at various locations around the world have collapsed under wind loads they were designed to withstand.

A 3-D finite element model was created using SAP 2000 to better understand the LAMS structural system. A load path analysis was conducted on the model to verify that the loads are transferred throughout the model properly. The model was also compared against preliminary data recorded using instrumentation set up on an in-service LAMS to model outputs. Data was recorded during several wind events in both the transverse and longitudinal directions. This data was then processed and scaled to replicate the demands on the structure during a 90-mph wind event. Design wind loads were calculated using the 90-mph design wind speed in the model. Nodes were created in the model at the locations of the instrumentation. The demand outputs of these nodes were then compared to the structural monitoring of the in-service LAMS.

The maximum forces, stresses, and support reactions were calculated based on the design wind loads. The locations of these maximum responses were also found. This was done to gain a better understanding of potential failures of LAMS.

Three alternative model analysis scenarios were studied to determine the effect of some of the uncertainties in the system. The stresses in the structure were calculated for the same location for the original and the alternative foundation case. The reactions of the supports were also calculated for the high wind kit cables and frame supports at the same locations of the reactions from the maximum demands study. For the other two alternative model scenarios, only the stresses in the purlins and frames were calculated and compared.

7.2 Conclusions

The load path analysis study revealed that the model transferred loads in a manner that produced confidence in the main framing system. This was true for both the transverse and longitudinal directions. The modeled response showed the structure acts as a system, and the individual frames do not act completely independently. This study provided evidence that for the transverse direction, the individual frames carried most of the direct load, but there was some distribution of the loads into the other frames due to the cable braces. For the longitudinal direction, the cables (both roof and wall), purlins, and frames each played important roles in the load path, illustrating the system behavior.

The comparisons of the model to the responses of the in-service, instrumented LAMS provided mixed results for the transverse wind loads. The axial forces in the high wind cables differed by around an order of magnitude in some cases. The axial forces and internal moments on the frame members had several comparisons that were within an order of magnitude. The deflection of the eave in the y-direction on the windward side of the model and in the z-direction on the leeward side of the model provided nearly identical comparisons. However, the y-direction deflections on the leeward side of the model were xx% greater than the measured response. Although the comparisons showed mixed results, the similarities in the patterns in the model and in-service LAMS provided enough evidence to state that the model correctly represents the structure when experiencing transverse wind loads.

The comparisons of the model results to the responses of the in-service LAMS did not agree well for the longitudinal wind loads. There are several uncertainties in the structure that are potential reasons for the poor comparisons. The slack of the roof cables and the excess play in the purlin connections in the in-service LAMS could have altered the way the loads were transferred throughout the structure. Temperature effects on strain measurements also gave uncertainty to the preliminary data measured in the in-service LAMS. The model outputs only recorded the axial forces in the purlins, however, any out-of-plane loading in the purlins could have been recorded in the data. Lastly, because of the uniqueness of the structure, it is uncertain if the wind loads are defined on the structure properly. Overall, the comparisons showed similar signs between the model outputs and in-service LAMS data, however, values varied by a large magnitude.

The maximum values calculated in the finite element model demonstrated the structural response of a typical LAMS under design wind load cases and possible systemic factors that may be contributing to premature failure were discovered. Based on the transverse wind load cases (wind conditions 1-4), the door frame was the only section that experienced stress larger than the allowable stress. This occurred on the leeward eave of the roof on the second door frame. Other than that, none of the vertical frames, end vertical frames, purlins, or cables experienced stresses or forces as large as their allowable stresses or forces. For the longitudinal load cases (wind conditions 5,7,9 and 6,8,10) both the end vertical frame and the most vertical door frame closest to the windward wall experienced stresses larger than the allowable stress. The door frame experienced stress nearly 3 times larger than the allowable stress. Other than that, none of the vertical frames, purlins, or cables experienced stresses or forces as large as their allowable stresses or forces for the longitudinal load cases.

The demands seen in the model under design loads align with the failures that are occurring in erected LAMS. Longitudinal winds have caused failure of the LAMS on the door frames. This is due to the door frames either being improperly designed or uncertainty in the design wind loads. With this information, a likely cause of failure has been identified including what wind direction is producing the failure, and where the failure is occurring.

The alternative model analysis scenario that included the spring support produced outputs that suggest the model is not affected greatly if movement occurs in one of the baseplates. The alternative model analysis scenarios provided evidence that there are large variabilities in the model outputs based on the longitudinal wind loads applied to the model. These findings demonstrate the importance of a wind tunnel study for irregularly shaped structures like the LAMS.

7.3 Future Work

While this study provides evidence that suggests when and where the failure of these large-area maintenance shelters occur, there are several uncertainties and aspects of the LAMS that need to be further evaluated.

The uncertainty of the design wind loads is very significant in the responses of the structure. Based on the alternative analysis scenarios, it was determined that differences in how the wind loads are designed largely effect the stresses felt throughout the structure. This was noticed particularly in the longitudinal direction. To validate the model in this study, it is critical to conduct further research on the wind loads to gain a better understanding of the aerodynamic coefficients that should be used in design.

The spliced connections of the frames were not modeled or investigated in this study. This is a critical aspect of the structure, and if the strength and stiffness of these splices are lower than the frame members, they could lead to significant deformations and the premature failures seen in LAMS. The strength of these connections along with how they affect the structure and model needs to be studied.

The support connections were not studied in this research. The uncertainty of the designed wind load could have led to the design and use of insufficient supports. Based on the alternative analysis scenario study in this research, the movement of a single baseplate did not have an effect on the structure. However, the impact of flexible supports was not evaluated over multiple stiffnesses, nor over all supports, so it's effects cannot be dismissed as of yet. There is also a high variability in the foundations of the LAMS. These differences could drastically change the strengths of the supports for the frames and high wind kit. This needs to be further studied to gain a better understanding of these variabilities and uncertainties.

The model in this study was designed assuming the cables, purlins, and fabric were all taut. The in-service LAMS showed that this is not the case. The looseness of these members could have a large effect on how the loads are transferred throughout the structure. Further work needs to be conducted to determine how to model these differences. Specifically, the purlins experienced possible out-of-plane forces on the in-service LAMS. The looseness of the purlins and cables can also lead to deflection of the frame lines that are not studied in the model.

References

ASCE. (2005). *ASCE/SEI 7-05 Minimum Design Loads for Buildings and Other Structures.* Reston, Virginia: American Society of Civil Engineers.

ASCE. (2016). *Tensile Membrane Structures (ASCE/SEI 55-16).* Reston, VA: American Society of Civil Engineers.

Bridgens, B., Gosling, P., & Birchall, M. (2004). Tensile Fabric Structures: Concepts, Practices & Developments. *Structural Engineer, 82*(14), 21-27.

Clamshell Buildings. (2019). *Validation Submittal Including Technical Description and Calculations For the LAMS Type AF VM Clamshell Model 50B-BBB-A5CC Part Number 50B-BBB-A5CC-V01.*

CSI. (2017). *CSI Analysis Reference Manual.* Computers and Structures, Inc. Retrieved from file:///C:/Program%20Files/Computers%20and%20Structures/SAP2000%2021/Manuals/CSiRefer.pdf

Fittro, T. (2018). *Fabric Structure Strength and Structural Integrity of Large Area Maintenance Shelters (LAMS).* Auburn University, Graduate Faculty.

Huntington, C. G. (2013). *Tensile Fabric Structures: Design, Analysis, and Construction.* American Society of Civil Engineers.

JOCOTAS. (2012). *Department of Defense Standard Family of Tactical Shelters.* U.S. Army Natick Soldier RD&E Center, Joint Committee On Tactical Shelters. Retrieved from https://apps.dtic.mil/dtic/tr/fulltext/u2/a568854.pdf

Legacy Building Solutions. (2015, May 1). *7 Common Mistakes in Fabric Building Construction*. Retrieved from Legacy Building Solutions: https://blog.legacybuildingsolutions.com/common-mistakes-in-fabric-building-construction

Liew, J., & Tran, T. (2006). Novel Deployable Strut-Tensioned Membrane Structures. *Journal of the International Association for Shell and Spatial Strutures, 47*(1), 17-29.

NIST. (2010). *Collapse of the Dallas Cowboys Indoor Practice Facility, May 2, 2009.* U.S. Department of Commerce National Institute of Standards and Technology, Building and Fire Reseach Laboratory. Retrieved from https://www.nist.gov/system/files/documents/2017/05/09/pptFinalReportRelease_DallasCowboysPracticeFacility_Jan2010.pdf

Seaman Corporation. (n.d.). *Style 8324 FRLTC Kynar/Opaque/White.*

Stiles, J. (2021). *Solutions for Wind-Induced Fabric Structure Failures with Case Studies in the United States Air Force.* United States Air Force, Air Force Civil Engineering Center.

The Aluminum Association. (2005). *Aluminum Design Manual.* Retrieved from chrome-extension://cbnaodkpfinfiipjblikofhlhlcickei/src/pdfviewer/web/viewer.html?file=file:///C:/Users/Culver%20Norred/Downloads/vdocuments.site_aluminum-design-manual-2005.pdf

Wang, C., Wood, L., Abdul-Rahman, H., & Mohd-Rahim, F. (2015, April). Defects of Tensioned Membrane Structures (TMS) in the Tropics. *Journal of Performance of Constructed Facilities*.

Wiegler, L. (2011, January 20). Tearing into the Metrodome: Are Other Air-Pressurized Stadiums Unsafe and Outmoded? *Scientific American*. Retrieved from https://www.scientificamerican.com/article/tearing-metrodome-pressurized-stadiums-unsafe/

Wilson, F. (2016, 12 May). *Failure Mechanisms of a Fabric Structure*. Retrieved from Shelter-Rite Architectural Fabrics: https://www.architecturalfabrics.com/blog/failure-mechanisms-of-a-fabric-structure